Utrecht University

Master's Thesis – master Energy Science

'A Characterization of Energy Drought Events in the Netherlands'

by

Isaï Magan

Utrecht University
Faculty of Geosciences

1st Supervisor: Dr. Jing Hu
2nd Supervisor: Dr. Vinzenz Koning
July 2023

Contents

Table of Figures

Table of Tables

List of acronyms

AIC	Akaike information criterion
BIC	Bayesian information criterion
CF	Capacity factor
CLC	CORINE land cover
CVaR	Conditional value at risk
DF	Degrees of freedom
DSO	Distribution system operator
ED	Energy drought
EEZ	Exclusive economic zone
ERA	ECMWF Re-Analysis
ES	Expected shortfall
EVA	Extreme value analysis
GEV	Generalized extreme value
GHG	Greenhouse gas
GP	Generalized Pareto
GW	Gigawatt
MERRA	Modern-Era Retrospective analysis for Research and Applications
MW	Megawatt
PV	Photovoltaic
Q-Q	Quantile-quantile
RCP	Representative concentration pathway
TSO	Transmission system operator
VaR	Value at risk
VRE	Variable renewable energy

Abstract

The increasing importance of renewable energy supply in the transition to carbon neutral energy systems highlights the need of an adequate understanding of the associated risks to energy supply. Variable renewable energy sources are inherently dependent on meteorological conditions, and as such could provide insufficient energy for certain periods of time. In this study, a characterization is performed on such energy drought events in the Netherlands. ERA-5 reanalysis and MERRA-2 climate data is used to model the performance of solar PV and wind power generation. Statistical approaches are used to investigate these events on provincial, sub-national and national scale. It has been found that the province least susceptible to energy drought occurrence is Zeeland, whereas Gelderland, Limburg, Noord-Brabant, Overijssel and Utrecht are most likely to experience energy droughts. Additionally, copula theory is used to investigate probabilities of the co-occurrence of energy drought events between regions and technologies. When provinces are aggregated to sub-national regions, this research shows that constructed copula models capture tail events in the distribution of power generation in the form of energy droughts well. A co-occurrence between 9.61% and 14.9% has been found for ED events between the two defined sub-national regions, with return periods between 67.7 and 117 days. Finally, extreme value theory is applied to investigate extremely long-lasting energy droughts. Using the Peak-Over-Threshold method, a VaR-95% value between 27.2 and 46 hours and a CVaR-95% value between 41.6 and 58.1 hours has been found for extreme energy drought duration in the Netherlands. Furthermore, 50-year and 100-year ED durations are found to be between 84 and 99 hours and 91 and 107 hours, respectively. The results of this study can be incorporated in the planning of future renewable energy installations, and for grid operators to determine and manage the risk of black outs more accurately.

Keywords – Energy; Variable Renewable Energy; Climate change; Energy drought; Dunkelflaute; Wind; Solar; Capacity factor; Netherlands; Copula; Co-occurrence; Extreme value analysis; Peak-over-threshold

1: Introduction

1.1 Renewable energy mix

Anthropogenic greenhouse gas (GHG) emissions are a main driver of human-induced climate change. The risks associated with the impacts of this climate change span across many domains such as ecosystems, human health, and economic sectors (Pörtner et al., 2022). As is stipulated in the goals of the 2015 Paris agreement, in order to mitigate these impacts, GHG emissions must be reduced in the near future (Schleussner et al., 2016). GHG emissions are especially prevalent in the global energy sector, accounting for up to 34% of total emissions in 2018 (Lamb et al., 2021). This highlights the need for a transformation towards a more renewable energy mix.

Reshaping the energy supply infrastructure from being primarily based on fossil fuels to more dependent on variable renewable energy (VRE) technologies such as solar and wind is a strategy currently employed in the various parts of the world, such as Europe. The development of renewable energy sources (RES) is stimulated in the European Union (EU) through directives from the European Commission and investment support by the European Central Bank (Simionescu et al., 2020).

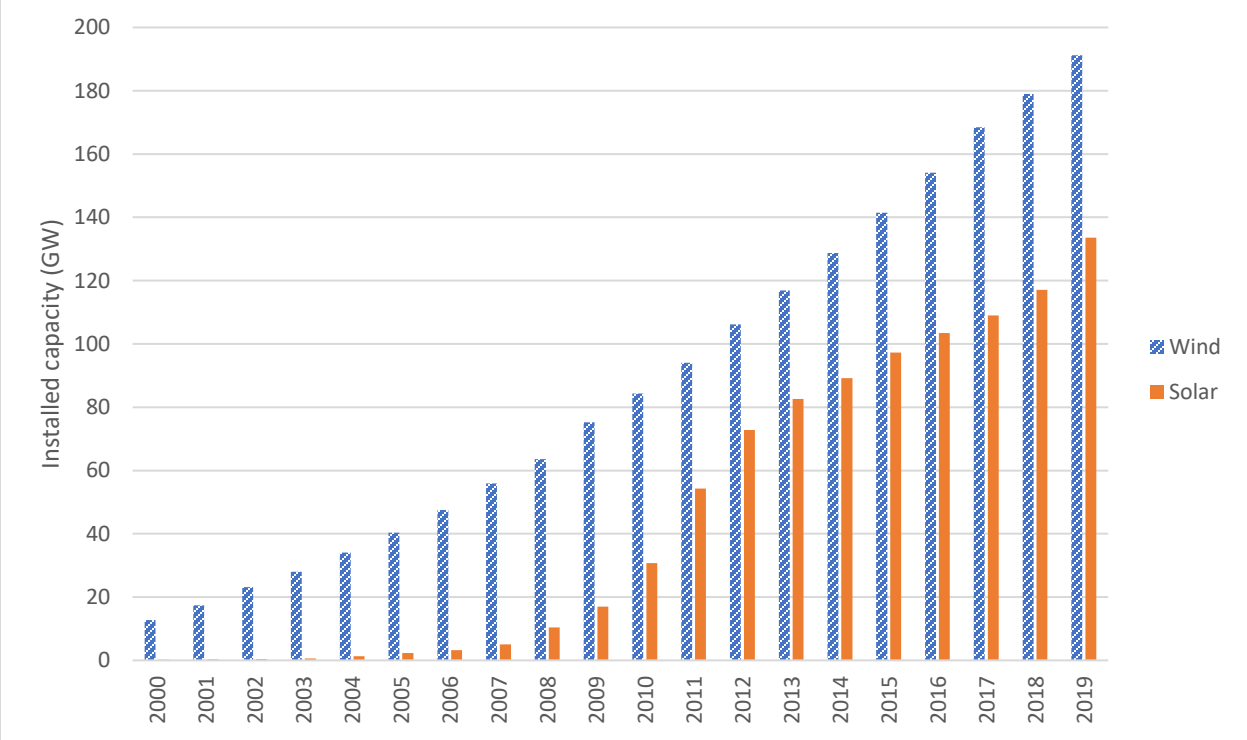

Figure 1: Total installed capacity (GW) in EU-27 countries and the UK in the period 2000-2019 (Eurostat, 2023).

As can be seen from Figure 1, the total installed capacity in the EU-27 countries and the UK have historically increased significantly (Eurostat, 2023). As a result, the gross electricity generation in the EU stemming from wind and solar sources has historically increased and is projected to increase further up to 2050 (Shivakumar et al., 2019).

1.2 Energy droughts

The performance of VRE technologies is inherently dependent on meteorological conditions. Variability in power production from these sources is therefore introduced through both space and time dimensions. This is unlike conventional power plants, which are mostly unaffected by temporal meteorological variability. Safeguarding the energy security of systems whose energy mix consists for a significant share of VRE sources therefore requires a different energy system design than was traditionally required (van der Wiel et al., 2019).

Periods in time where a relatively low energy production occurs due to specific weather conditions are of concern to ensure fulfilling the simultaneous energy demand. These periods of low energy production from VRE sources are described in literature as “Dunkelflaute” (German expression for the absence of light and wind) as well as “dark doldrums” (Matsuo et al., 2020) or “energy droughts” (EDs) (Otero et al., 2022). Meteorological studies occasionally refer to these type of events as “anticyclonic gloom” (Li et al., 2021b).

The impacts of EDs are associated with the periods of time where the power output of VRE technologies is minimal. Transmission system operators (TSOs) require precise power forecasts to be able to guarantee stability of the power system (Steiner et al., 2017). Unforeseen extreme events in the form of EDs could potentially lead to blackouts of the system and would result in temporary unfulfillment of energy demand. Historically however, TSOs have employed balancing measures to account for the sudden loss in power supply (Hirth & Ziegenhagen, 2015). These balancing measures result in increased operational costs of the power system (Ueckerdt et al., 2015).

From a societal perspective, the measures taken to account for the impact of EDs partly come at the cost of the electricity consumer. One form this could present itself in is an increased price of electricity during EDs. This increased price is the result of the temporary dispatch of power plants to account for the loss in VRE output or other measures taken by the TSOs to ensure balance (Hirth, 2013). For example, in 2021 an ED event in the form of a wind drought in Europe caused a surge in the price of natural gas leading to high electricity costs (Ohba et al., 2023). Other costs inflicted on the consumer could be in the form of rolling blackouts or brownouts. These balancing measures are taken by grid operators, and result in the unavailability of all or some electricity consumption respectively for a specific time period (Agarwal & Khandeparkar, 2021).

Collectively, these impacts present problems in the form of energy insecurity, as they have the potential to interrupt obtainability of energy sources as well as worsen energy affordability (Gökgöz & Güvercin, 2018). This is exacerbated even further by considering the impact of fluctuating energy demand, especially when EDs are synchronous with periods of time in which there is a high demand of energy. With the potential impact of ED events in mind, plans for expanding VRE installations which require new energy system designs consequently require an understanding of such ED events.

A country that is particularly susceptible to the impacts of EDs is the Netherlands. In comparison to the rest of the EU-27 countries, the penetration of solar and wind sources in the energy mix is relatively high (Eurostat, 2023). Additionally, the demand for energy per capita is relatively high (Statista, 2023b, 2023a). A compounding issue for the Netherlands with regard to ED is frequent congestion issues in the national power grid (TenneT, 2022b). These congestion issues result in more vulnerable power grids as TSOs are limited in their options for maintaining balance should an ED occur. Finally, in contrast with other EU-27

countries such as Germany or Spain, it has a small surface area. This reduces the effect spatial smoothing could have on decreasing the variability of energy production from VRE sources and mitigating EDs (Jurasz et al., 2020). An example of a historical ED event in the Netherlands is described by Li et al., where on April 30th, 2018, the TSO of the Netherlands (TenneT) was forced to issue an emergency warning in the Netherlands for energy consumption and purchased power from cross-border regions at high market prices to ensure stability (2021b).

1.3 Literature review

Research in the field of EDs is a relatively recent phenomenon, although it draws inspiration from classical forms of drought research in the fields of hydrology, statistics, and meteorology. The literature that exists comprises of different research aims, and consequently different scopes and methodologies. Research aims range from the identification of co-occurring extreme weather phenomena in the context of EDs (Tedesco et al., 2022), to the characteristics of the EDs themselves (Raynaud et al., 2018), to the quantification of how to predict such ED events (Li et al., 2020).

Some research only considers wind power (Ohlendorf & Schill, 2020), whereas others include hydropower as an energy producing technology (Raynaud et al., 2018). Further distinction can be made between studies that focus on regional (Amonkar et al., 2022), national (Ohba et al., 2022) and multi-national (Otero et al., 2022) scales.

Differences in methodological approach are often a result of differences in research aim and scope. Most commonly, climate data has been utilized to simulate and study the conditions in which EDs take form, such as was done by Li et al. using mesoscale modeling (2021b). Since the consideration for what constitutes as an ED differs between studies, an attempt has been made by Allen & Otero Felipe to standardize the monitoring of EDs through the use of indices (2022). Some studies are mostly focused on the extreme event occurrence for ED events rather than the occurrence of general ED events (Plötz & Michaelis, 2014).

To research EDs, a definition must first be proposed of what exactly it entails. As mentioned previously, studies on this topic have utilized differing definitions, an overview of which can be found in Table 1.

Table 1: Collection of studies and their respective definitions of the term 'energy drought', or equivalent term used in their research.

Study	Definition
Raynaud et al. (2018)	Two definitions: Energy Production Drought – "a contiguous sequence of days during every day of which the production is below a given low-production threshold." (p.580) Energy Supply Drought – The imbalance between energy production and demand
Otero et al. (2022)	Two definitions: Energy drought of low production – Period of time where energy production is below threshold Energy drought of residual load – Period of time where demand minus solar/wind production exceeds threshold
van der Wiel et al. (2019)	Two types of extreme event with threshold of expected average return period of determined length: One associated with low energy production, and the other associated with high energy shortfall. This was done for events of relatively short, medium, and long duration.
Amonkar et al. (2022)	Periods of time in which the realized energy production falls below a certain target threshold
Gangopadhyay et al. (2022)	Shortfalls in energy production based on the mean energy production for that particular day across timeframe (multiple years)
Li et al. (2021a)	Periods of time where the capacity factor for both solar and wind simultaneously fall below threshold
Ohba et al. (2022)	Period of time where the continuous daily power generation falls below capacity factor threshold
Allen & Otero Felipe (2022)	Definition based on conversion of energy production and residual load to indices: Energy drought considered to be values of indices where energy production is below threshold or residual load exceeds threshold
Ohlendorf & Schill (2020)	Two definitions: Narrow definition – period of time where consecutive hours of aggregated capacity factors for wind and solar are constantly below a threshold value Broad definition – period of time where average capacity factor for solar and wind falls below a threshold value
Mockert et al. (2022)	Period of time where the mean combined capacity factor of solar and wind are below a threshold continuously for a minimum amount of time
Plötz & Michaelis (2014)	Power supply – Long phases with little or no wind power feed in, where the long phases are defined by different minimum durations and the power feed in by a threshold value

While none of the studies in Table 1 maintain the exact same definition as any other, all studies seem to place emphasis on a chosen minimum period of time where the energy production is below an arbitrary

threshold. Most commonly, the proxy for measuring energy production is retrieved from determined capacity factor values for both solar and wind. Most studies do not consider energy production in isolation, as they additionally consider energy demand patterns for the determination EDs. The chosen thresholds for what constitute as an ED in terms of energy production or residual demand differed between studies, although it should be mentioned that this is mainly due to the type of data used in their computations and the scope and aim of their research.

Regarding EDs, the Netherlands has been investigated seldomly. The studies that have done so found that compared to other countries in Europe, the Netherlands has a strong correlation of ED events happening simultaneously in neighboring countries such as Belgium (Li et al., 2021a). Additionally, it has been found that the Netherlands, along with Sweden, would benefit most from employing strategies aimed at mitigating the impact of ED events such as pooling energy production through interconnection between large areas (Li et al., 2021a).

Other studies on EDs in the Netherlands have not necessarily considered the general characteristics of all ED events that occurred over a certain time period. Rather, these studies analyzed specific historical ED events, based on additional selection criteria, and their context to generate simulations through mesoscale modeling. Li et al. (2021b) found that for a simulation based on a 9-day ED event occurring around Belgium, the Netherlands and Germany in 2017 there was a presence of frequent mixing of the marine boundary in addition to weak wind speeds and cloudy conditions. Additionally, based on one specific historical ED event in the Netherlands, Li et al., (2020) found that during the passage of a cold front there was a low-level jet current present when the ED occurred. Finally, meteorological conditions of ED events in the Netherlands along with other European countries have been studied by van der Wiel et al. (2019). This study found that shorter ED events (1-day) are characterized by large high-pressure systems, whereas longer ED events are characterized by atmospheric blocking.

Based on the available literature on this topic, it seems that there is a research gap on ED events in the Netherlands. More specifically, compounding EDs are not fully investigated. These types of EDs are characterized by complementary occurrences of events, which compound to an enhanced overall effect. For example, compounding characteristics of EDs could be based on the investigated technologies, namely wind and solar. For example, the compounding effect of solar photovoltaic (PV) and wind simultaneously producing little renewable energy compounds into a greater overall effect. For the existing literature, these components of energy production are commonly aggregated to arrive at a single energy production parameter. However, the technologies are yet to be investigated separately for the Netherlands. This form of ‘simple’ ED allows to investigate the contribution of solar and wind energy technologies individually to compounding EDs.

Additionally, further analysis of compounding EDs can be broken down in the spatial domain. Through splitting the Netherlands at the sub-regional level, specific regions can be investigated for ED events and compared. No existing literature has considered co-occurrence of EDs at the sub-regional level and their contribution to the national EDs in the Netherlands. Finally, literature has not yet considered extreme ED events in the Netherlands. More specifically, the extremities that occur with regard to their duration. Such extreme events are characterized as occurring rarely, with an extremely long duration compared to most other events. Extreme events are important for risk management and have been studied in many different fields. Most notably, the concept of expected shortfall (ES) is often studied to describe tail behavior of distributions (Acerbi et al., 2001; Nadarajah et al., 2014). This concept has not yet been investigated for the duration of ED events in the Netherlands.

1.4 Research aim

Resulting from the research gaps previously described, this study characterizes ED events in the Netherlands from 1960 until 2020. It places an emphasis on investigating the frequency, duration, and estimated return periods of these events. While the studied period is historical, Yang et al. (2022) found that future solar and wind energy production potential does not differ considerably between 2010 and 2100 based on an ensemble of climate scenarios. The observed decrease in potential for solar PV amounted to 0.01-2.71% depending on location and representative concentration pathway (RCP) scenario, while an increase between 0.6-2.3% is observed for wind. The conclusion of this study relates to average production, while the research of this thesis focusses on the tail distribution of production. However, the assumption is made that the weather is stationary over time and therefore does not consider the impact of climate change. Therefore, it is reasonable to assume that the characterization of EDs from the selected historical time period holds merit for the near future. Even though this stationarity is assumed, this study makes use of two climate datasets with hourly timesteps spanning 60 and 40 years, respectively. This is likely to capture the statistics accurately due to the size of the data samples, even if the results are based on the previously mentioned stationarity assumption. The main research question is stated as follows:

How are energy drought events in the Netherlands between 1960 and 2020 characterized?

The characterization of these events describes their frequency, duration and return periods. However, in order to answer this research question in more detail and fill the established research gap, both 'simple' and compounding EDs are analyzed. Simple EDs are considered to be analyzed from the perspective of only one technology, such as solar or wind. Additionally, separate analysis is performed on extreme long duration events to estimate appropriate return periods for the most extreme events. Therefore, the relevant sub questions for this research are as follows:

1) *What is the characterization of simple energy droughts?*
2) *What is the characterization of technologically compounding energy droughts?*
3) *What is the characterization of spatially compounding energy droughts?*
4) *What is the characterization of extreme long duration energy droughts?*

Compounding events are characterized by their amplification of impacts through co-occurrence or rapid succession of individual events (Zscheischler et al., 2020). Therefore, the periods of time with co-occurrence are of interest for investigating the EDs. For example, for technological compounding when both solar and wind are concurrently below a threshold of production, or for spatial compounding with multiple regions experiencing ED events simultaneously. Regardless of the type of compounding event, inevitably the impacts of EDs are exacerbated. For extreme events, the interest is centered around describing how often the occurrence is estimated, determining the risk associated with such events and what the associated duration is of extreme events for defined return periods.

From a scientific perspective, this research aims to fill the research gap and provide knowledge on the compounding characteristics of technology, space, and time of EDs. More specifically, this study employs copula-based models to quantify the extent of co-occurrence of events categorized by technology type and region. Furthermore, this study develops a methodology that combines principles of extreme value analysis (EVA) for more accurate tail analysis that have not been used in the field of EDs in the Netherlands before. Finally, this research employs a more sophisticated method of threshold selection for the EVA

than comparable studies such as the one by Plötz & Michaelis (2014) where extreme events in wind power analysis are studied.

From a societal perspective, this research aims to improve the current understanding of ED events. The relevance for this is societally tied to its impacts. As previously mentioned, (rolling) blackouts or brownouts interrupt access to energy whereas grid balancing measures tend to increase electricity prices for consumers. Similar to investigating conventional extreme events such as droughts or floods, risk assessment is imperative in understanding the scale of the problems this could pose, both currently and in the future (Grounds et al., 2018). Therefore, this study describes the expected return periods for ED events based on their characteristics. To conclude, this study aims to provide knowledge on ED events specifically for the Netherlands. Consequently, the risk of implementing additional VRE sources in the national energy mix is better understood and can be accounted for in the design and planning of future energy systems.

The results of this research can benefit multiple stakeholders. Firstly, the characterization of simple and technologically compounding ED events can provide valuable information for policy makers and parties involved in VRE installation planning. Since this information is inherently spatial, the effectiveness and risk of planned projects can be assessed with the possibility of ED event occurrence. Additionally, the characterization of spatially compounding ED events can provide valuable information for the Dutch TSO. The simple ED event occurrence in one region can theoretically be offset by power production in another, however this is not possible for co-occurring ED events in the spatial domain. Therefore, the characterization of spatially compounding ED events could provide insights on risk management and grid planning for the TSO. Finally, the characterization of extremely long duration ED events can provide valuable information to grid operators such as the aforementioned TSO and distribution system operators (DSOs). These operators are responsible for employing ancillary services in the case of a sudden reduced supply of power. Similar to research on other extreme events such as flooding or droughts, extreme events should be considered in the form of ED event duration as the ancillary services should be able to bridge these periods of time.

2: Methodology

The general approach of the methodology for this research is displayed in Figure 2.

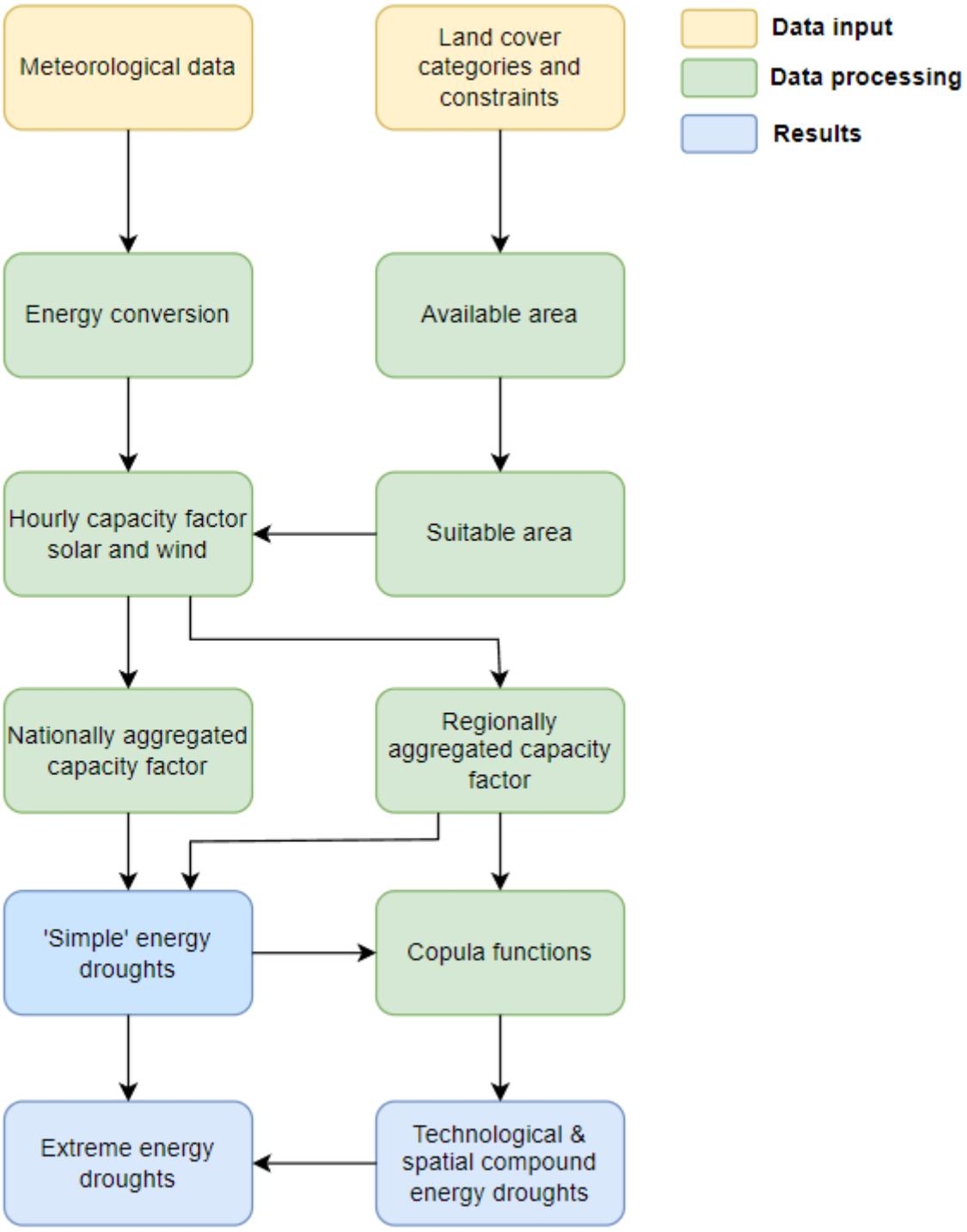

Figure 2: Flowchart depicting the methodology for this research

2.1 Data

The data that is used as an input for the wind and solar energy conversion is the ECMWF Re-Analysis (ERA)-5 reanalysis data. This dataset was created by the European Center for Medium-Range Weather Forecasts (ECMWF). It contains hourly estimates of numerous weather components on a global scale, with a resolution of 0.25° x 0.25° on the longitude-latitude grid. The specific range of coordinates that is used are latitudes between 50° and 55°, and longitudes between 2° and 8°. This range covers the land area of the Netherlands as well as the exclusive economic zone (EEZ) of the Netherlands. For further sensitivity analysis, GES-Modern-Era Retrospective analysis for Research and Applications-2 (MERRA) data is also taken as an input for the energy conversion and will be referred to as MERRA data. Since this data is available at a different resolution than the ERA5 data, it is transformed to similar resolution using re-gridding tools. Specifically, bilinear interpolation is selected as the conversion method. This method considers the four nearest grid cells of the original data in two directions and is appropriate to use given the size of the available data (Rajulapati et al., 2021). The total area comprises of 525 grid cells. The specific components retrieved from the dataset for further calculation are:

- 100m u- and v- components of wind (m s^{-1})
- 10m u- and v- components of wind (m s^{-1})
- 2m temperature (K)
- Forecast albedo (Dimensionless)
- Surface downwards solar radiation (W m^{-2})

Additionally, data is used for spatially attributing installed capacity of solar and wind technologies to each grid cell. The data on currently installed capacity is available on a provincial level. The installed solar and onshore wind capacity per province in 2021 can be found in Table 2 (Rijksoverheid, 2022 & RvO, 2022). The installed capacity per offshore wind farm in the Dutch EEZ in 2018 and their respective turbine types can be found in Table 3 (RvO, 2018). The installed capacity is expressed in megawatts (MW).

Table 2: Installed solar and onshore wind capacity (MW) per province in 2021 (Rijksoverheid, 2022 & RvO, 2022).

Province	Installed solar capacity (MW)	Installed onshore wind capacity (MW)
Drenthe	881	221
Flevoland	581	1346
Friesland	841	574
Gelderland	1825	174
Groningen	1114	728
Limburg	1164	73
Noord-Brabant	2577	299
Noord-Holland	1411	713
Overijssel	1219	75
Utrecht	744	34
Zeeland	559	558
Zuid-Holland	1499	490
Total	14415	5285

Table 3: Installed offshore wind capacity (MW) per installation in the Dutch EEZ in 2018 and respective turbine types (RvO, 2018).

Installation	Total offshore wind capacity (MW)	Turbine type
Borssele I and II	752	Siemens Gamesa 8.0 MW – 167 DD
Borssele III and IV	731.5	Vestas V164 – 9.5 MW
Borssele V	19	Vestas V164 – 9.5 MW
Gemini Windpark	600	Siemens SWT-4.0-130
Luchterduinen	129	Vestas 112
Prinses Amaliawindpark	120	Vestas V80
Egmond aan Zee (OWEZ)	108	Vestas V90
Total	2459.5	-

2.2 Data allocation

The data for installed capacity does not follow a similar resolution as the weather data. Therefore, installed capacity is distributed across grid cells based on total province installed capacity. The allocation of capacity across grid cells is determined by performing a spatial analysis that identifies the most suitable locations for the installation of VRE technologies. It is assumed that no capacity is installed in areas that are deemed unsuitable by the spatial analysis.

Limiting factors for land areas are numerous and include the presence of protected nature areas or slope and elevation limitations. Offshore area availability is affected by the presence of limiting factors such as a maximum distance to port or the presence of oil rigs. Furthermore, the type of landcover is used to determine the share of area that is suitable for installing VRE technologies. The method of spatial analysis follows the work of previous research conducted in this field (Hu et al., 2019, 2023; Jung & Schindler, 2023) and the land cover data is retrieved from the CORINE Land Cover (CLC) inventory (Copernicus, 2023). The resulting available area is transformed into potential installed capacity through the use of specific array spacing. Further detailed methodology for the spatial analysis and suitable area allocation can be found in Appendix A.

Offshore wind installations are allocated to the provinces with which they have connections to generate their generated power. Therefore, this allocation is targeted at the provinces of Groningen, Noord-Holland, Zuid-Holland, and Zeeland. This method is preferred over simply dividing the energy output across provinces evenly due to the distance of transmission being a limiting factor for efficient power consumption.

2.3 Wind energy conversion

The input data is used in the conversion of wind energy to establish capacity factors for wind energy for each grid cell at each timestep. For onshore wind, it is uncertain what type of wind turbines are installed in the grid cells located in the provinces. Therefore, it is assumed that the most suitable wind turbine is installed relative to the average wind speed at that location. The wind turbine classification based on these wind speeds is derived from guidelines by the International Electrotechnical Commission (IEC),

based on this classification three industry-standard wind turbine models are chosen and their specifications are given along with the classifications in Table 4 (Quarton, 2005). Specifications for the wind turbine models are retrieved from Wind-turbine-models (2023a, 2023b, 2023c).

Table 4: Wind turbine classification and model specifications based on average wind speed (Quarton, 2005 & Wind-turbine-models.com 2023a, 2023b, 2023c).

Wind turbine classification according to average wind speed	Usage	Representative commercial turbine module	Rated capacity (MW)	Rotor diameter (m)	Specific power (W/m)	Cut-in speed (m/s)	Rated speed (m/s)	Cut-off speed (m/s)
Class I: 8.5-10 m/s	Onshore	Vestas 105-3.3	3.3	105	381.8	3	13	25
Class II: 7.5-8.5 m/s	Onshore	Vestas 117-3.3	3.3	117	306.9	3	13	25
Class III: 0 - 7.5 m/s	Onshore	Vestas 126-3.3	3.3	126	264.7	3	12	22.5

For offshore wind, no assumption is made for classification on the basis of average wind speed. Floating offshore wind turbines are not considered, as the spatial analysis resulted in no suitable installable area for this type of wind turbine. Since the turbine types per installation are known, each offshore wind farm is assigned its own turbine type and consequently that turbine type's respective specifications. This allows for more accurate calculation in the energy conversion step. The calculation for the capacity factor (CF) of wind power is as seen in (1).

$$CF = \frac{0.5 C_p \rho A v^3}{P_{rated}} \quad (1)$$

Where C_p is the power coefficient of the turbine, ρ the density of air, A the air flow area, v the wind speed and P_{rated} the rates capacity of the turbine. The power coefficient of the turbine is derived from their power curve, which is dependent on technical characteristics. These characteristics are specific to a particular turbine type. To illustrate the power curve of one of the turbine types considered in this study, Figure 3 presents the power curve of a Vestas 164 – 9.5 MW offshore turbine from the Borssele III – V wind farms (The Wind Power: Wind Energy Market Intelligence, 2023). From the figure it can be seen that the output of the turbine is maximum from windspeeds of 14 m/s to 25 m/s, after which the cut-off rate is reached, and power output drops to zero. The power curve of all onshore and offshore wind turbine types is presented in Appendix B.

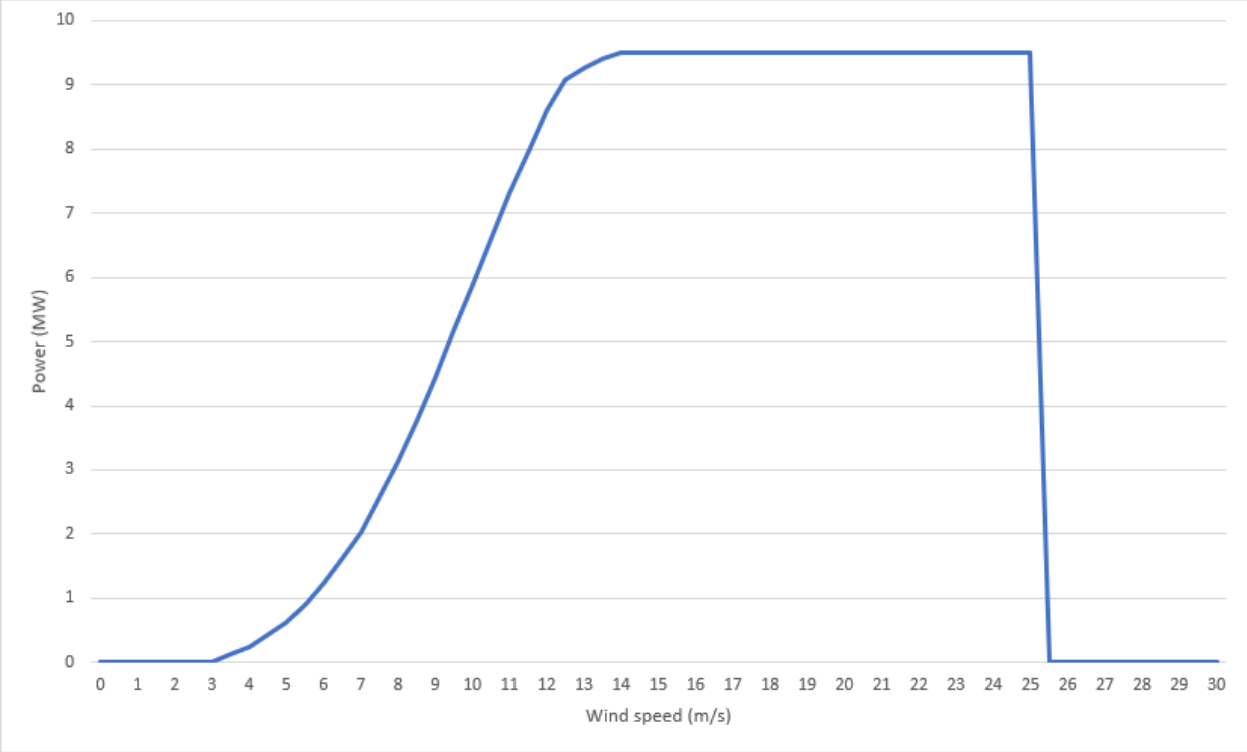

Figure 3: Power curve of the Vestas V164 - 9.5 MW offshore turbine used in the Borssele III - V wind farms

Several adjustments are made to correct for technical and environmental factors that influence power production. These adjustments follow the work of Hu et al., in which the authors consider similar steps to perform the energy conversion more accurately (2019).

The first correction is made for the difference between wind speed values retrieved from the ERA5 (or GES-MERRA-2) data and the wind speed values at the respective turbine heights, these differ due to differences in air density, behavior of modern pitch-regulated turbines, and other adjustment components (Ryu et al., 2022 & Eurek et al., 2017).

The second correction is made with regard to the difference between power production from a singular turbine compared to aggregated wind turbine power output. The power output for a cluster of turbines differs from singular turbines through a spatial smoothing effect. The extent of this effect depends on the maximum and minimum distance between the wind turbines, as well as other spatial parameters. To correct for the smoothing effect of such aggregated wind turbine power output, a Gaussian filter is applied to the single-turbine power curve (Beurskens & Brand, 2012).

Finally, other efficiency losses for the energy conversion are considered. The efficiency losses are categorized into two parts. The first part considers wake losses as a result of reduced wind power availability for downstream wind turbines. These wake losses are incorporated using a dataset compiled through a study that measured wake losses in a large observed set of wind turbines (Windpowerlib, 2023). The second part considers other losses (mechanical, electrical) and is attributed a fixed 5% efficiency loss value.

2.4 Solar energy conversion

The general approach for solar energy conversion involves converting weather data (solar irradiation) to energy production. Similar to wind energy conversion, this follows steps made in the work by (Hu et al., 2023). The panel tilt angle is determined to be the most optimal angle for utility PV, and a uniform pitch angle of 35 ° is assumed.

The total irradiance received by the PV panel is calculated as seen in (2) - (6).

$$I_p = I_{dir,p} + I_{dif,p} + I_{r,p} \quad (2)$$

$$I_{dir,p} = \frac{I_{dir,h}\cos(\theta)}{cos\,(90-\alpha)} \quad (3)$$

$$cos(\theta) = sin(\alpha)cos(\beta) + cos(\alpha)sin(\beta)cos(Z_p - Z_s) \quad (4)$$

$$I_{dif,p} = \frac{1+cos\beta}{2} I_{dif,h} \quad (5)$$

$$I_{r,p} = \frac{1-cos\beta}{2}(I_{dir,h} + I_{dif,h})Alb \quad (6)$$

Where β is the panel tilt angle, Z_p is the azimuth angle, θ is the incidence angle, Alb is the surface albedo, $I_{dif,h}$ and $I_{dir,h}$ are respectively the diffuse and direct components of hourly irradiation. To account for the decrease in performance of PV panels as a result of temperature fluctuation, corrections are made. The hourly CF of solar energy can be determined as seen in (7) - (9).

$$CF = \left(\frac{I_p}{I_{STC}}\right)[1-\delta(T_{NOCT} - T_{cell})]PR \quad (7)$$

$$T_{cell,t} = T_{modback}\left(\frac{I_p}{I_{STC}}\right)\Delta T_{cond} \quad (8)$$

$$T_{modback} = I_p exp^{(a+b*v_{2m})} + T \quad (9)$$

Where I_{STC} is solar irradiance at standard test conditions (1000 W/ m^2), PR is a performance ratio, T_{cell} and T_{NOCT} (44°C) are respectively cell operating temperature and nominal operating cell temperature, δ is the power temperature coefficient, $T_{modback}$ is the PV module back temperature, v_{2m} is the wind speed at 2 m height, T is the ambient temperature, a, b and ΔT_{cond} are respectively the empirical convection coefficient, the heat transfer coefficient, and the temperature drop due to conduction.

Following this procedure, the CF values for wind and solar are determined per grid cell in hourly timesteps for the entire time period. The input of ERA5 reanalysis data is bias adjusted, whereas the input of the MERRA data is not. In general, the ERA-5 data contains less bias, higher correlation, and better diurnal variability (Jourdier, 2020). Therefore, the outcome for the MERRA is adjusted to the mean ERA5 outcome for every grid cell. This adjusted MERRA data is used along with ERA-5 data to serve as input for the characterization of ED events.

2.5 Simple energy drought events

Based on the literature review results in Table 1, ED events are classified in this study as periods of exceptionally low amounts of energy production from VRE sources. Specifically, such events are considered as periods of time where for a minimum of five hours the capacity factors for solar or wind are consistently below 10%. This threshold has been established due to the characteristic of grid-scale battery energy storage systems (BESS) being able to generally provide reliable capacity at peak demand for a maximum of four hours (Bowen et al., 2019; Yang et al., 2013). ED events lasting less than four hours are therefore less impactful if such storage systems are implemented in the energy system. Furthermore, these thresholds are chosen in line with similar research on this topic and provide frequent ED events for the selected time period. Therefore, the minimum duration of 5 hours is applied consistently throughout the rest of the study unless mentioned otherwise, for example when considering ED events based on daily average CF values. The CF threshold value of 10% is applied unless stated otherwise, for example when considering ED events based on 5% or 2% CF thresholds.

The frequency is characterized by the number of events that occur in the provided timeframe. An analysis can additionally be made to see for what time of the year the highest and lowest frequency of ED events occur. Seasonal trends are investigated where possible, as well as interannual trends such as the co-occurrence with solar cycles. The duration of the ED events is considered to be the total time period in which the threshold values are exceeded. The event duration is measured in hours. Similarly, the mean and maximum values of the duration of ED events per region are provided. Regions that are considered are provinces, collections of provinces and the Netherlands in its entirety. In addition to solar EDs, adjusted solar EDs are also provided. These consider EDs based on all time periods in which the solar altitude angle is above 0, indicating the possibility of sunlight generating power. This category is added to observe the solar ED trends without including night times and observing the difference between the overall solar ED characteristics.

2.6 Compounding energy droughts: technological and spatial

For technological compound events, two methods are used for their characterization. The first method is to establish a weighted mean capacity factor that combines solar and wind technologies and to consider this value if it is below the established threshold. The second option is based on strictly considering moments in time where both solar and wind are below the threshold proposed previously. Rather than taking a weighted mean capacity factor, this method likely results in less frequent events however provides different information. As it considers the co-occurrence of minimal production by both sources, these events could describe an extreme event where both technologies are significantly underperforming. In contrast, the approach that takes the weighted mean capacity factor is more dependent on the influence of the technology with the highest share of overall installed capacity.

The co-occurrence of ED events can be determined through the use of copulas. Due to possible nonlinear dependencies, these dependence structures cannot be described by common calculation tools such as Kendall's tau or Spearman's rho (Ida et al., 2014). However, copulas are able to describe such dependence relations. Specifically, copulas are useful tools to capture the tail dependencies of variables. Since ED events are situated in the tail of CF distributions, copulas are a useful tool to employ. Copula functions are multivariate distributions and are defined as can be seen in (10) and (11).

$$C : [0,1]^n \rightarrow [0,1] \tag{10}$$

$$C(u_1, u_2, \dots, u_n) = P(U_1 \leq u_1, U_2 \leq u_2, \dots, U_n \leq u_n) \tag{11}$$

Where marginalizing gives $U_i \sim Uniform(0,1)$ (Tedesco et al., 2022). As described by Otero et al., the joint cumulative distribution function of two variables X and Y can be given as seen in (12), where the marginal distribution functions of X and Y are presented by (13) and (14) respectively.

$$F_X Y\ (x, y) = P(X \leq x, Y \leq y) = C(F_X(x), F_Y(y)) \tag{12}$$

$$F_X(x) = P(X \leq x) \tag{13}$$

$$F_Y(y) = P(Y \leq y) \tag{14}$$

The variables X and Y represent the capacity factors of the two technologies considered, solar and wind. Unlike the analysis for simple EDs and extreme ED events, the copula analysis considers the format of CF for both wind and solar PV as being measured in days rather than hours. To this purpose, the mean daily value is calculated based on the available hours. This allows the continuity requirement for working with copula functions to be upheld by eliminating zero returns, for instance for solar PV during the night, by ensuring synchronicity of ED events with similar durations. Additionally, it has been found that inter-temporal cross-correlation (or lagged correlation) is eliminated when switching from hourly to daily data frequency (Grothe & Schnieders, 2011). This technique of assessing co-occurrence is similarly applied to spatial compounding ED events. To characterize this type of compounding event, the Netherlands is divided into two regions.

The liberalized electricity market in EU countries is designed around zonal pricing (Klopčič et al., 2022). The appropriateness of the size of the bidding zone is partly determined by the share of VRE sources in its power generation, as its intermittent nature complicates scheduling (Pototschnig, 2020). The configuration of the Dutch electricity market is currently described by a single bidding zone (TenneT, 2022a). However, as a result of structural congestion, the European Union Agency for the Cooperation of Energy Regulators (ACER) has instructed the TSO of the Dutch power system (TenneT) to investigate alternative bidding zone configurations (TenneT, 2022a). The proposed alternative configuration is two bidding zones that split the Netherlands and can be found in Figure 4. The dots in the figure represent network elements, which are allocated between the N1 and N2 regions. Based on a case study that includes the Netherlands, an increase in the number of bidding zones could lead to improved zonal market outcomes (van den Bergh et al., 2016).

To investigate spatial compounding ED events, the N1 and N2 zones are taken to assess co-occurrence of events. Similar to technological compounding, this is done through working with the previously described copula functions. A similar approach has been taken by Otero et al. to describe the co-occurrence of EDs between regions at the country level (2022).

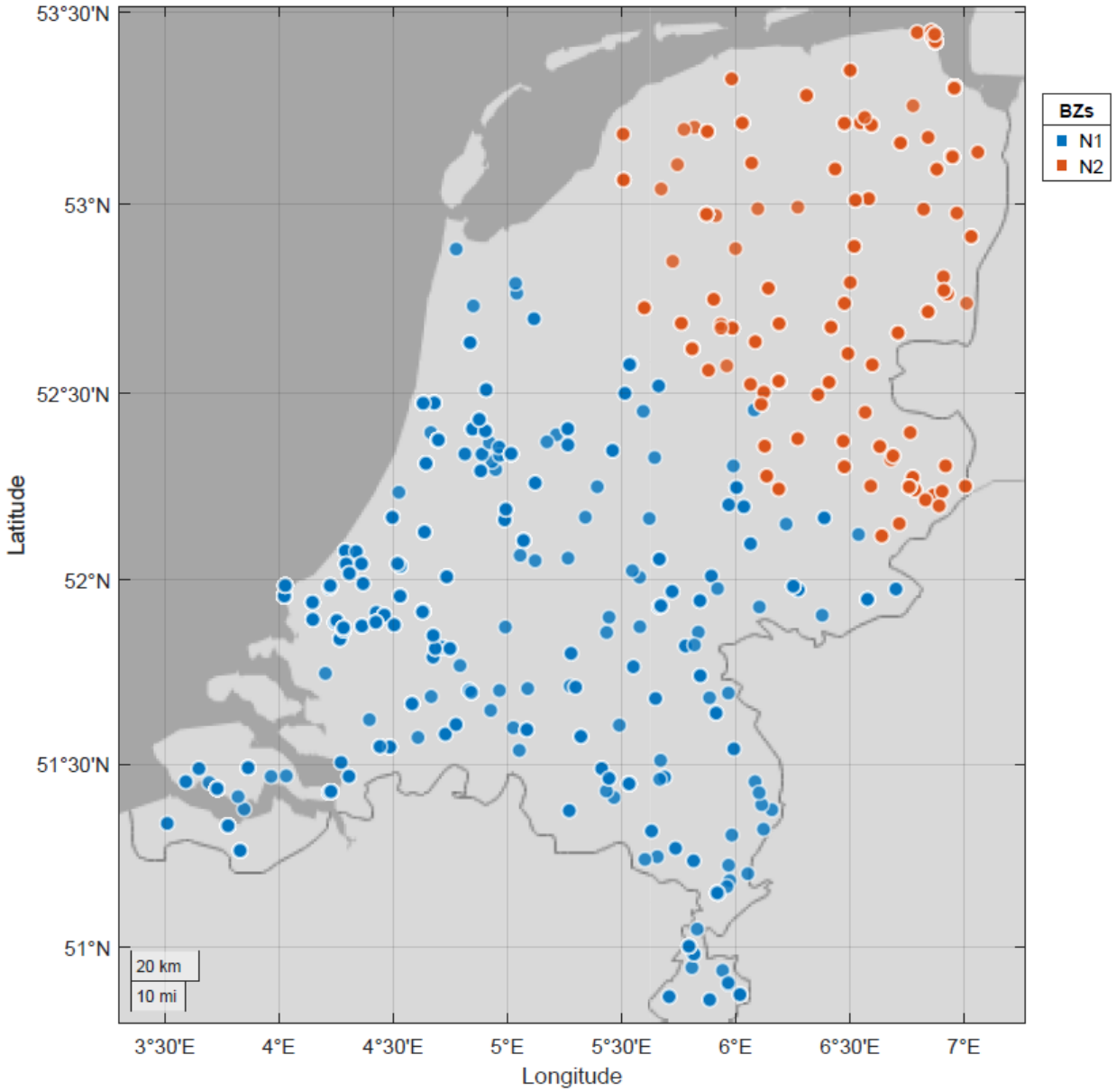

Figure 4: Proposed alternative configuration of bidding zones in the Netherlands (TenneT, 2022)

2.7 Extreme energy droughts

The final sub-question of this research considers the extremes of the temporal aspect of ED events. Specifically, it investigates the extreme event distribution of ED event occurrences in the entire timeframe for the Netherlands. Extreme value theory (EVT) is used in numerous fields of research such as finance (Gilli & Këllezi, 2006), meteorology (Osei et al., 2021), and engineering (Rinaldi et al., 2007) to assess risk. Similarly extreme ED events and their associated duration can be estimated for certain return periods.

The selection of extreme ED events in the dataset is performed using the Peak-Over-Threshold (POT) method. This method selects all events with durations lasting longer than the established threshold value (Mararakanye et al., 2022), which are subsequently fitted according to a distribution. In the field of EVT, two classes of distributions are considered. These classes are the generalized extreme value (GEV) distributions (Fréchet, Weibull, Gumbel) and the generalized Pareto (GP) distributions (Pareto, exponential, uniform) (Bali, 2003). The latter is more suitable for the POT approach (Pickands III, 1975) and is therefore used for fitting. The threshold for the POT approach is established following the methodology of Thompson et al. (2009), in which extreme wave height was analyzed. The authors developed an automatic threshold selection method that can be applied in this research, where the main criteria applied is statistical significance through p-value assessment. This method was developed to increase the accuracy of return level estimates of extreme events and improves the validity of found results for this study compared to alternative (mostly arbitrary) methods of threshold selection. The *extRemes* R package (Gilleland & Katz, 2016) is used to analyze the datasets containing extreme events.

The distribution of the duration of ED events has been found to be characterized by a thick right-tail in some instances, as the shape parameter $\xi > 1$, even without considering an upper threshold. Consequently, the conventional methodology for fitting this distribution might not be adequate for estimating the mean, variance, or risk of extreme ED events (Hain et al., 2023). With a shape parameter value above one, the tail may not converge to a finite value. To correct for this, the study by Cirillo & Taleb (2016) proposed a new methodology for these instances to be more accurately described. This is done by introducing an upper bound value for the range of ED durations and then transforming the bounded distribution into a shadow variable *Z* as shown in equation (15). The upper threshold for this research has been set at 150% of the highest recorded empirical value of the respective dataset that this method has been applied to.

$$Z = \phi(Y) = L - H \log\left(\frac{H - Y}{H - L}\right) \quad (15)$$

Where *Y* is the original distribution, *Z* is the shadow variable, *L* is the lower bound, and *H* is the upper bound. The upper tail of Z can now be characterized, specifically the tail parameters such as shape and scale. These parameters can be used to return to Y and assess its properties. The mean of the readjusted Y is given by equation (16).

$$E[Y|Y \geq L] = (H - L)\, e^{\frac{\sigma}{H\xi}} \left(\frac{\sigma}{H\xi}\right)^{\left(\frac{1}{\xi}\right)} \Gamma\left(\frac{\xi - 1}{\xi}, \frac{\sigma}{H\xi}\right) + L \quad (16)$$

Where ξ is the shape parameter, σ is the scale parameter, and Γ is the incomplete gamma function. The R package *pracma* (Borchers & Borchers, 2022) is used to calculate the incomplete gamma function. Finally,

the value-at-risk (VaR) and conditional value-at-risk (CVaR) of the readjusted Y can be computed as described in equations (17) and (18).

$$VaR_p = e^{-\frac{\sigma\,(1-p)^{-\xi}}{H\xi}}\,(L\,e^{\frac{\sigma}{H\xi}} - H\;e^{\frac{\sigma}{H\xi}} + H\;e^{\frac{\sigma(1-p)^{-\xi}}{H\xi}}) \quad (17)$$

$$CVaR_p = VaR_p + (H-L)\,e^{\frac{\sigma}{H\xi}}\left(\frac{\sigma - H\xi\,log\left(\frac{H-VaR_p^*}{H-L}\right)}{H\xi}\right)^{\left(\frac{1}{\xi}\right)}\Gamma\left(\frac{\xi-1}{\xi}, \frac{\sigma}{H\xi} - log\left(\frac{H-VaR_p^*}{H-L}\right)\right) \quad (18)$$

Where *p* is the probability of the VaR and CVaR, and VaR_p^* is estimated as described in equation (19).

$$VaR_p^* = VaR_p - \frac{\sigma}{\xi}\left(1 - \frac{n_u}{n}\right) \quad (19)$$

Where n is the number of events in the original distribution, and n_u is the number of events crossing the threshold determined in the POT threshold selection.

VaR and CVaR are commonly used in the field of finance as valuable tools for risk management. Where the VaR is a percentile of a loss distribution, and the CVaR approximates the average loss under worst-case scenarios (Sarykalin et al., 2008). These worst-case scenarios are contextually described as losses that exceed the previously mentioned VaR value. This principle is presented in an example ED duration distribution in Figure 5. The VaR and CVaR are calculated as their definition states, unless otherwise specified. Additionally, once in 50-year and once in 100-year extreme ED event durations are presented as a method of assessing return periods.

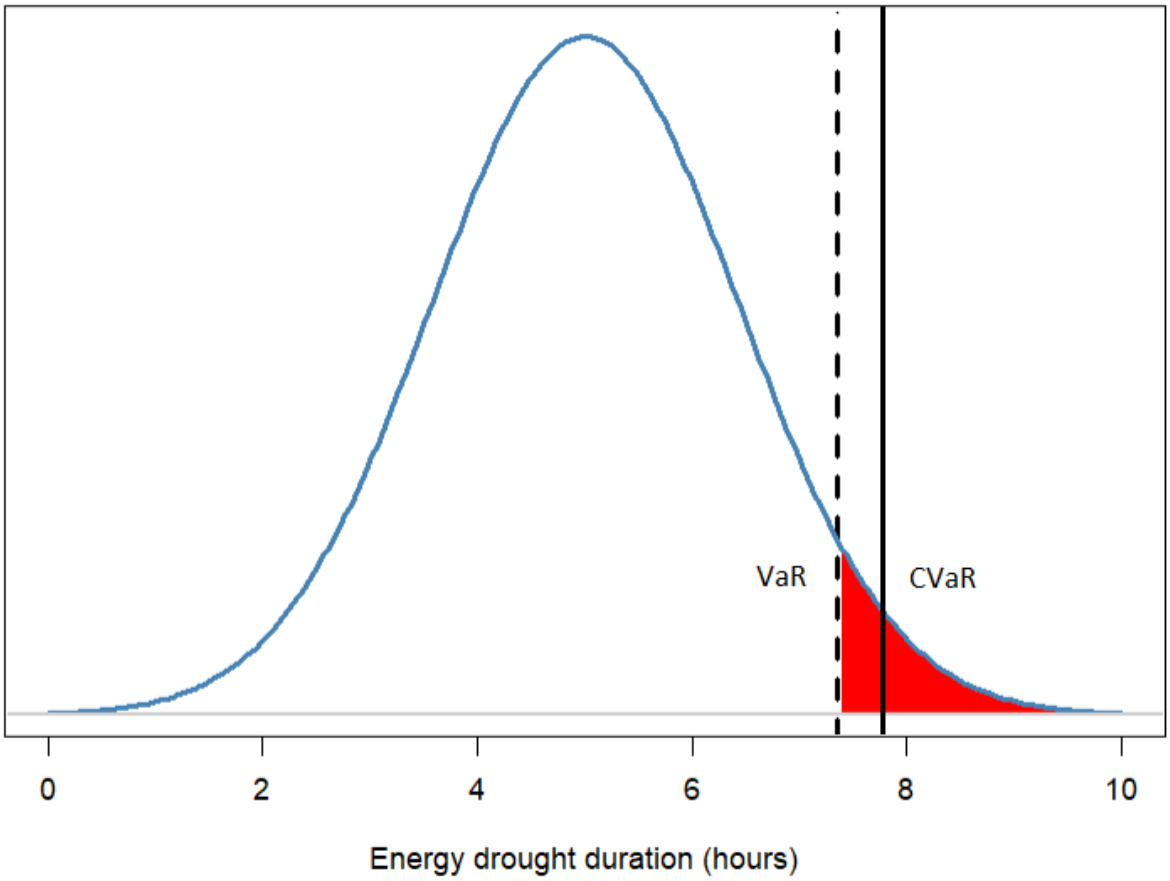

Figure 5: Example distribution of ED durations

As can be seen from the figure, there is a dashed line that indicates a threshold, in this case a percentile, value of the example distribution. Any value found to be higher than this threshold value is marked in red. The VaR value can be considered as the value where the dashed line is positioned, whereas the CVaR is the expected value once this threshold value has been exceeded. The CVaR is represented by the value corresponding to the solid line. The CVaR value is also considered to be ES value. Since the EVA of this research considers the longest found ED durations through the POT method, the VaR and CVaR are considered to be adequate risk assessment tools to analyze the most extreme ED durations.

3: Results

3.1 Spatial analysis

As is outlined in Appendix A, the spatial analysis was performed on the Netherlands to retrieve potential area suitable for solar panel and wind turbine installation per grid cell. The grid cells are sized similar to the retrieved data from the ERA-5 and MERRA database. The result of the spatial analysis can be found in Figure 6.

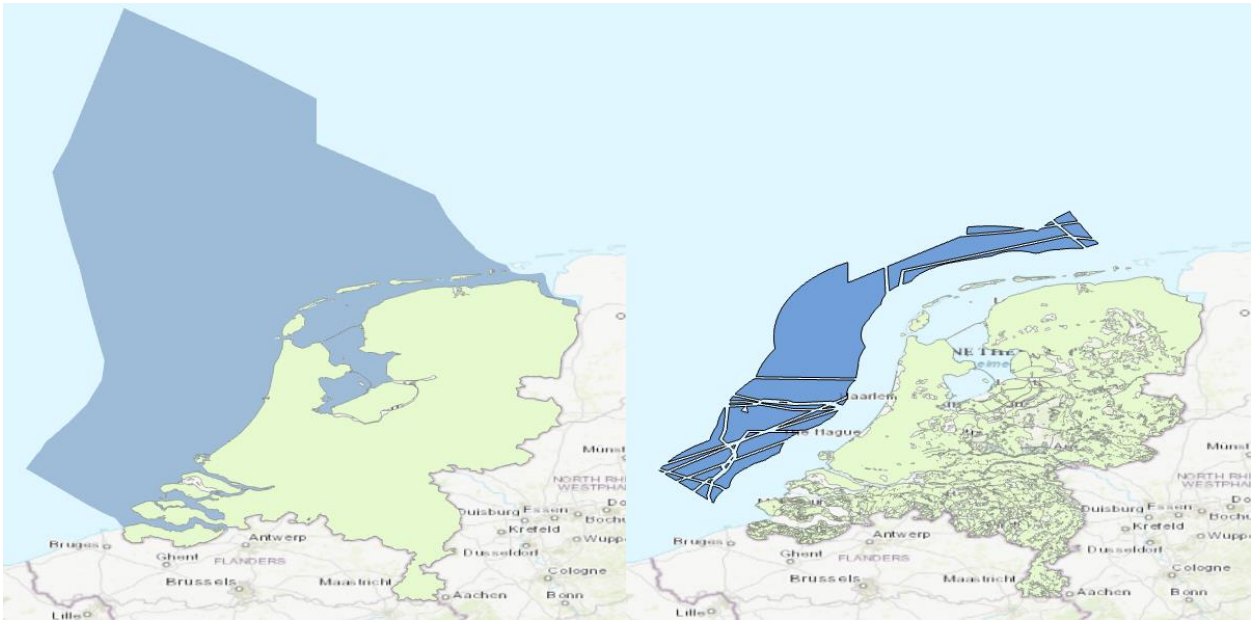

Figure 6: Spatial extent of Dutch offshore and onshore area (left) and available area for installing VRE capacity (right).

The results of the spatial analysis are used to determine the potential installed capacity per grid cell. As is outlined in Appendix A, the specific array-spacing used for assessing potential installed capacity for wind is an area of six times the rotor diameter in length and width. This spacing considers the most suitable wind turbine type per grid cell, or offshore where applicable. For the solar PV spacing, the calculated shadow factor to prevent self-shading is established per grid cell. While this value varies per grid cell, on average the required area is increased with a factor of 1.4 compared to the surface area of the PV unit. The potential installed capacity for wind is presented in Figure 7.

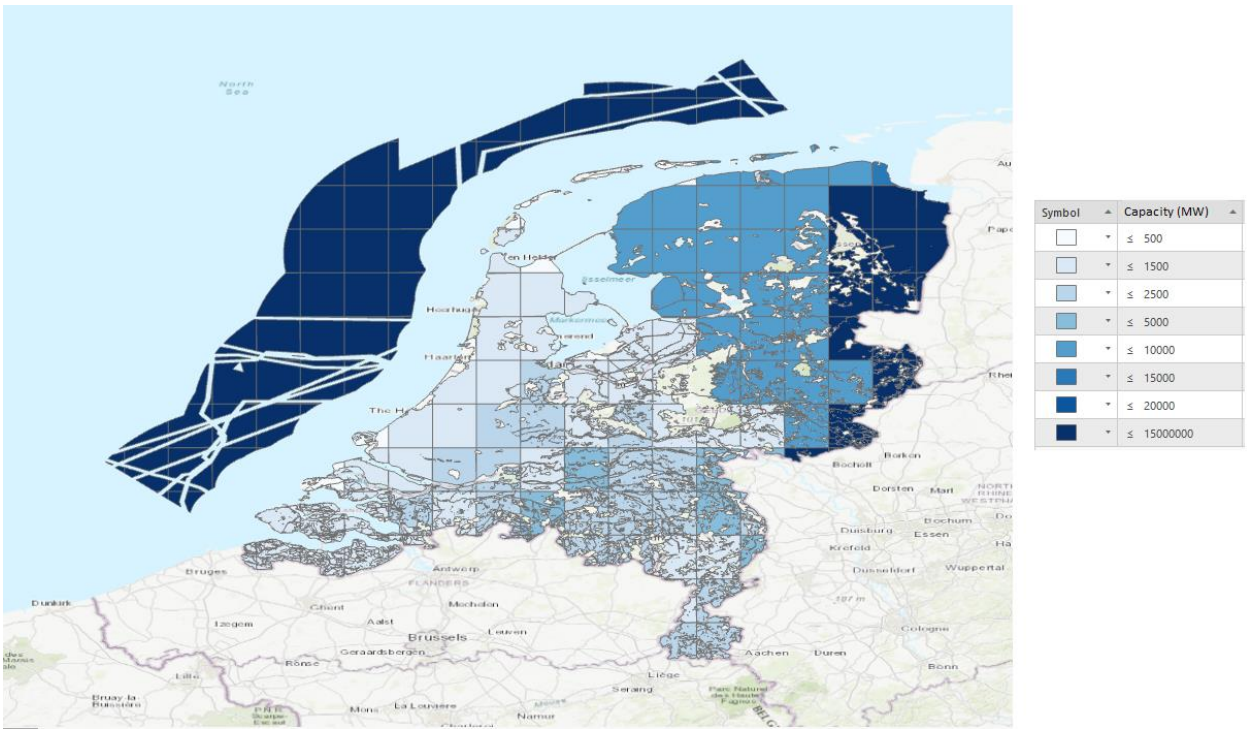

Figure 7: Potential installed capacity for wind onshore and offshore per grid cell

It should be mentioned that the high upper limit for the installed capacity of wind in the legend is established based on the highest amount of installable wind capacity in the offshore region, which amounts to roughly 14 TW. This is in stark contrast to the maximum installable wind capacity for the onshore region, which is roughly 4 Gigawatt (GW) per grid cell. From the onshore region it can be observed that generally the installable capacity per grid cell is highest in the north-eastern section of the country, in the provinces of Groningen, Drenthe and Overijssel. Within these provinces, the highest value per grid cell is consistently found near the border with Germany. In contrast, relatively low values for installable capacity are observed in the 'Randstad' region, which is characterized by its high urban density and roughly comprises the regions of Noord-Holland, Zuid-Holland and Utrecht (Mashhoodi, 2018).

As was mentioned previously, the offshore region outperforms any onshore region with regard to installable wind capacity. The offshore wind area, and therefore capacity, is mainly restricted by distance to port. This suitability factor prevents any installable potential for floating offshore wind. Without this limitation, small amounts of installable potential are found near the Western section of the EEZ, in the relative vicinity of English waters.

The potential installed capacity for solar PV is presented in Figure 8.

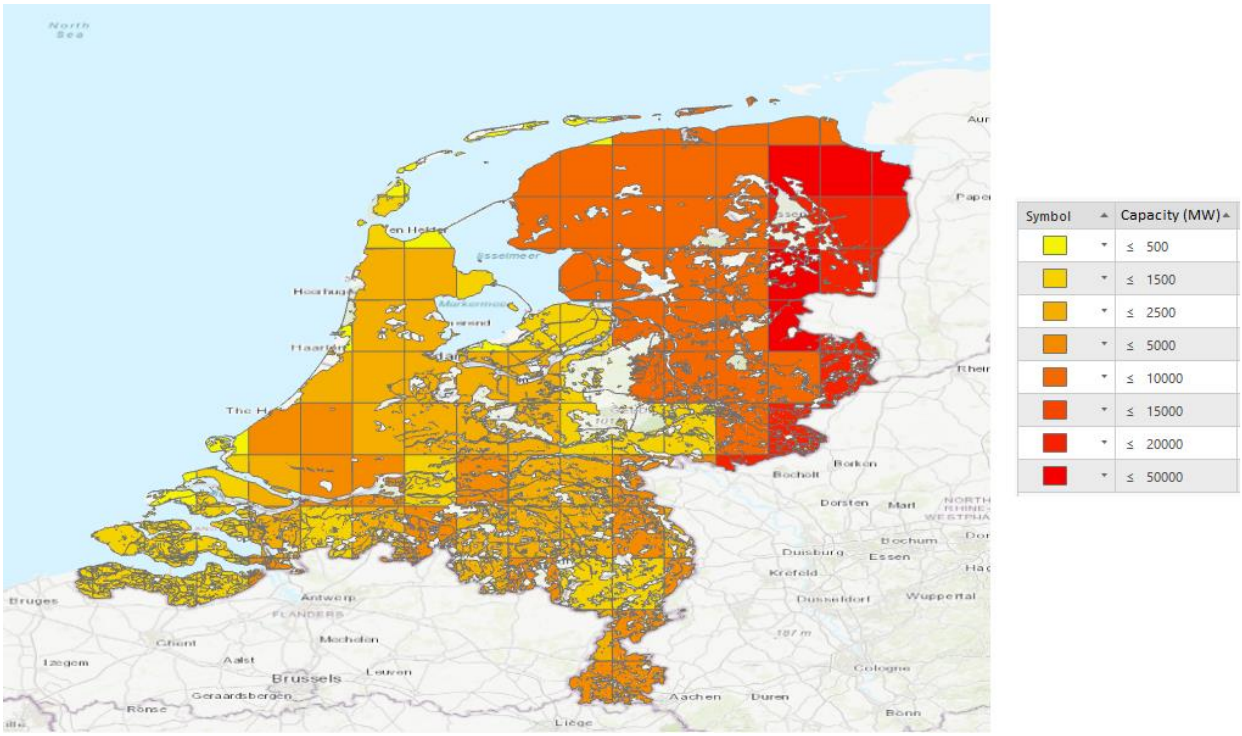

Figure 8: Potential installed capacity for solar PV per grid cell

Similar to the results for installed potential capacity for the wind technology, a trend that can be observed is relatively high potential in the north-eastern section of the country. This area contains the provinces of Groningen, Drenthe and Overijssel, and similar to the wind technology assessment, values are highest along the border with Germany. This is due to similar geographic constraints and suitability assessment for the observed land covers. A noticeable difference is observed in the 'Randstad' region, where unlike wind technology, relatively high potential is observed. This is most likely the result of the urbanized areas in this region, as this land cover type is suitable for solar PV installation. The maximum amount of installable capacity per grid cell is roughly 47 GW.

3.2 Wind conversion

The results for the wind conversion based on ERA-5 data is presented in Figure 9.

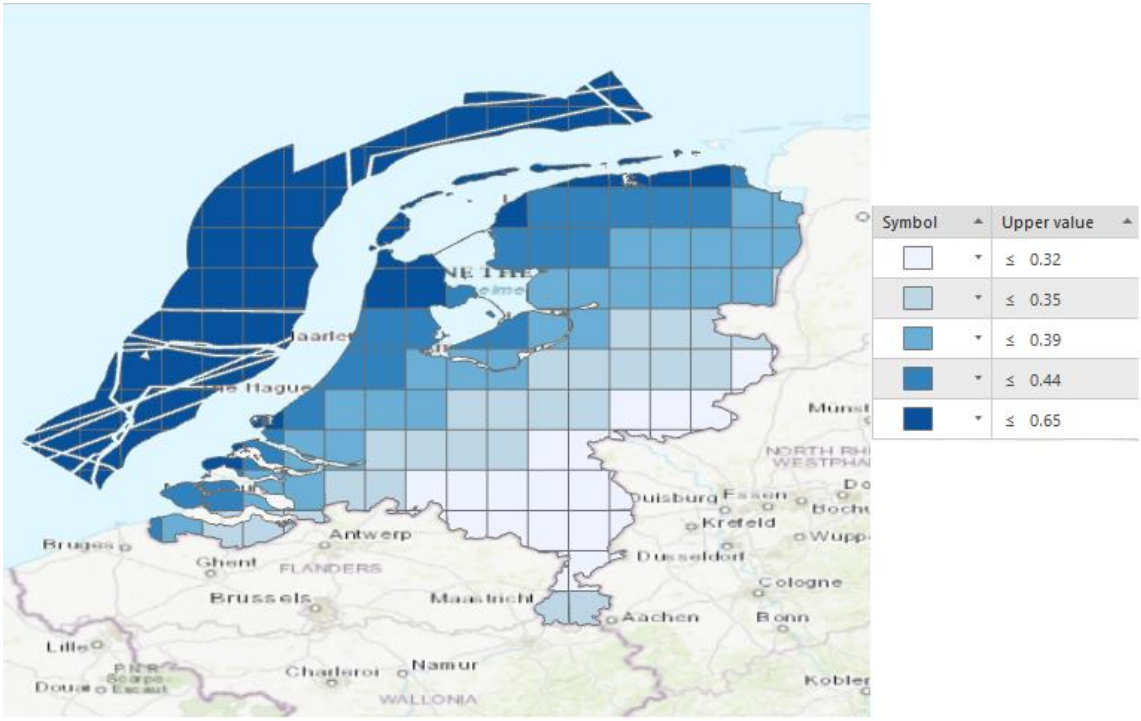

Figure 9: Onshore and offshore mean wind CF values per grid cell based on ERA-5 data

The results for the wind conversion based on MERRA data is presented in Figure 10.

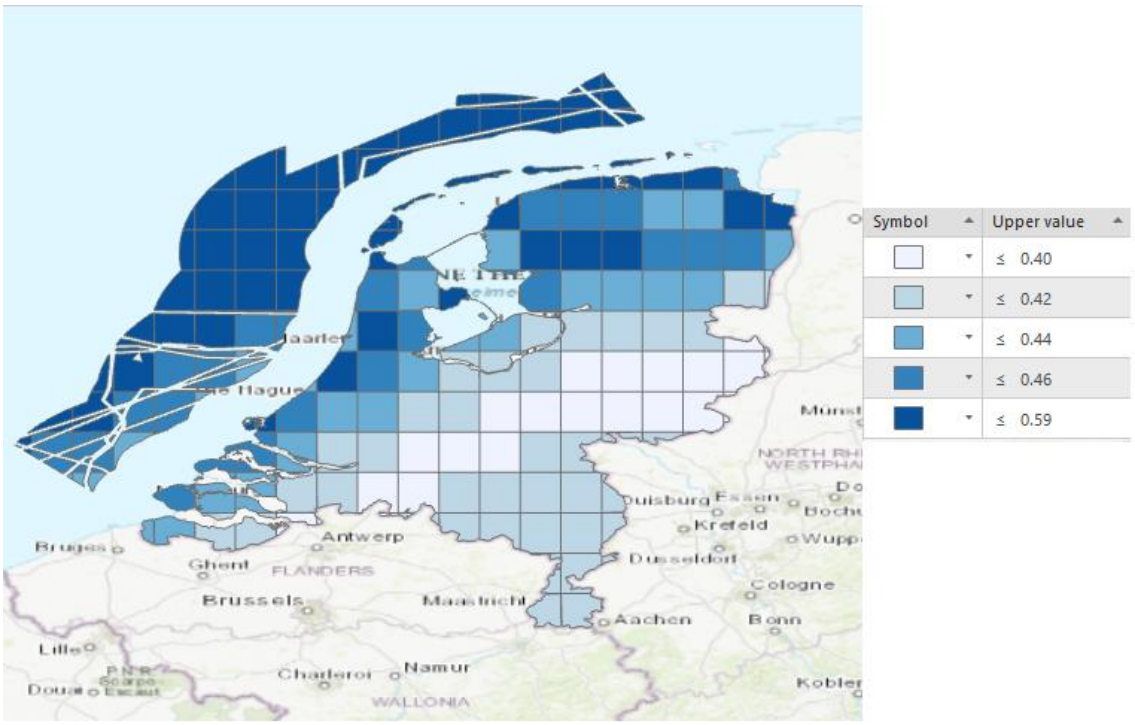

Figure 10: Onshore and offshore mean wind CF values per grid cell based on MERRA data

For the ERA-5 data conversion, the modelled performance of onshore wind reflects values that have been observed by Nortier et al. (2022). In this study, estimated onshore performance of wind turbines ranges between 0.1 and 0.45. Additionally, the modelled performance of offshore wind is in line with literature, which estimates a mean regional offshore wind capacity factor of 58% for the Netherlands (Bosch et al., 2018). The spatial distribution of mean CF values follows a pattern of decreasing performance moving land inwards. This closely resembles the pattern for mean wind speed values in this area (Stepek & Wijnant, 2011) which is an indicator of wind turbine performance, and therefore mean CF values.

For the MERRA data conversion, the modelled performance of onshore wind shows higher mean CF values when compared with the ERA-5 data conversion. It seems that even with bias adjustment, the MERRA data conversion generates CF values that are slightly higher than described in literature (Bosch et al., 2018; Nortier et al., 2022). Similar to ERA-5 data conversion, offshore wind is characterized by higher mean CF values than onshore wind. However, the trend of decreasing CF values when moving land inward is less noticeable for MERRA results.

3.3 Solar conversion

The results for the solar conversion based on ERA-5 data is presented in Figure 11.

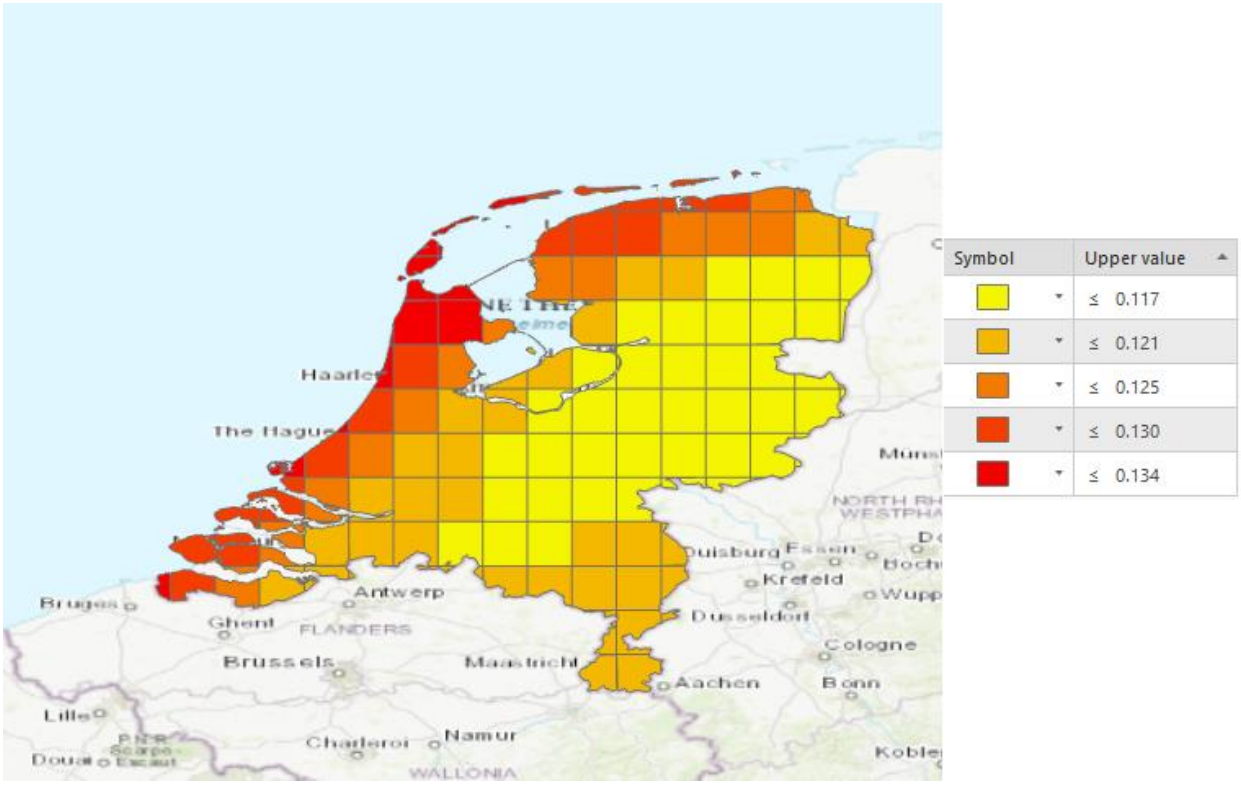

Figure 11: Solar mean CF value per grid cell based on ERA-5 data solar conversion

The results for the solar conversion based on MERRA data is presented in Figure 12.

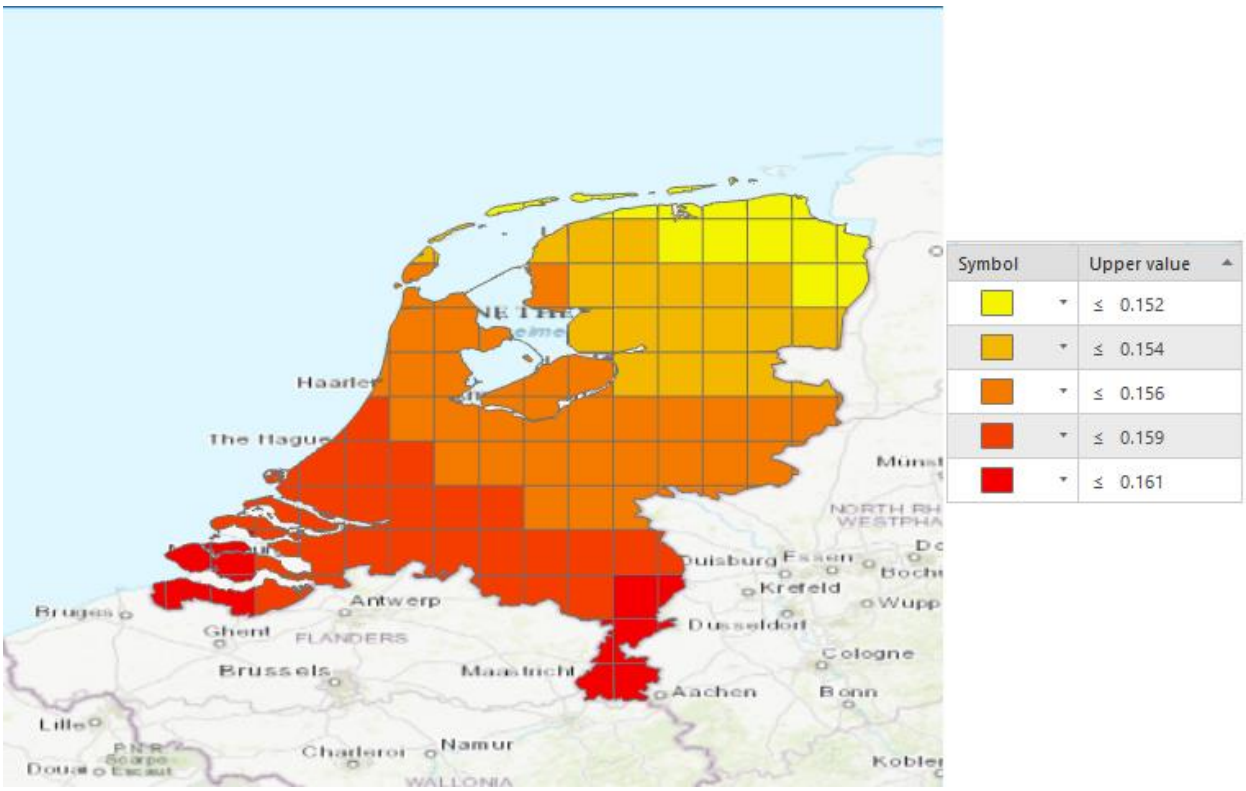

Figure 12: Solar mean CF value per grid cell based on MERRA data solar conversion

The availability of studies presenting observed mean capacity factors of solar PV for the Netherlands is limited. However, for the ERA-5 data conversion, the modelled performance of solar PV reflects the results found in other studies modelling Dutch or European mean solar PV capacity factors. The values presented in these studies estimate a mean from 0.13-0.14 (Zappa & Van Den Broek, 2018) to roughly 0.20 (Moraes Jr et al., 2018). However, it must be stated that for the higher values in the range of 0.20, these are determined by analyzing only summer months. Additionally, the distribution of performance for the grid cells from high to low CF closely follows the pattern for solar irradiance amounts in the Netherlands (SOLARGIS, 2020).

For the MERRA data conversion, the modelled performance of solar PV similarly reflects the estimates found in simulations from other studies (Moraes Jr et al., 2018; Zappa & Van Den Broek, 2018). Similar to the wind conversion results, the MERRA results present higher mean CF values than the ERA-5 results. Finally, the spatial trend is slightly different from the trend found for the ERA-5 results. The MERRA results follow a trend in which the southernly located grid cells result in higher mean CF values than the northernly located grid cells.

The difference between the results using the ERA-5 and MERRA datasets is considerable for both solar PV and wind. Previous research has shown that ERA-5 data outperforms MERRA data in accuracy for wind power simulation (K. Gruber et al., 2022). Additionally, it has been shown that ERA-5 data outperforms MERRA data in terms of solar irradiation estimation under cloudy-sky conditions (Amjad et al., 2021). Taking this into account, the results from ERA-5 data conversion seem to depict mean wind and solar PV CF values better than the results from MERRA data conversion. As is stated in the methodology section of

the report, the MERRA results are bias adjusted to resemble the ERA-5 results more closely, and used in the next section of this study which is the characterization of ED events.

3.4 Energy drought characterization

For ERA-5 ED characterization, the number of yearly ED events for solar PV, adjusted solar PV, onshore wind and the combination of solar PV and onshore wind is presented in Table 5. Overall, the technology with the least amount of ED events is onshore wind. The adjustment of solar PV on average results in a decrease of ED events by 20.6%, yet still results in more events than onshore wind and for some provinces, the combination of solar PV and onshore wind. The large discrepancy between ED events based on the combination of solar PV and onshore wind for the difference provinces is most likely the result of the various configurations of installed capacity per technology for each province. The provinces of Gelderland, Limburg, Noord-Brabant, Overijssel and Utrecht show a high amount of ED events even with solar PV and onshore wind combined. These provinces share the same trait of having proportionally high amounts of solar PV installed capacity as part of the share of this VRE land combination and are therefore more influenced by solar PV performance trends.

Table 5: Number of yearly ED events for solar PV, solar PV adjusted, onshore wind and the combination of solar and onshore wind (VRE land combined) as well as offshore wind and all VRE combined from ERA-5 data

Province	Solar PV	Solar PV adjusted	Onshore wind	VRE land combined	Offshore wind	All VRE combined
Drenthe	333	271	119	277	-	277
Flevoland	335	273	115	127	-	127
Fryslân	336	276	100	167	-	167
Gelderland	336	267	133	349	-	349
Groningen	334	274	111	182	46	105
Limburg	338	259	137	346	-	346
Noord-Brabant	338	258	132	353	-	353
Noord-Holland	339	270	98	180	45	146
Overijssel	334	268	127	342	-	342
Utrecht	337	267	125	343	-	343
Zeeland	340	258	121	165	53	68
Zuid-Holland	339	265	120	249	47	208
Mean	336.6	267.2	119.8	256.7	47.75	235.9

For ERA-5 ED characterization, the mean, maximum and standard deviation of the ED events per province is presented in Table 6. The maximum duration is on average 10.7 times as high as the mean duration. The province with the lowest mean ED duration is Flevoland, however Noord-Holland has a significantly lower maximum ED duration as well as the lowest standard deviation of the ED durations. The provinces with the highest mean ED duration are Overijssel and Utrecht, with both provinces additionally having ED events lasting for over 200 hours.

Table 6: Mean, max and standard deviation of the ED duration observed per province from ERA-5 data

Province	Mean ED duration (hours)	Max ED duration (hours)	Standard deviation of ED duration (hours)
Drenthe	14.4	167	6.77
Flevoland	12.3	176	8.21
Fryslân	12.4	126	6.53
Gelderland	18.0	166	7.94
Groningen	11.2	125	5.96
Limburg	18.3	191	8.49
Noord-Brabant	17.4	167	6.81
Noord-Holland	11.8	93	5.68
Overijssel	18.6	215	9.59
Utrecht	18.6	239	9.29
Zeeland	9.85	70	5.44
Zuid-Holland	12.8	119	6.02
Mean	15.1	161.8	7.50

In addition to solar PV and onshore wind, offshore wind is considered as a separate category for ED events. For ERA-5 ED characterization, the model results depict 24 ED events per year for offshore wind. This value is significantly lower than solar PV and onshore wind. The maximum duration of an ED event for offshore wind is 55 hours. Similarly, this value is significantly lower than results for solar PV and onshore wind. The mean value for ED events is 9.72 hours, with the standard deviation being 5.86 hours.

For MERRA ED-characterization, the number of yearly ED events for solar PV, adjusted solar PV, onshore wind and the combination of solar PV and onshore wind is presented in Table 7. The results are similar to the results from the ERA-5 ED characterization with the exception of the adjusted solar PV category. The adjusted solar PV on average has 153.3 yearly ED events for the MERRA data results, whereas for the ERA-5 data this number is 267.2. This difference could be caused by a relatively high energy conversion of solar PV in the MERRA solar conversion compared to ERA-5 solar conversion in the following or leading the filtered 'dark' hours where the solar altitude angle is below 0. Other differences are characterized by lower mean ED duration for onshore wind and VRE land combined.

Table 7: Number of yearly ED events for solar PV, solar PV adjusted, onshore wind and the combination of solar and onshore wind (VRE land combined) from MERRA data

Province	Solar PV	Solar PV adjusted	Onshore wind	VRE land combined	Offshore wind	All VRE combined
Drenthe	335	160	108	272	-	272
Flevoland	336	160	105	113	-	113
Fryslân	336	160	95	151	-	151
Gelderland	337	154	122	348	-	348
Groningen	334	157	102	162	48	101
Limburg	340	151	127	347	-	347
Noord-Brabant	340	149	123	354	-	354
Noord-Holland	340	148	95	171	48	140
Overijssel	335	156	116	342	-	342
Utrecht	338	155	114	343	-	343
Zeeland	341	144	111	147	56	70
Zuid-Holland	340	146	109	232	52	193
Mean	337.7	153.3	110.6	248.5	51.00	231.2

For MERRA ED characterization, the mean, maximum and standard deviation of the ED events per province is presented in Table 8. As can be seen from the table, comparable results for the mean and standard deviation are presented as observed in the ERA-5 ED characterization, although slightly lower values for the MERRA results. However, the maximum ED duration is significantly shorter for the MERRA ED-characterization than for its ERA-5 counterpart. Generally, the observed difference between ERA-5 and MERRA energy conversion is highest for the solar PV technology. The results from the ERA-5 and MERRA data are similar for onshore and offshore wind.

Table 8: Mean, max and standard deviation of the ED duration observed per province from MERRA data

Province	Mean ED duration (hours)	Max ED duration (hours)	Standard deviation of ED duration (hours)
Drenthe	13.5	108	5.74
Flevoland	11.4	158	7.14
Fryslân	11.7	117	5.35
Gelderland	17.0	119	7.70
Groningen	10.8	93	5.22
Limburg	17.1	118	7.93
Noord-Brabant	16.5	92	6.15
Noord-Holland	11.3	63	4.81
Overijssel	17.5	165	9.25
Utrecht	17.4	118	8.83
Zeeland	9.81	66	4.89
Zuid-Holland	12.0	67	4.95
Mean	14.2	107.3	6.61

Similar to ERA-5, the offshore wind performance for MERRA ED-characterization shows a significantly lower number of events and shorter maximum and mean duration of events than for solar PV, onshore

wind, or its combination. For MERRA ED-characterization, the model depicts 28 ED events per year, with a mean and maximum duration of 10.1 hours and 69 hours respectively. The standard deviation for the duration of these events is 6.36 hours. These values are even lower than for ERA-5 offshore wind, highlighting a relatively high performance of offshore wind.

For the ED characterization of the bidding zones, the two regions are formed to contain different provinces. The N1 region contains the provinces of Flevoland, Gelderland, Limburg, Brabant, Noord-Holland, Utrecht, Zeeland, and Zuid-Holland. In contrast, the N2 region contains the provinces of Drenthe, Friesland, Groningen and Overijssel. Furthermore, all solar and onshore wind capacity from the provinces is allocated to the two different regions. Additionally, for offshore wind, the locations of the different wind farms are taken into consideration. The wind farm to the north of Groningen (Gemini, 600MW) is allocated to the N2 region. All other offshore wind farms are allocated to the N1 region, as they are off the coast of Zeeland, Zuid-Holland, and Noord-Holland.

The yearly number of events, and the mean, maximum and standard deviation of their durations is presented in Table 9. These results are based on hourly timesteps. The yearly number of events is determined by dividing the total occurred ED events by the number of years that span the dataset. As can be seen from the results, the N1 region has a lower number of recorded events, with lower mean and maximum durations as well as lower standard deviation of the durations compared to the N2 region. This could be caused by the different share of technologies in their generation portfolio. The N2 region only has access to one offshore wind farm, which is shown from the general characteristics above to be the technology that leads to the least amount of ED events if deployed. Additionally, the N1 region comprises of a larger surface area than the N2 region. This difference could lead to the N1 region experiencing the effect of spatial smoothing more than the N2 region.

As outlined in the methodology, the regions are also characterized based on daily mean CF values, serving as input for the co-occurrence determination in section 3.5. The results for the yearly number of events and the mean, maximum and standard deviation of their duration based on daily mean CF values is also presented in Table 9. Similar to the results based on hourly timesteps, the results based on daily timesteps show less ED events, with lower mean and maximum durations in the N1 region. The difference in the maximum duration of the recorded ED events is greater than the one observed in the results based on hourly timesteps, with the maximum duration in the N2 region being nearly twice as high as the one in the N1 region.

Table 9: Yearly number of events, mean, max and standard deviation of ED events based on ERA-5 data and hourly and daily timesteps for the bidding zone regions

	Yearly number of events	**Mean duration (hours)**	**Maximum duration (hours)**	**Standard deviation (hours)**
N1 hourly	328	14.4	94	5.23
N2 hourly	358	16.8	118	5.44
	Yearly number of events	**Mean duration (days)**	**Maximum duration (days)**	**Standard deviation (days)**
N1 daily	29	2.25	22	2.20
N2 daily	34	2.85	39	3.72

For the MERRA ED-characterization, the yearly number of events, and the mean, maximum and standard deviation of their duration based on hourly CF values is presented in Table 10. In contrast to the ERA-5

ED-characterization, the number of events is lower, and their mean and maximum duration lower than for the ERA-5 data. Similar to the ERA-5 ED-characterization, the N2 region has more events than the N1 region, and its events last longer and have a higher maximum duration. Additionally, the yearly number of events and the mean, maximum and standard deviation of their duration based on daily mean CF values is presented in Table 10. The results are overall lower than for the ERA-5 ED characterization, with the main difference being a significant decrease for the maximum duration of the ED events in the N1 region.

Table 10: Yearly number of events, mean, max and standard deviation of ED events based on MERRA data and hourly timesteps for the bidding zone regions

	Yearly number of events	**Mean duration (hours)**	**Maximum duration (hours)**	**Standard deviation (hours)**
N1 hourly	318	13.9	68	4.33
N2 hourly	358	15.9	92	5.16
	Yearly number of events	**Mean duration (days)**	**Maximum duration (days)**	**Standard deviation (days)**
N1 daily	26	1.87	13	1.53
N2 daily	35	2.23	21	2.22

Finally, the aggregated CF for the entire Netherlands is used to characterize the ED events. All technologies are included in this characterization. The results for the ED characterization of the Netherlands based on ERA-5 data as input and hourly timesteps is presented in Table 11. In addition to the ED events based on the 10% CF threshold, events for 5% and 2% CF thresholds are described. Additionally, the results for the ED characterization of the Netherlands based on ERA-5 data as input and daily timesteps is presented in Table 11. Similar to the hourly assessment, regular and adjusted CF thresholds are assessed.

Table 11: Yearly number of events, mean, max and standard deviation of ED events based on ERA-5 data and hourly timesteps for the Netherlands for regular and adjusted CF thresholds

	Yearly number of events	**Mean duration (hours)**	**Maximum duration (hours)**	**Standard deviation (hours)**
NL hourly – 10% CF	357	15.1	117	4.88
NL hourly – 5% CF	175	11.6	47	4.22
NL hourly – 2% CF	47	8.92	20	3.44
	Yearly number of events	**Mean duration (days)**	**Maximum duration (days)**	**Standard deviation (days)**
NL daily – 10% CF	29	2.46	22	2.64
NL daily – 5% CF	5	1.67	10	1.24
NL daily – 2% CF	<1	1	1	-

For the ERA-5 data as input, the outcome of the ED-characterization for the Netherlands presents near daily ED events when based off of hourly timesteps as input. For the method that uses mean daily CF values, ED events occur between two to three times per month on average. The maximum duration is 22 days, which is significantly higher compared to the result based off of hourly timesteps, as this results in 117 hours as the max duration of ED events. As is expected, lowering the threshold CF value reduces the event occurrence. Additionally, the mean and maximum duration reduces as the threshold is lowered. In the case of assessing ED events based on average daily CF values, the 2% CF threshold results in seven ED

events across the entire time-period. The frequency of such events occurring is therefore less than once every nine years.

The results for the ED characterization of the Netherlands based on MERRA data as input and hourly and daily timesteps are presented in Table 12. To compare with ERA-5 results, regular and adjusted CF thresholds are assessed.

Table 12: Yearly number of events, mean, max and standard deviation of ED events based on MERRA data and hourly timesteps for the Netherlands for regular and adjusted thresholds

	Yearly number of events	**Mean duration (hours)**	**Maximum duration (hours)**	**Standard deviation (hours)**
NL hourly – 10% CF	339	14.2	70	4.21
NL hourly – 5% CF	182	11.5	42	3.84
NL hourly – 2% CF	53	9.2	20	3.47
	Yearly number of events	**Mean duration (days)**	**Maximum duration (days)**	**Standard deviation (days)**
NL daily – 10% CF	26	2.00	15	1.73
NL daily – 5% CF	3	1.24	4	0.51
NL daily – 2% CF	<1	1	1	-

The MERRA results show a smaller number of events, and lower mean and maximum duration for both hourly and daily timesteps than the results from the ERA-5 ED characterization. This observation is also made when comparing the results for similar CF threshold values. Similar to the ERA-5 results, lowering the CF threshold results in a lower number of ED events. For the ED events based on average daily CF values for a 2% CF threshold, only one ED event occurs across the entire time period.

The seasonal trends of the recorded ED events are assessed by considering the percentage share of the overall duration of all events per month of the year. The share of total ED duration per month is presented in Figure 13.

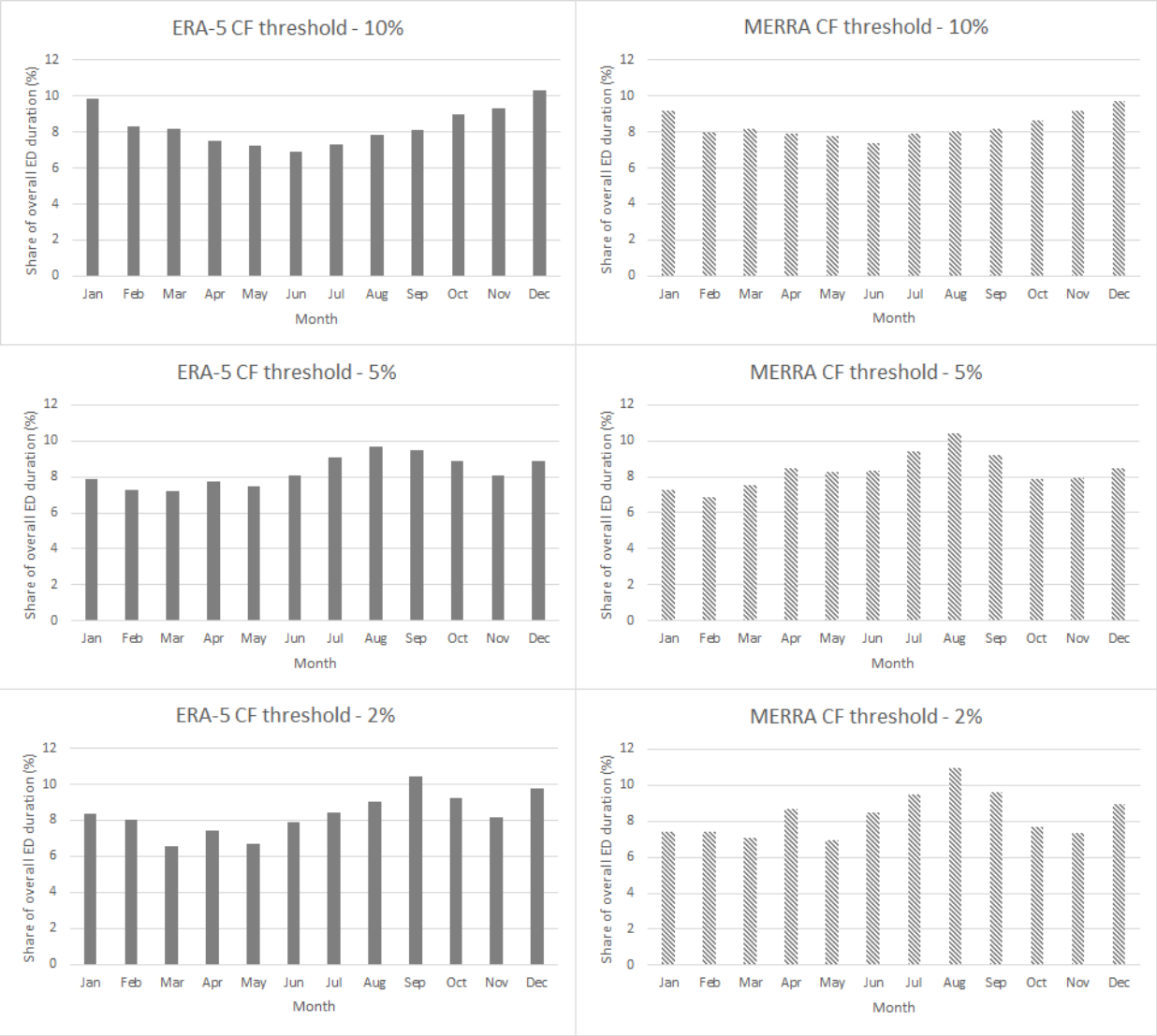

Figure 13: Percentage shares of overall ED duration per month for both ERA-5 and MERRA datasets and corresponding to 10%, 5% and 2% CF thresholds for ED event definition

The year-to-year variability in ED duration is presented in Figure 14. The variability is determined for both datasets and expressed in a percentage share of the overall duration of all ED events recorded. As can be seen from the figure, for both datasets the interannual variability increases as the threshold CF value for defining ED events is reduced. Furthermore, a trend can be observed that earlier years in the dataset contain a slightly higher share of the overall ED duration compared to the latest years. This is observable in both datasets, however for the ERA-5 data the trend is more noticeable as a larger time period is considered.

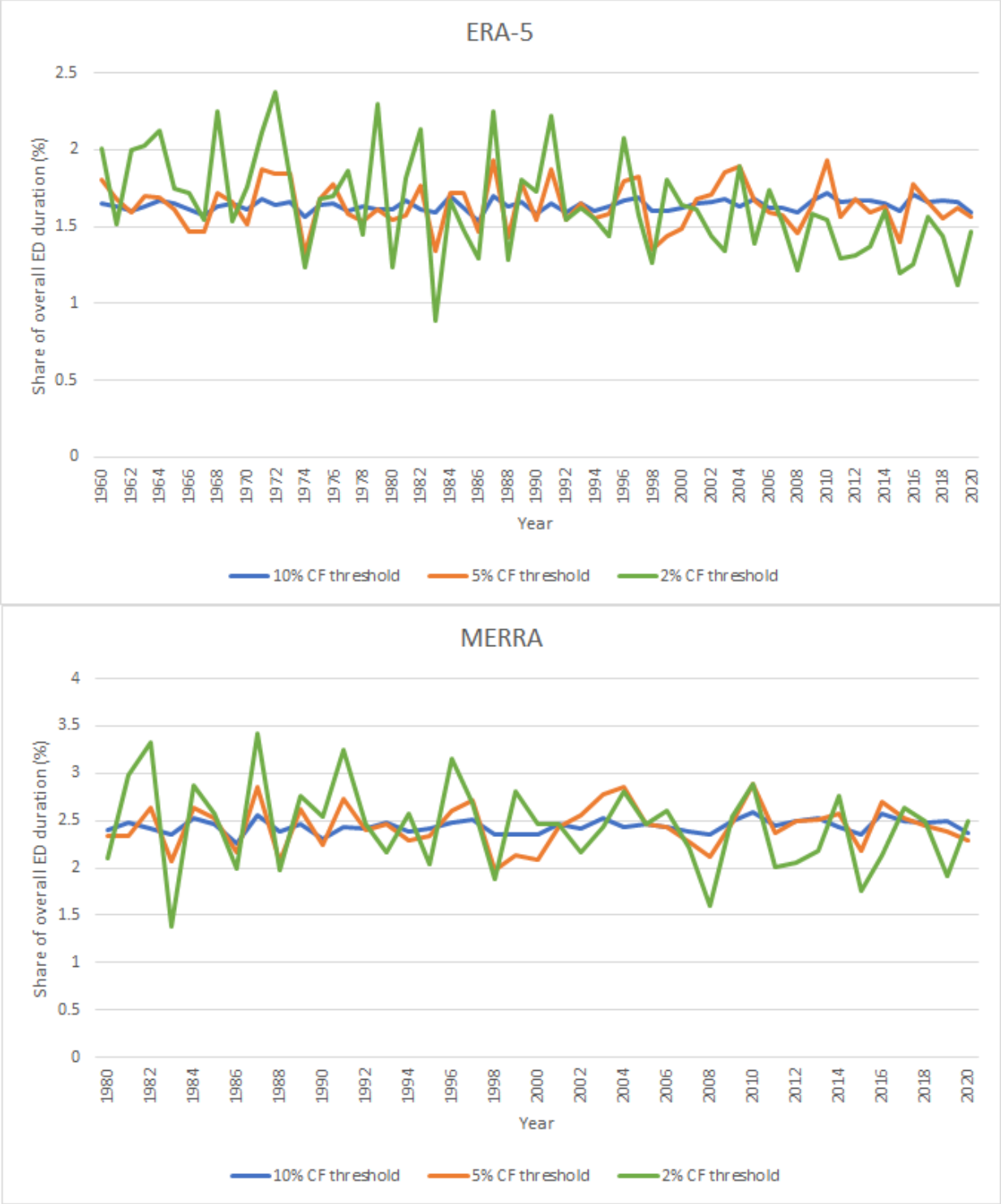

Figure 14: Year-to-year variability of the share of overall ED duration for 10%, 5% and 2% CF thresholds for ERA-5 (upper) and MERRA (lower) data

3.5 Co-occurrence

To accurately determine the co-occurrence between the two regions, the individual regions are first statistically characterized. The aggregated daily CF values of the two regions are fitted using a Cullen and Frey plot. These plots provide information on the skewness and kurtosis of the distribution of the CF values and how they compare to other distribution types (Shehata & Yousof, 2022). The Cullen and Frey plot for region N1 can be found in Figure 15.

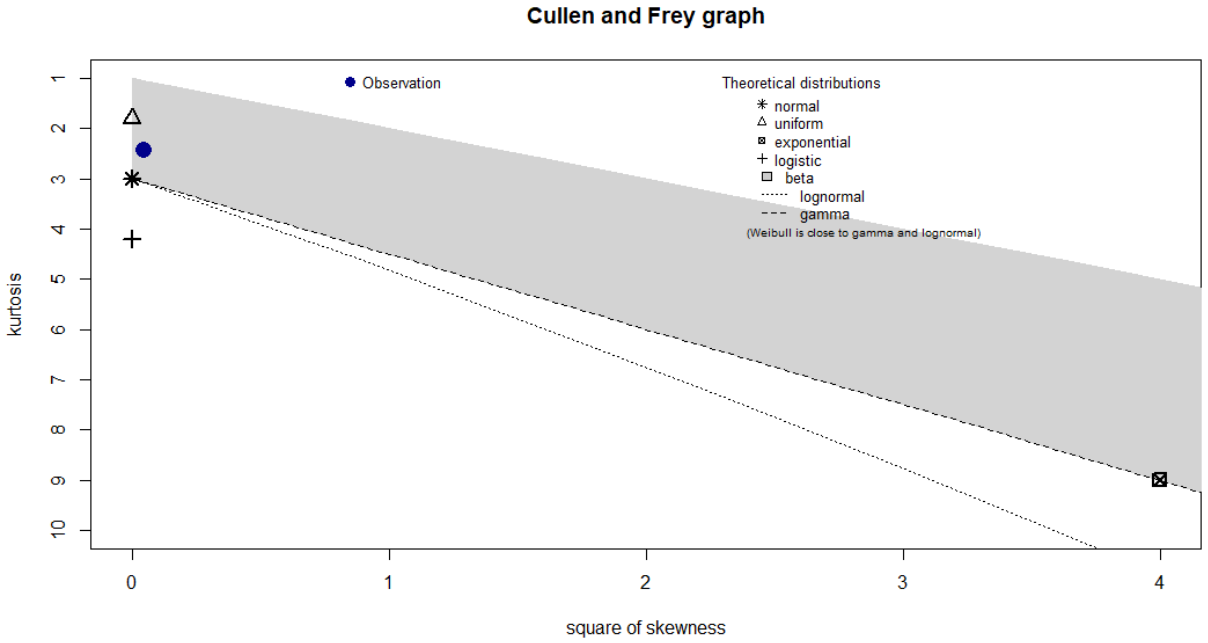

Figure 15: Skewness-kurtosis plot of the distribution of daily mean CF values of the N1 region according to ERA-5 data

The daily CF values of the N1 region seem to be thin tailed, as the kurtosis is lower than that of a normal distribution. The distributions that could fit the dataset for the N1 region are Weibull, normal, gamma, lognormal and uniform. To determine which distribution fits the data the best, the Aikake information criterion (AIC) and Bayesian information criterion (BIC) are used. The AIC provides information on the minimized mean squared error of model fittings to a certain distribution (Vrieze, 2012). The BIC provides information on the asymptotic approximation to a transformation of the Bayesian posterior probabilities of considered models, which in simpler terms is described as the plausibility of the fitting of the model to the data (Neath & Cavanaugh, 2012). Both values of the possible distributions are estimated, and the lowest AIC and BIC values determine the fit that is used. Both values are determined using the *fitdistrplus* R package (Delignette-Muller et al., 2015). The results are presented in Table 13. As can be seen from the table, the Weibull distribution has the lowest AIC and BIC values and is therefore chosen as the fit.

Table 13: AIC and BIC values of the Weibull, normal, gamma, lognormal and uniform distributions for the N1 region daily mean CF values based on ERA-5 data

	Weibull	**Normal**	**Gamma**	**Lognormal**	**Uniform**
AIC	-61070.12	-60335.46	-60039.63	-57913.70	-45856.99
BIC	-61054.09	-60319.44	-60023.61	-57897.68	-45840.97

The goodness of fit of the selected distribution can be visually assessed through the use of a quantile-quantile (Q-Q) plot. The Q-Q plots in this section are expressed in terms of aggregated CF values for the considered regions. The Q-Q plot for the selected distribution is presented in Figure 16. As can be seen in the figure, the Weibull distribution fits the data well, with slight deviations in the lower and upper tails. In these tails, the empirical distribution seems to be thinner tailed than the simulated data.

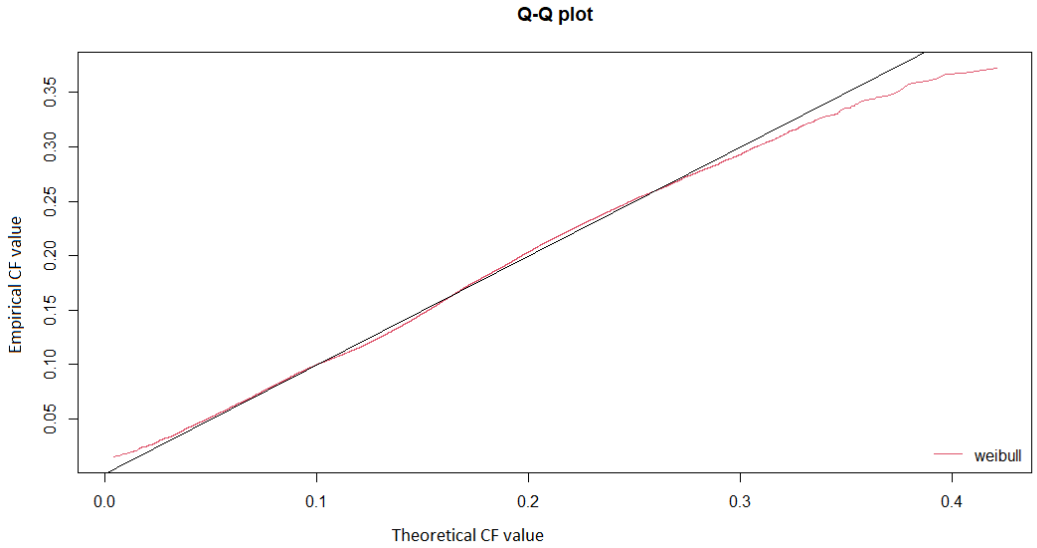

Figure 16: Q-Q plot of the Weibull distribution to fit the daily mean CF values of the N1 region based on ERA-5 data

Additionally, a histogram is constructed to compare simulated and empirical data. This histogram is presented in Figure 17.

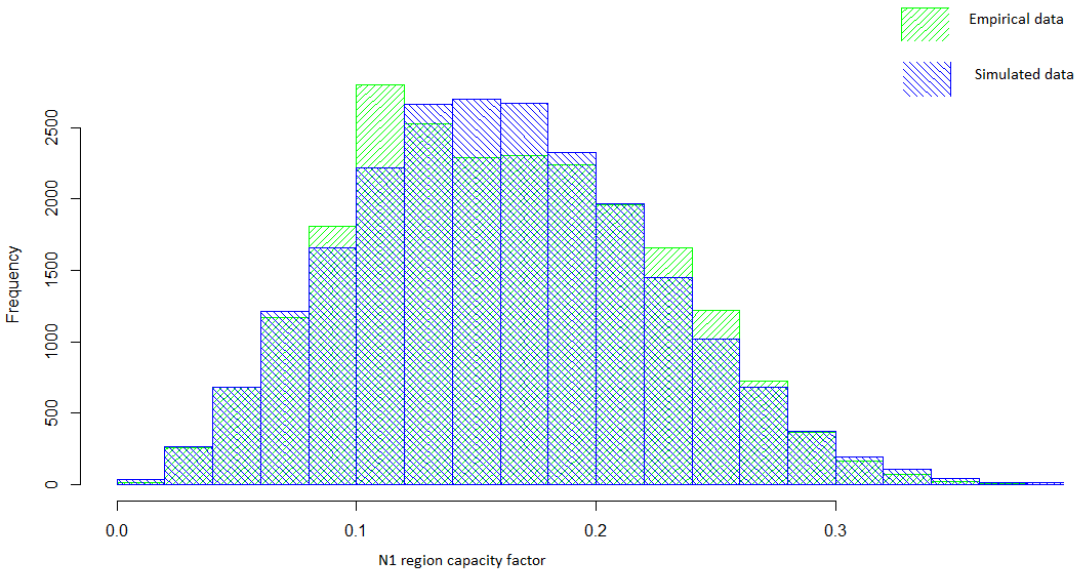

Figure 17: Histogram of empirical and simulated data for the Weibull fitting of the mean daily CF values for the N1 region based on ERA-5 data

The skewness-kurtosis plot for the N2 region based on ERA-5 data is presented in Figure 18.

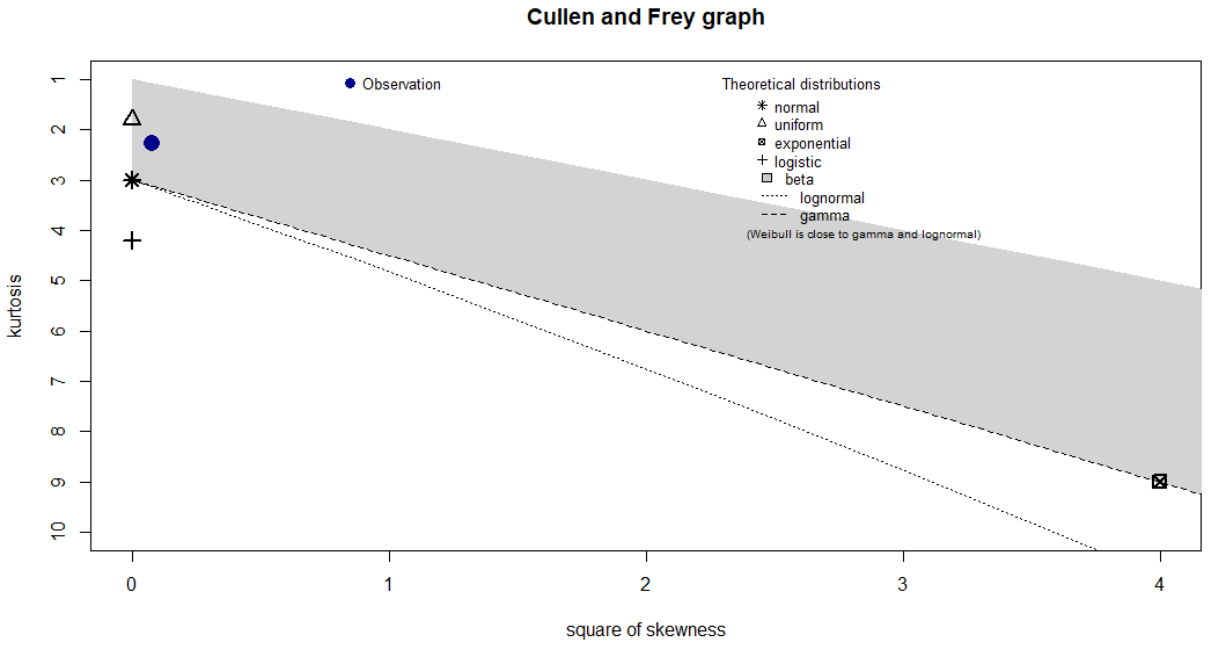

Figure 18: Skewness-kurtosis plot of the distribution of daily mean CF values of the N2 region according to ERA-5 data

The Weibull, normal, gamma, lognormal and uniform distributions are assessed based on AIC and BIC values. The AIC and BIC values of the different distributions for the N2 region based on ERA-5 data are presented in Table 14.

Table 14: AIC values of the Weibull, normal, gamma, lognormal and uniform distributions for the N2 region daily mean CF values based on ERA-5 data

	Weibull	**Normal**	**Gamma**	**Lognormal**	**Uniform**
AIC	-59424.70	-58134.23	-58663.14	-56753.85	-46610.12
BIC	-59408.68	-58118.21	-58647.12	-56737.83	-46594.10

As can be seen from the table, the distribution with the lowest AIC and BIC values is the Weibull distribution. This distribution is further assessed in the form of a Q-Q plot, and a histogram fitting in Figure 19 and Figure 20 respectively.

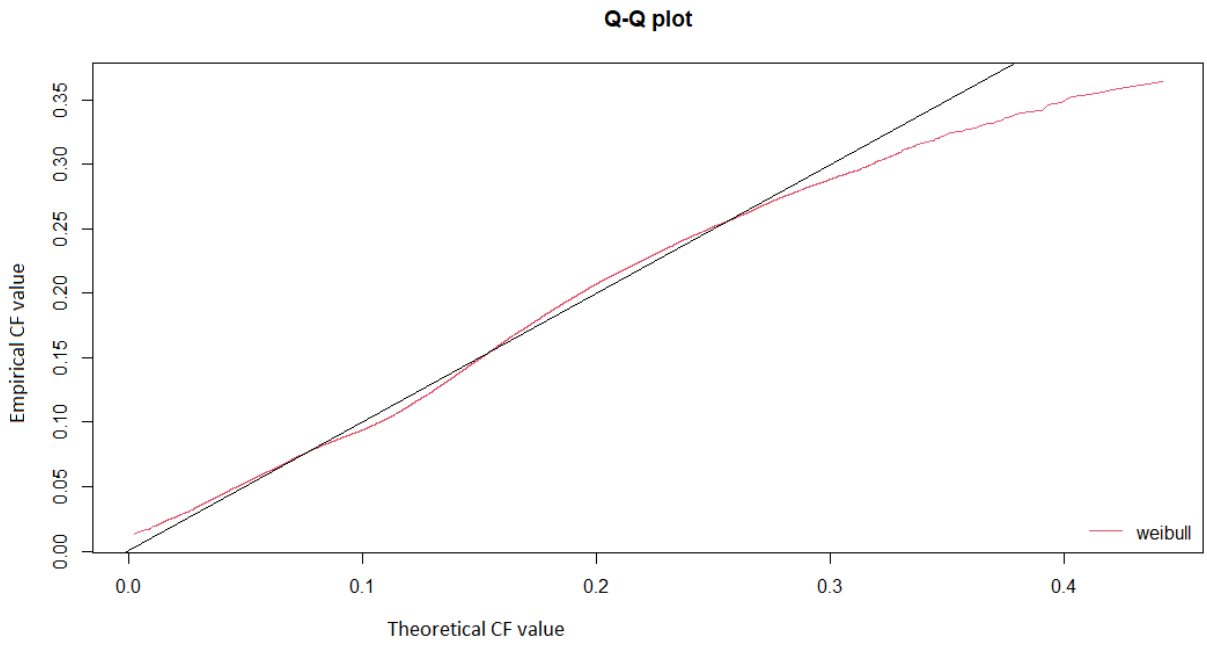

Figure 19: Q-Q plot of the Weibull distribution to fit the daily mean CF values of the N2 region based on ERA-5 data

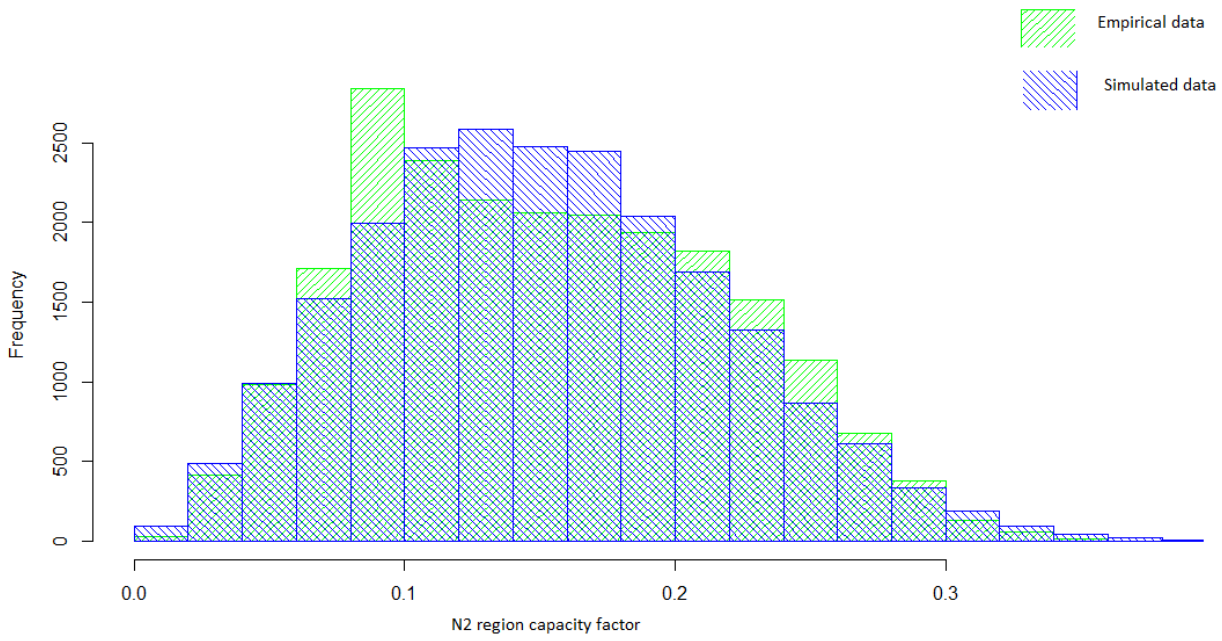

Figure 20: Histogram of empirical and simulated data for the Weibull fitting of the mean daily CF values for the N2 region based on ERA-5 data

The type of copula to use is based on the margins of the two distributions used, namely the N1 and N2 mean daily CF values. The correlation of the original data is calculated to be 0.72 based on Kendall's tau. The copula is characterized by a value of 12 for the degrees of freedom (df). Due to the dependence

between the variables, the t-copula is determined to be the best copula to use. This is determined through the use of the *VineCopula* package in R (Schepsmeier et al., 2015). The distributions of the mean daily values for N1 and N2 are plotted against each other as presented in Figure 21.

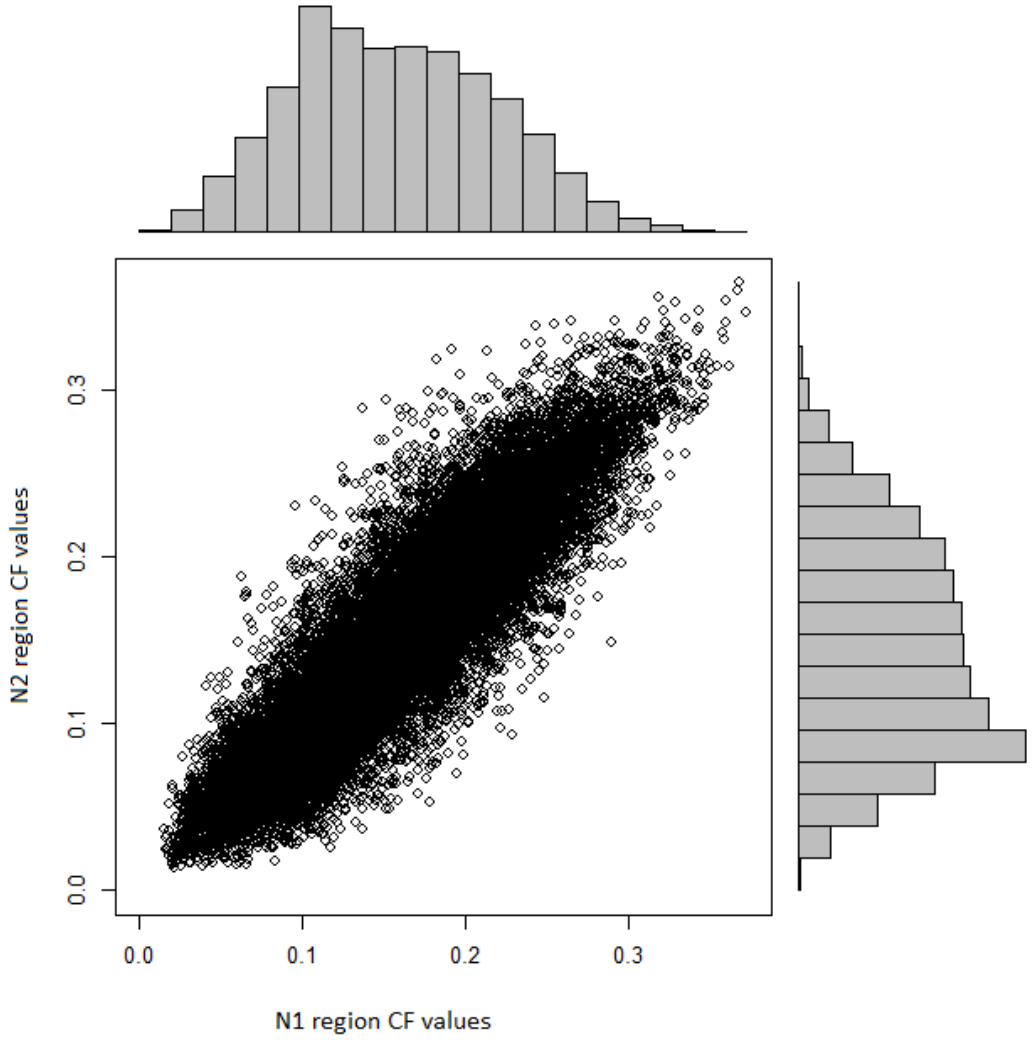

Figure 21: Distributions of the daily mean CF of the N1 and N2 region based on ERA-5 data

The transformed uniform marginals of the N1 and N2 distributions for the ERA-5 data are presented in Figure 22.

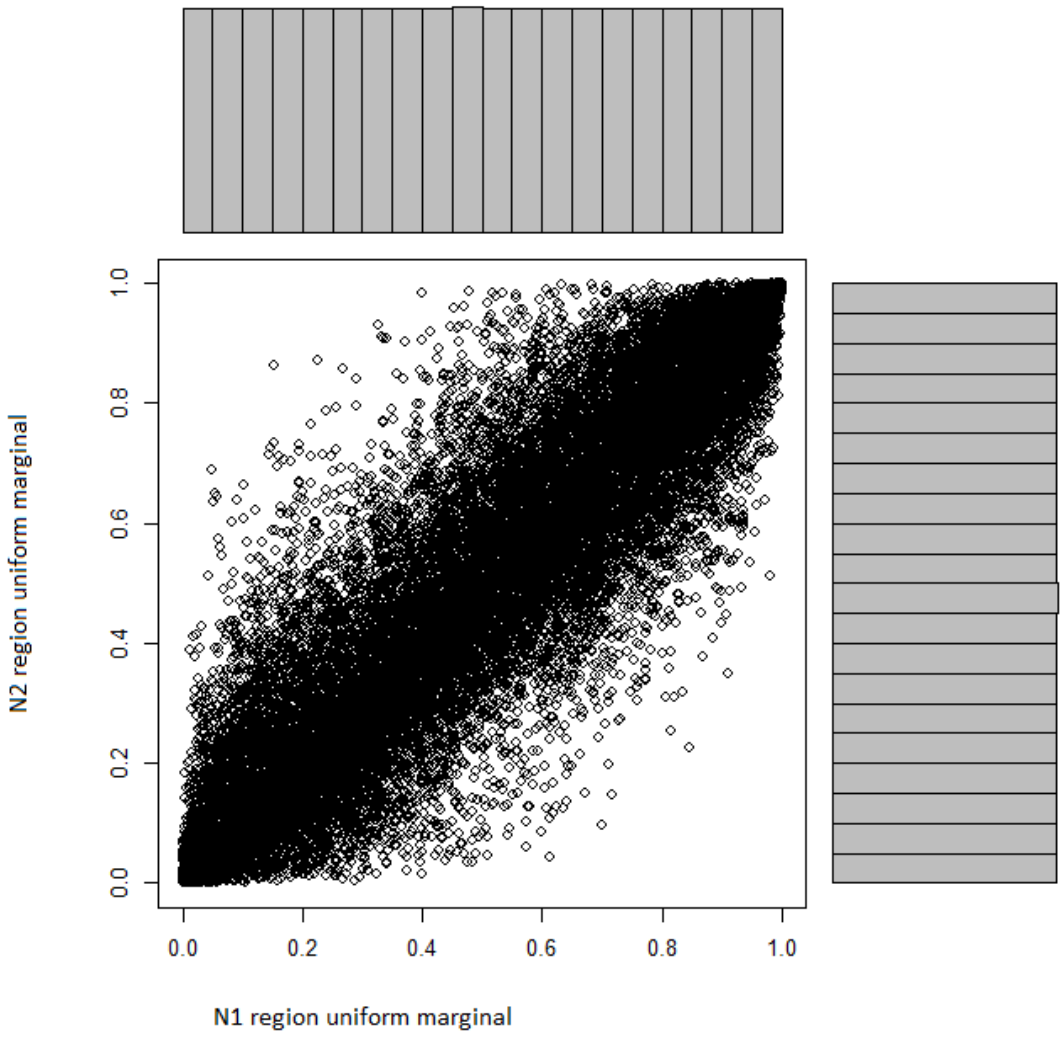

Figure 22: Uniformed marginals of the mean daily CF values of the N1 and N2 region according to ERA-5 data

From the uniformed marginals, the joint probability distribution between the two regions can be constructed and is presented in Figure 23.

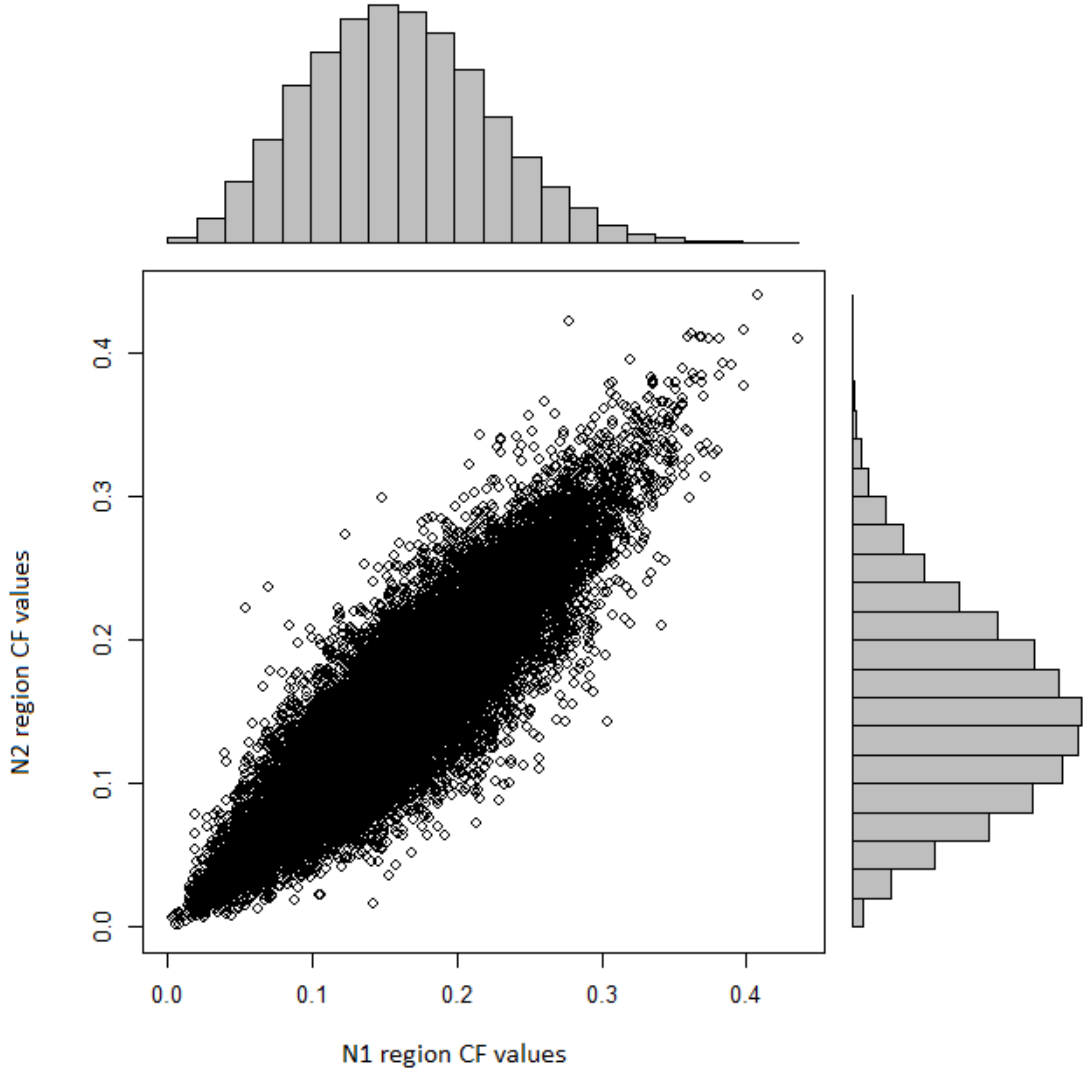

Figure 23: Joint probability distribution of the mean daily CF values of the N1 and N2 region based on ERA-5 data

The density plot and cumulative distribution function (CDF) of the transformed data is presented in Figure 24.

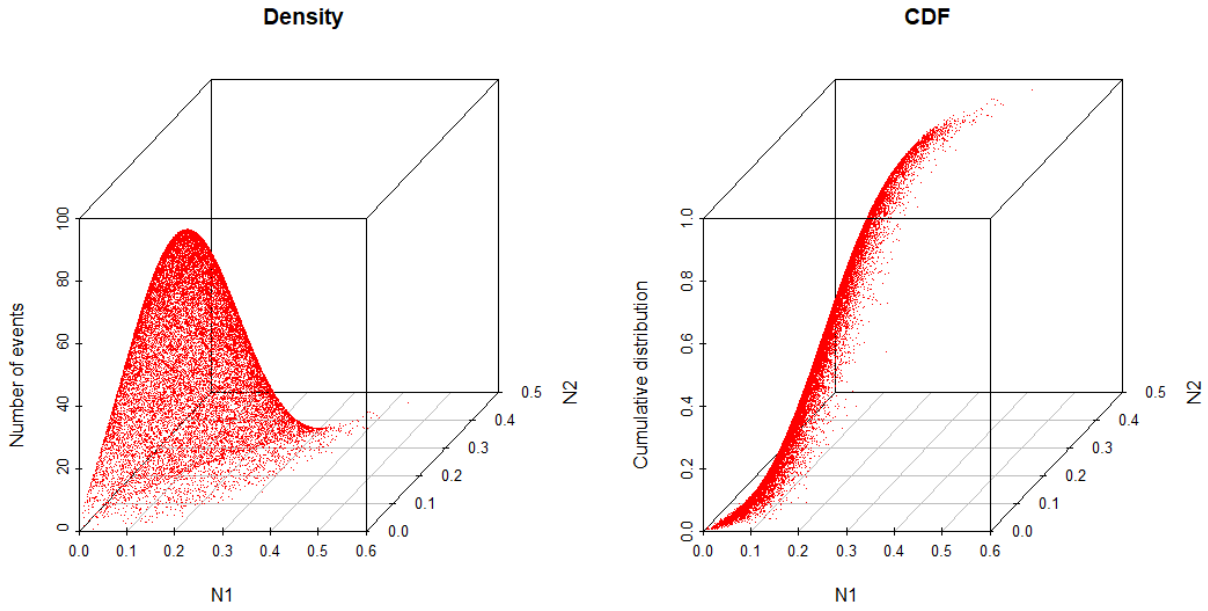

Figure 24: Density and CDF plot for the transformed data of the mean daily CF values of the N1 and N2 regions based on ERA-5 data

The density function of the transformed data for the distribution between the mean daily CF values of N1 and N2 based on ERA-5 data and its contour plot are presented in Figure 25.

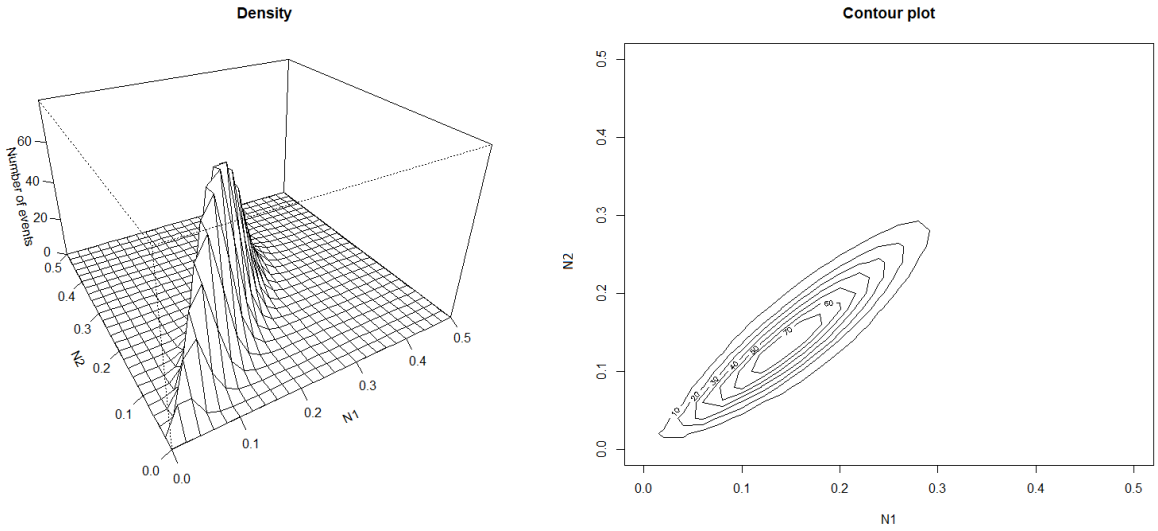

Figure 25: Density and contour plot for the transformed data of the mean daily CF values of the N1 and N2 regions based on ERA-5 data

The CDF of the transformed data for the distribution between the mean daily CF values of N1 and N2 based on ERA-5 data and its contour plot are presented in Figure 26.

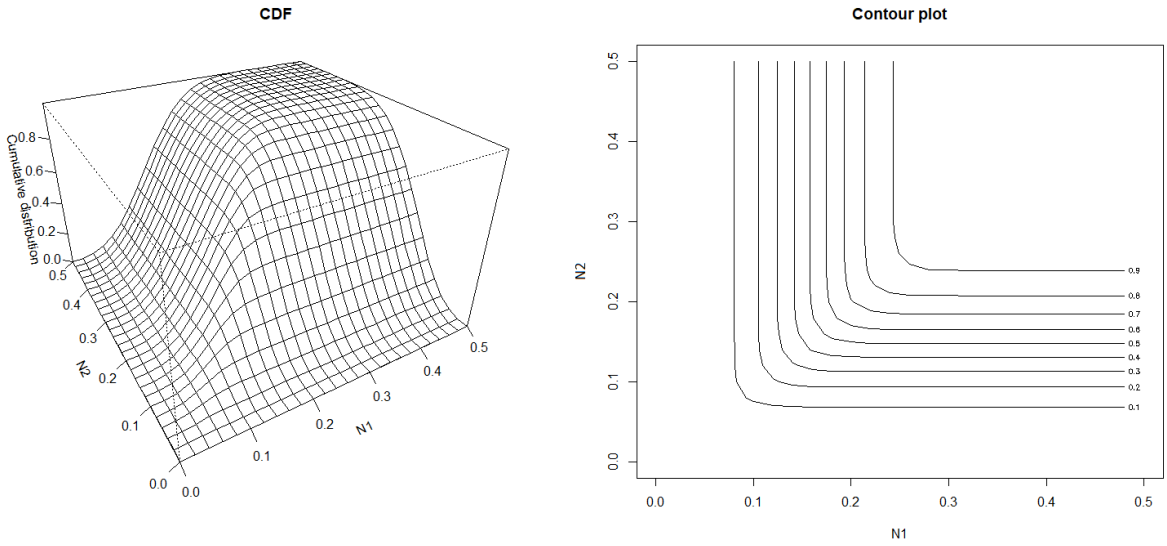

Figure 26: CDF and contour plot for the transformed data of the mean daily CF values of the N1 and N2 regions based on ERA-5 data

The empirical probability of the co-occurrence of ED events in the two regions can be established with the originally produced CF data, whereas the modelled probability of such events can be established through simulated data stemming from the constructed copula. The empirical and modelled probabilities of co-occurrence of ED events between the two regions for different CF thresholds using ERA-5 data are presented in Table 15. Additionally, a visualization of the captured events between empirical data and the modelled data is presented in Figure 27.

Table 15: Empirical and modelled probabilities of ED co-occurrence between N1 and N2 regions at different CF thresholds using ERA-5 data

	Empirical probability (%)	**Modelled probability (%)**
10% CF threshold	15.24	14.93
5% CF threshold	1.517	2.163
2% CF threshold	0.000	0.166

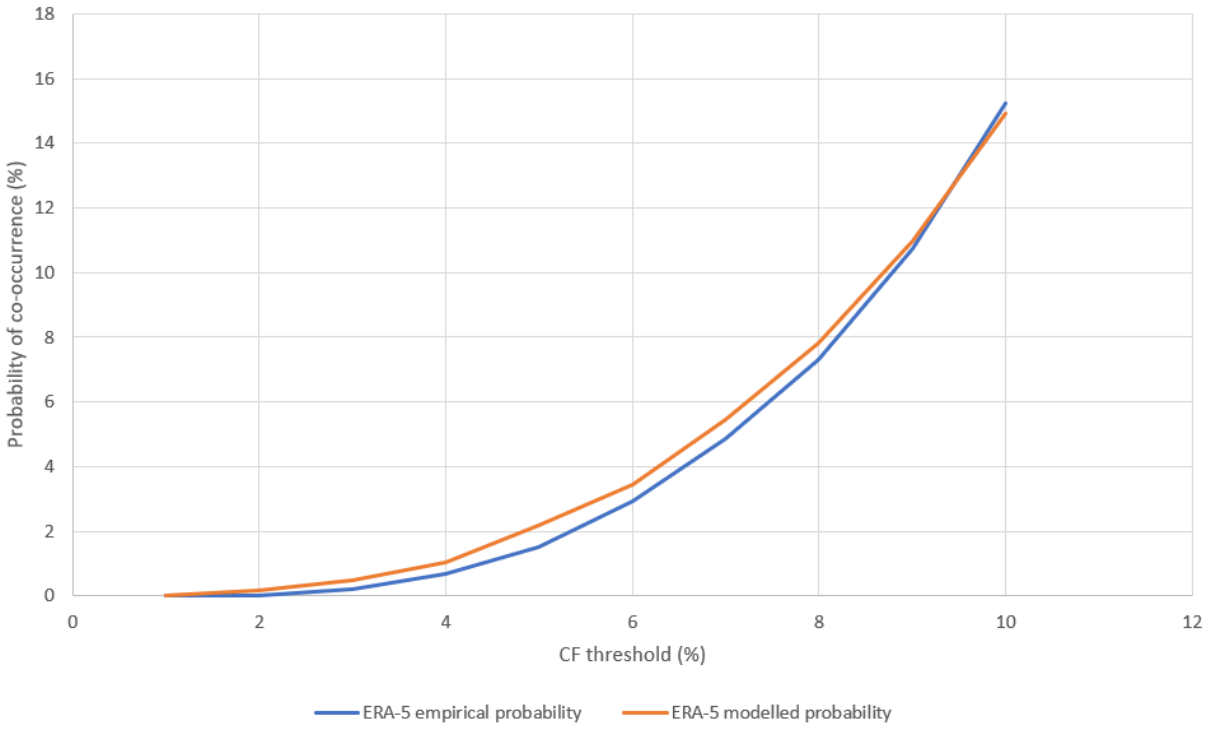

Figure 27: Empirical and modelled probability of co-occurrent ED events between the N1 and N2 regions based on ERA-5 data

As can be seen from the results, the model captures more ED events at the 5% and 2% CF thresholds. At the 10% CF threshold, the model captures slightly less events than are present in the empirical dataset. The results indicate that the copula model is a useful tool to capture the tail behavior of the co-occurring CF values, and therefore co-occurring ED events between the regions. This is especially relevant for the 2% CF threshold where no empirically recorded events are found. Due to the limited amount of empirical data, the simulated data provides a method of assessing these co-occurrence events in absence of them occurring historically. Finally, the return periods for co-occurrent ED events between the N1 and N2 regions based on ERA-5 data are 6.70 days, 46.2 days, and 602 days for the 10%, 5% and 2% CF thresholds, respectively.

The skewness-kurtosis plot of the distribution of daily mean CF values of the N1 region according to MERRA data is presented in Figure 28.

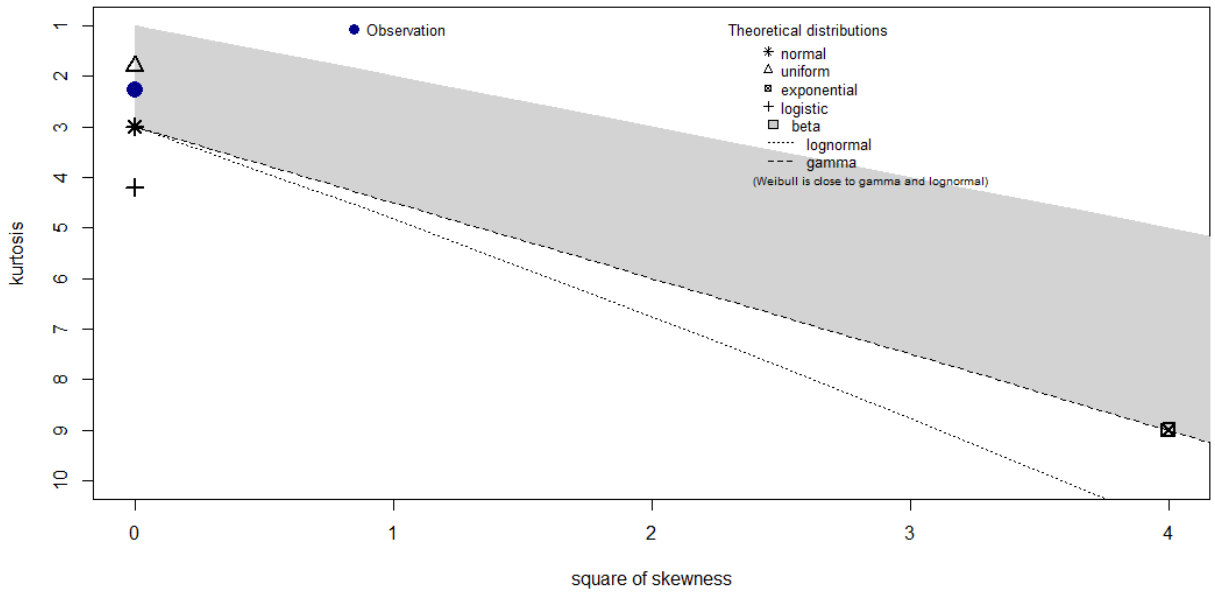

Figure 28: Skewness-kurtosis plot of the distribution of daily mean CF values of the N1 region according to MERRA data

Similar to the skewness-kurtosis plots of the distributions based on the ERA-5 data, the distributions that are seemingly suitable for fitting are the Weibull, normal, gamma, lognormal and uniform distributions. The AIC and BIC values of these distributions are presented in Table 16.

Table 16: AIC and BIC values of the Weibull, normal, gamma, lognormal and uniform distributions for the N1 region daily mean CF values based on MERRA data

	Weibull	**Normal**	**Gamma**	**Lognormal**	**Uniform**
AIC	-43998.09	-43698.58	-42734.59	-41241.04	-35582.82
BIC	-43982.86	-43683.35	-42719.37	-41225.82	-35567.59

As can be seen from the table, the lowest AIC and BIC values belong to the Weibull distribution. This distribution is used to fit the data. This distribution is further assessed in the form of a Q-Q plot, and a histogram fitting in Figure 29 and Figure 30 respectively. Compared to the Q-Q plot of the N1 region according to ERA-5 data, the fitting is skewed slightly further in the upper tail. The histogram fits the data adequately, with slight deviations presenting primarily near the mean of the data. Deviations are additionally observed in the tails of the distribution.

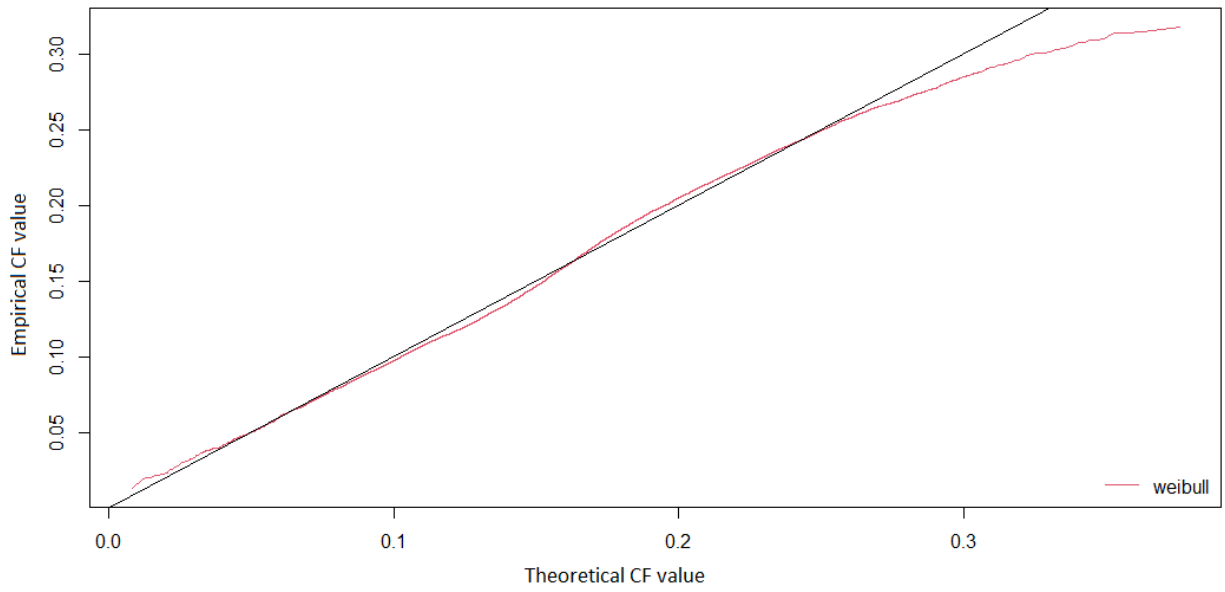

Figure 29: Q-Q plot of the Weibull distribution to fit the daily mean CF values of the N1 region based on MERRA data

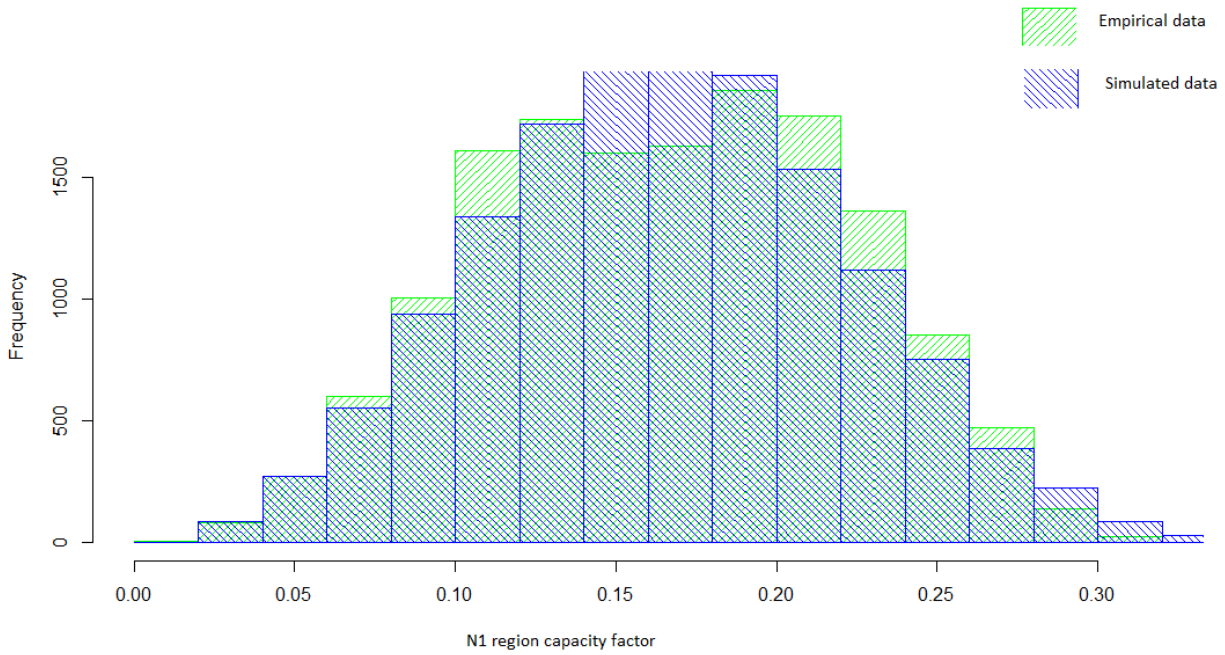

Figure 30: Histogram of empirical and simulated data for the Weibull fitting of the mean daily CF values for the N1 region based on MERRA data

The skewness-kurtosis plot of the distribution of daily mean CF values of the N2 region according to MERRA data is presented in Figure 31.

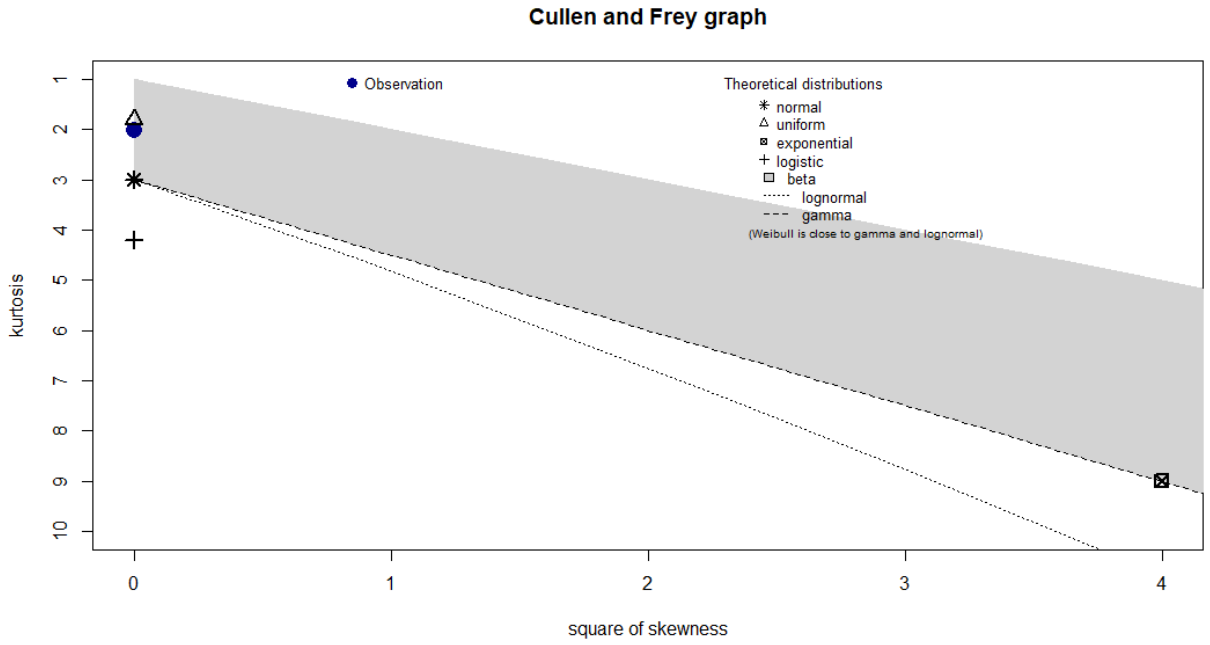

Figure 31: Skewness-kurtosis plot of the distribution of daily mean CF values of the N2 region according to MERRA data

Similar to the skewness-kurtosis plots of the distributions based on the N1 region, the distributions that are seemingly suitable for fitting are the Weibull, normal, gamma, lognormal and uniform distributions. The AIC and BIC values of these distributions are presented in Table 17.

Table 17: AIC and BIC values of the Weibull, normal, gamma, lognormal and uniform distributions for the N2 region daily mean CF values based on MERRA data

	Weibull	**Normal**	**Gamma**	**Lognormal**	**Uniform**
AIC	-42215.62	-41723.55	-41126.69	-39688.64	-36398.51
BIC	-42200.40	-41708.32	-41111.46	-39673.41	-36383.28

As can be seen from the table, the Weibull distribution is associated with the lowest AIC value and is chosen to fit the data. This distribution is further assessed in the form of a Q-Q plot, and a histogram fitting in Figure 32 and Figure 33 respectively. The Q-Q plot shows that the Weibull distribution does not fit the N2 region as well as the N1 region. Similar to the N1 region, the Q-Q plot shows a larger deviation of the simulated data from the empirical data in the right tail.

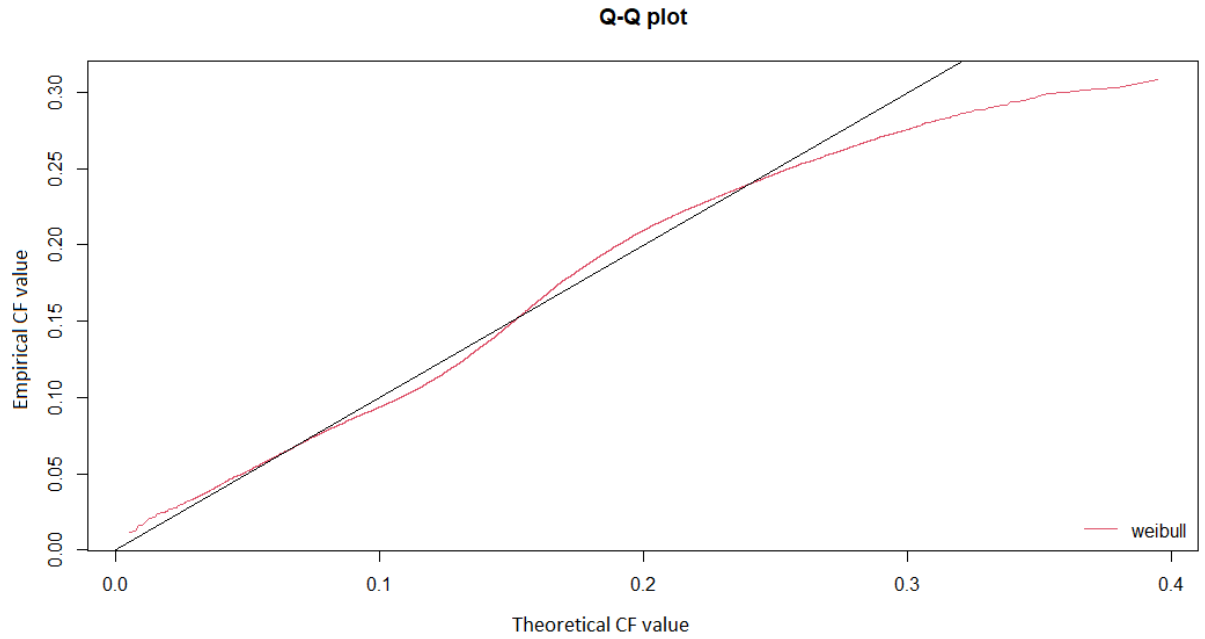

Figure 32: Q-Q plot of the Weibull distribution to fit the daily mean CF values of the N2 region based on MERRA data

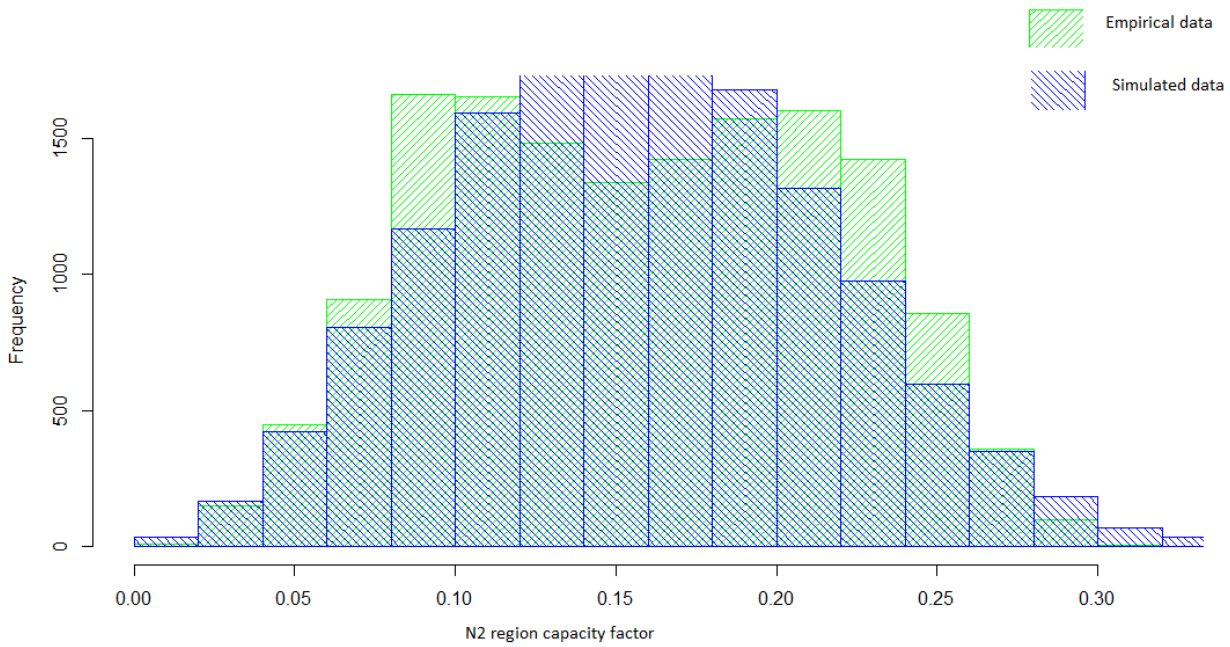

Figure 33: Histogram of empirical and simulated data for the Weibull fitting of the mean daily CF values for the N1 region based on MERRA data

Unlike the copula for the ERA-5 data, the copula type selected for the MERRA data is the Frank copula. The selection of the copula type is again determined by the *VineCopula* package in R. While the Frank

copula and t copula are selected as potential suitable fits, after visual assessment the t copula has again been chosen as most suitable. A visual comparison between the Frank copula and t copula can be found in Appendix C. The correlation of the original data is 0.70 based on Kendall's tau, and the constructed t copula is characterized by a df of 13.

The distribution between the mean daily CF values of the N1 and N2 region based on MERRA data is presented in Figure 34.

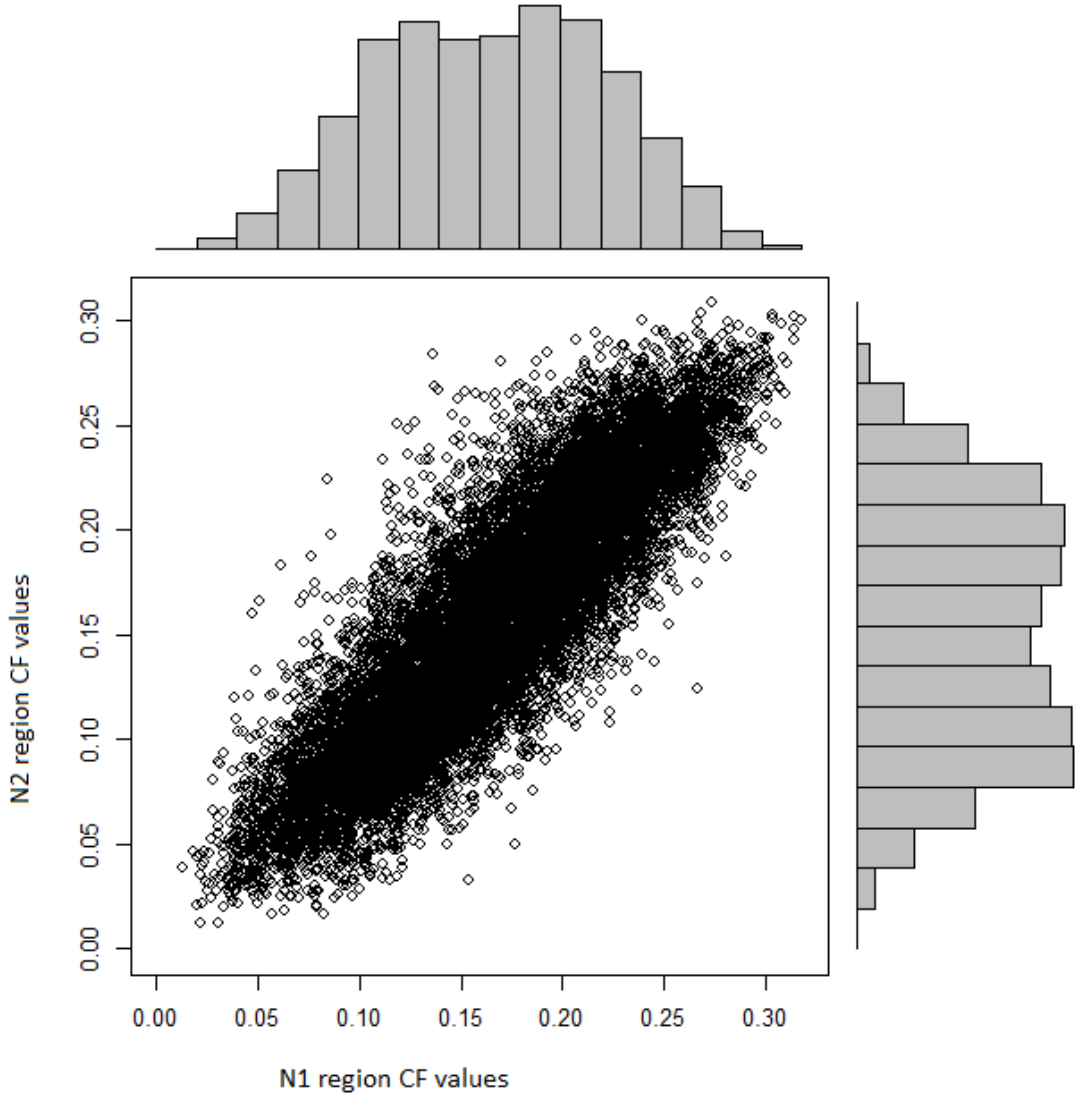

Figure 34: Distributions of the daily mean CF of the N1 and N2 region based on MERRA data

The uniformed margins of the distribution of mean daily CF values of the N1 and N2 regions based on MERRA data is presented in Figure 35.

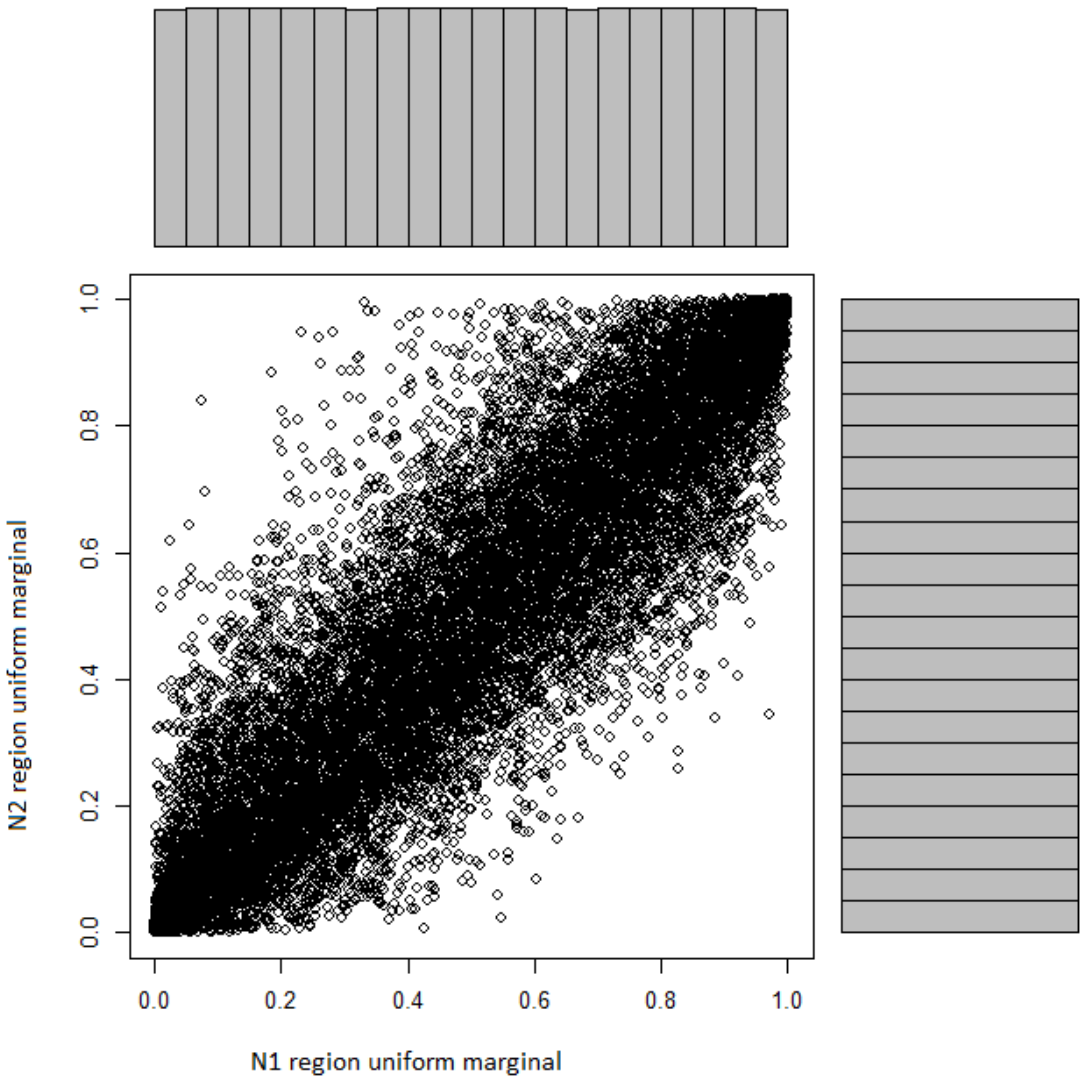

Figure 35: Uniformed marginals of the mean daily CF values of the N1 and N2 region based on MERRA data

The joint probability distribution of the mean daily CF values of the N1 and N2 region based on MERRA data is presented in Figure 36.

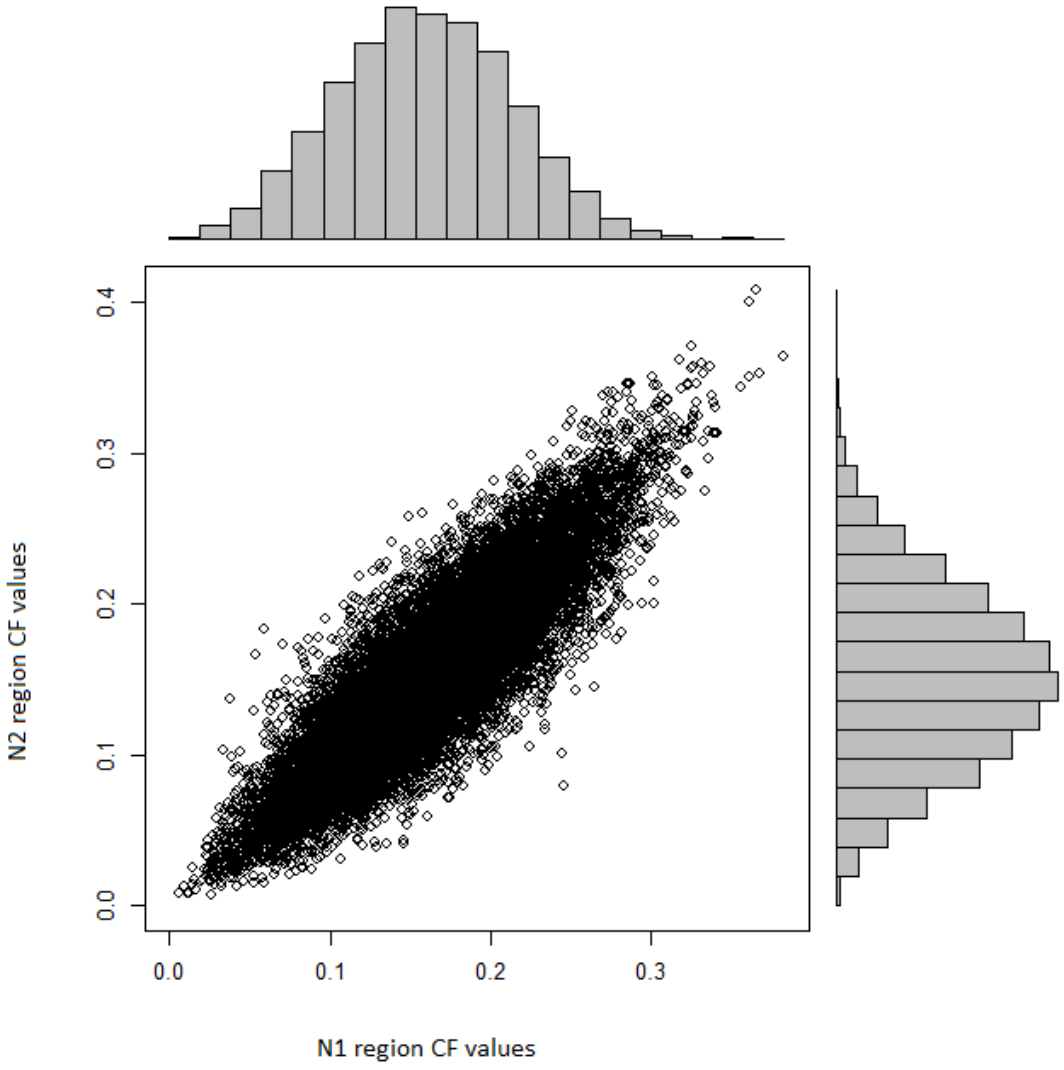

Figure 36: Joint probability distribution of the mean daily CF values of the N1 and N2 region based on MERRA data

The 3D density distribution and CDF plot for the mean daily CF values of the N1 and N2 regions based on MERRA data is presented in Figure 37.

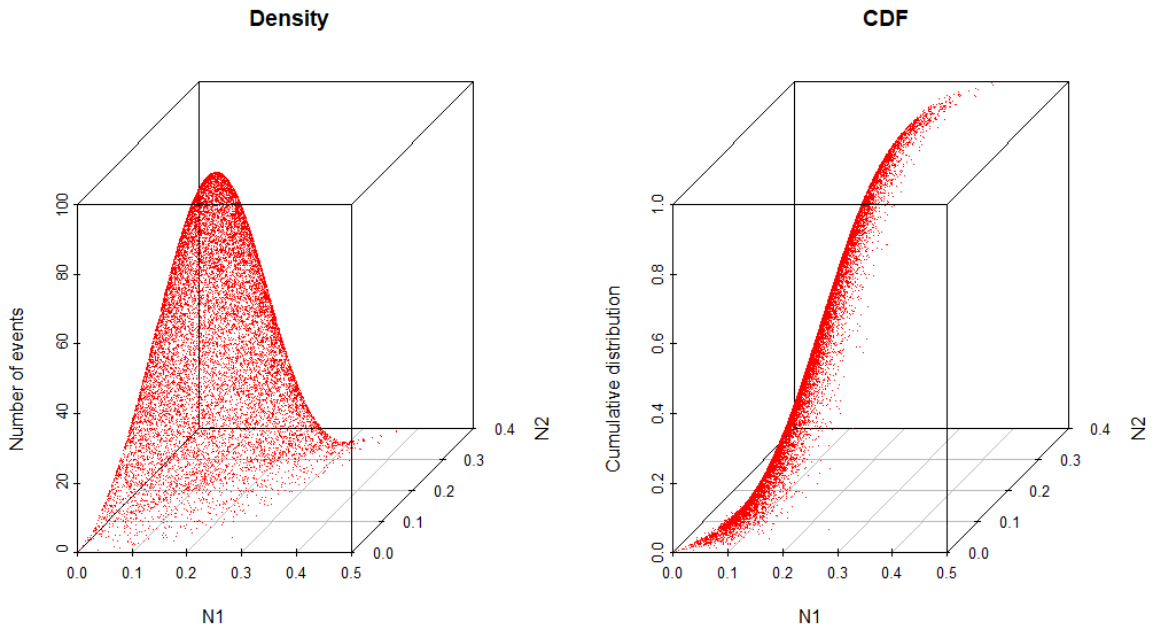

Figure 37: Density and CDF plot for the transformed data of the mean daily CF values of the N1 and N2 regions based on MERRA data

The density and contour plot for the transformed data of the mean daily CF values of the N1 and N2 regions based on MERRA data is presented in Figure 38.

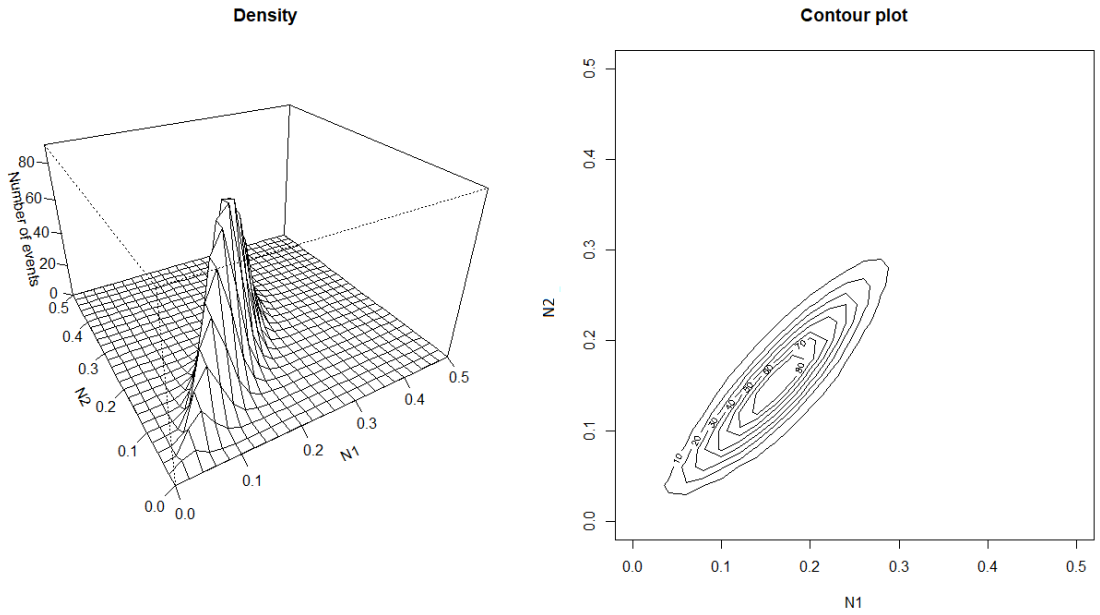

Figure 38: Density and contour plot for the transformed data of the mean daily CF values of the N1 and N2 regions based on MERRA data

The CDF and contour plot of the transformed data of the mean daily CF values of the N1 and N2 regions based on MERRA data is presented in Figure 39.

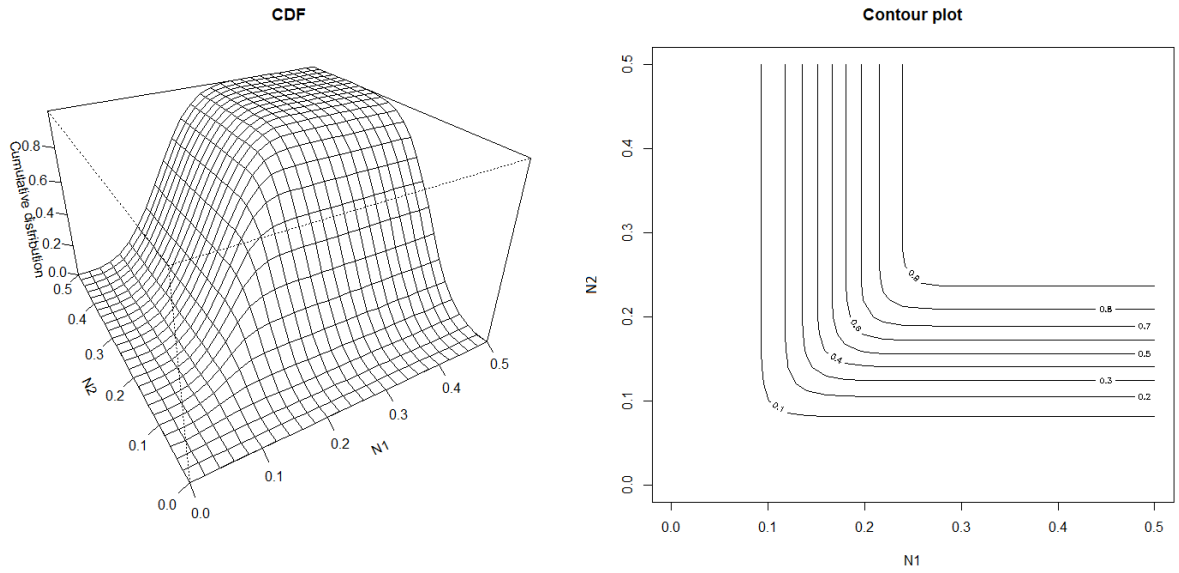

Figure 39: CDF and contour plot for the transformed data of the mean daily CF values of the N1 and N2 regions based on MERRA data

The empirical and modelled probabilities of co-occurrence of ED events between the two regions for different CF thresholds using MERRA data are presented in Table 18. Additionally, a visualization of the captured events between empirical data and the modelled data is presented in Figure 40.

Table 18: Empirical and modelled probabilities of ED co-occurrence between N1 and N2 regions at different CF thresholds using MERRA data

	Empirical probability (%)	**Modelled probability (%)**
10% CF threshold	10.70	9.609
5% CF threshold	0.681	1.055
2% CF threshold	0.000	0.013

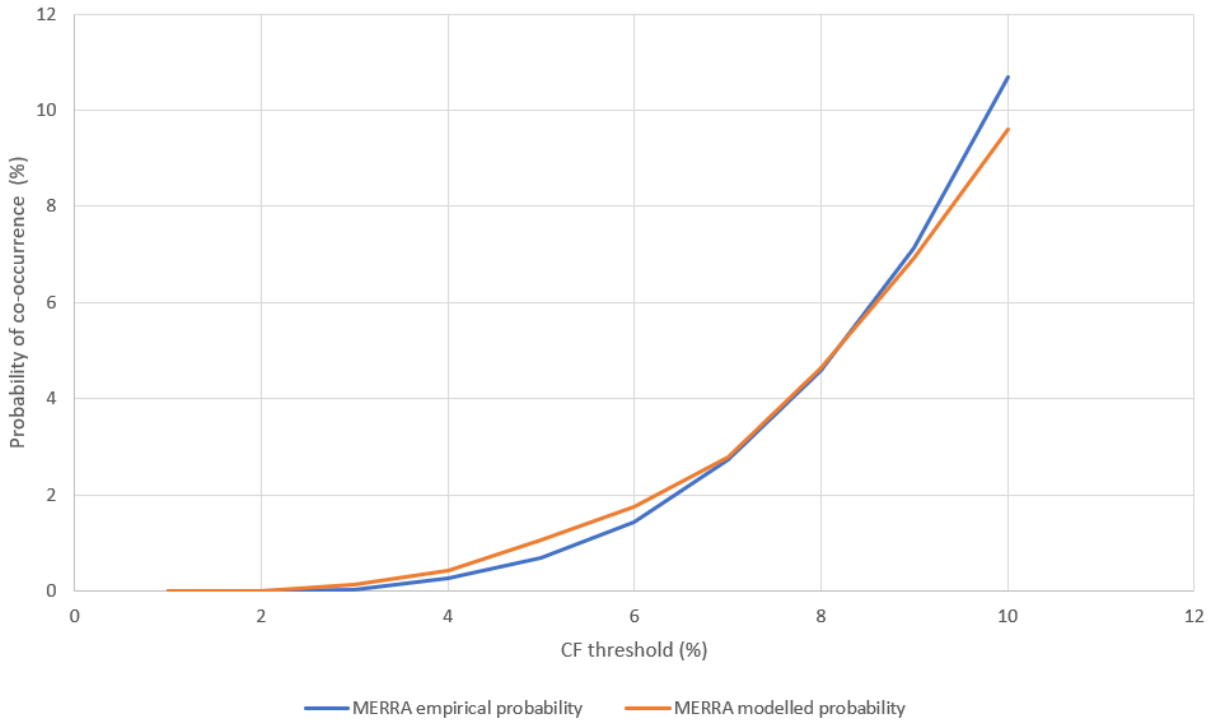

Figure 40: Empirical and modelled probability of co-occurrent ED events between the N1 and N2 regions based on MERRA data

The modelled data captures less ED events at the 10% CF threshold, while more events are captured at the 5% and 2% CF thresholds. Similar to the analysis of the copula analysis for the ERA-5 data, no recorded events at the 2% CF threshold are found in the empirical data but have been simulated in the generated model. As was found when analyzing the ERA-5 data, the established copula model provides a useful method of assessing the co-occurrence of ED events between the N1 and N2 regions, especially at the 2% CF threshold definition. Finally, the return periods for co-occurrent ED events between the N1 and N2 regions based on MERRA data are 10.4 days, 94.8 days, and 7692 days for the 10%, 5% and 2% CF thresholds, respectively.

In addition to modelling the co-occurrence of ED events between the N1 and N2 regions, the co-occurrence between solar PV and wind ED events in the Netherlands based on ERA-5 data is modelled. A t copula with a df value of 18 is constructed based on the margins for wind and solar PV. However, the results are most likely similar for a Gaussian copula based on the high df value (Malevergne & Sornette, 2003). The margin of wind is characterized by a Weibull distribution with a shape parameter of 1.82 and a scale parameter of 0.48. The margin of solar PV is characterized by a Weibull distribution with a shape parameter of 1.44 and a scale parameter of 0.12. The results of the dependency modelling are presented as the empirical and modelled probabilities of the co-occurrence of ED events between solar PV and wind and can be found in Table 19.

Table 19: Empirical and modelled probabilities of ED co-occurrence between solar PV and wind technologies at different CF thresholds using ERA-5 data

	Empirical probability (%)	**Modelled probability (%)**
10% CF threshold	1.912	1.477
5% CF threshold	0.148	0.085
2% CF threshold	0.000	0.000

As can be observed from the results, the model captures less events based on its simulated data when compared to the available empirical data for the ED co-occurrence of solar PV and wind based on the 10% and 5% CF thresholds. For the 2% CF threshold, no empirical events are recorded nor simulated by the model. The return period of co-occurring ED events between the technologies is 67.7 days and 1176 days for the 10% and 5% CF thresholds, respectively.

Furthermore, the co-occurrence of ED events between solar PV and wind in the Netherlands is modelled for the MERRA data. Instead of a t copula, a normal copula is constructed due to the high df value of an attempted t copula. It is constructed based on the margins for wind and solar PV. The margin of wind is characterized by a Weibull distribution with a shape parameter of 1.93 and a scale parameter of 0.48. The margin of solar PV is characterized by a Weibull distribution with a shape parameter of 1.70 and a scale parameter of 0.13. Similar to the results for the ERA-5 data, the results of the dependency modelling are presented as the empirical and modelled probabilities of the co-occurrence of ED events between solar PV and wind. These results can be found in Table 20.

Table 20: Empirical and modelled probabilities of ED co-occurrence between solar PV and wind technologies at different CF thresholds using MERRA data

	Empirical probability (%)	**Modelled probability (%)**
10% CF threshold	1.342	0.855
5% CF threshold	0.073	0.033
2% CF threshold	0.000	0.000

The results present similar findings to the ones derived from ERA-5 data, as the model captures less co-occurrence events than are empirically found for the 10% and 5% CF thresholds. For the 2% CF threshold, no empirical events are recorded nor simulated by the model. The return period of co-occurring ED events between the technologies is 117 and 3030 days for the 10% and 5% CF thresholds, respectively.

3.6 Extreme event analysis

For the ERA-5 data, the suitable threshold found for p-values of over 0.05 is at 19 hours and longer. The threshold is established at 21 hours due to suitable amount of data. It is the smallest threshold that covers enough extreme events. Any event lasting 21 or more hours is therefore included in the extreme event dataset. The selection of extreme events is visualized in Figure 41. In this figure, the red dots are representative of selected extreme events, as they all have a duration of 21 or more hours.

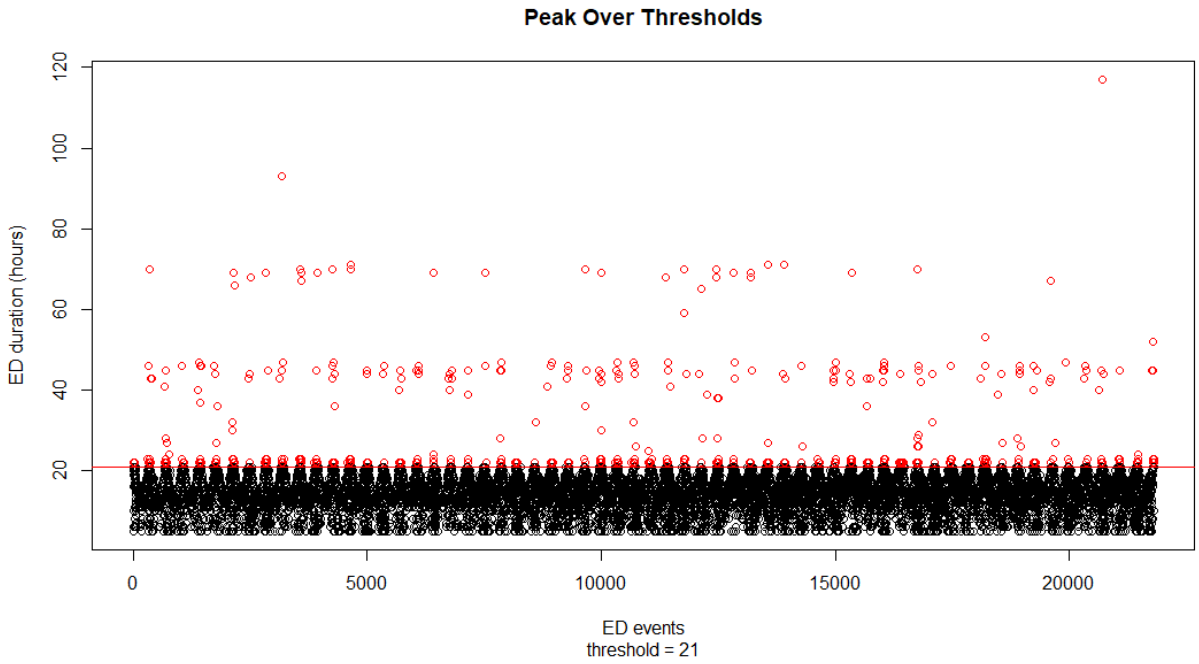

Figure 41: Extreme event selection according to the POT method, where red dots are included as extreme events based on ERA-5 data

This extreme event dataset based on ERA-5 data is fitted to an exponential distribution. The resulting fit presents information on the distribution. The scale parameter of the distribution is 10.4. The AIC value of the distribution is 3420, and the BIC value is 3424. The fitting is presented in Figure 42 as a plot displaying empirical and modelled ED durations. As can be seen from the figure, plot shows that the simulated data follows the empirical data well. Since the Pareto distribution was not chosen as a fit, the shadow variable approach in calculating the VaR and CVaR was not applied as outlined previously. Rather, a conventional method is chosen to calculate the CVaR, which can be found in Appendix D. The VaR is calculated as defined in the methodology.

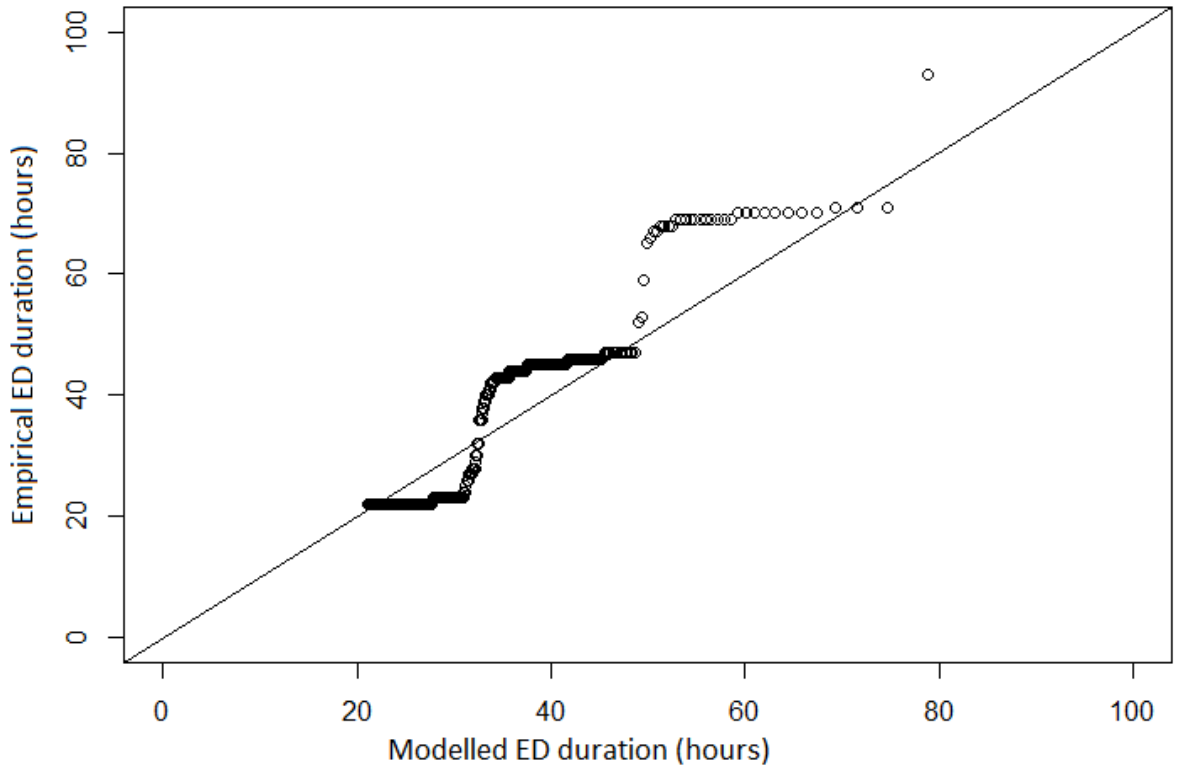

Figure 42: Plot of the extreme ED event dataset when fitted against a simulated exponential distribution based on ERA-5 data

The mean tail value, VaR-95%, CVaR-95%, 50-year ED duration and 100-year ED duration based on the tail of the extreme dataset based on ERA-5 data is presented in Table 21. The values for the 50 and 100-year ED durations are higher for the different thresholds than the VaR-95% and CVaR-95% values. This indicates the tail of the distribution is thin tailed.

Table 21: Mean tail, VaR-95%, CVaR-95%, 50-year ED duration and 100-year ED duration values of the extreme event dataset based on ERA-5 data

	Mean tail value (hours)	**VaR-95% (hours)**	**CVaR-95% (hours)**	**50-year ED duration (hours)**	**100-year ED duration (hours)**
Extreme event risk – 10% CF threshold	25.3	46.0	58.1	84.2	91.4
Extreme event risk – 5% CF threshold	17.3	21.0	21.6	39.5	41.5
Extreme event risk – 2% CF threshold	15.4	19.0	19.4	20.0	20.1

For the MERRA data, the suitable threshold found for p-value of over 0.05 is at 17 hours and longer. However, similar to the selection based on the ERA-5 data, the threshold is established at 21 hours due to a suitable amount of data. It is the smallest threshold that covers enough extreme events. Any event lasting 21 or more hours is therefore included in the extreme event dataset. The selection of extreme events is visualized in Figure 43. In this figure, the red dots are representative of selected extreme events, as they all have a duration of 21 or more hours.

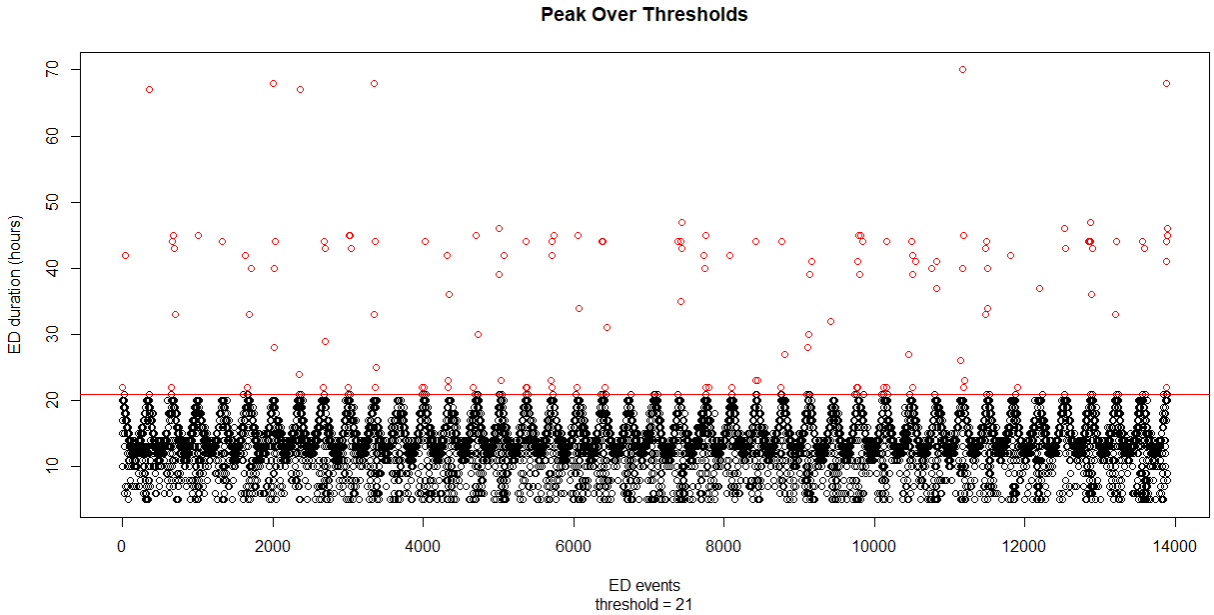

Figure 43: Extreme event selection according to the POT method, where red dots are included as extreme events based on MERRA data

This extreme event dataset based on MERRA data is fitted to a GP distribution. The shape parameter of the distribution is 1.19, whereas the scale parameter of the distribution is 0.25. The AIC value of the distribution is 1651, and the BIC value is 1661. The plot of this fitting is presented in Figure 44. As can be seen from the figure, the simulated data fits the empirical data well, with the simulated data being slightly higher than the empirical data.

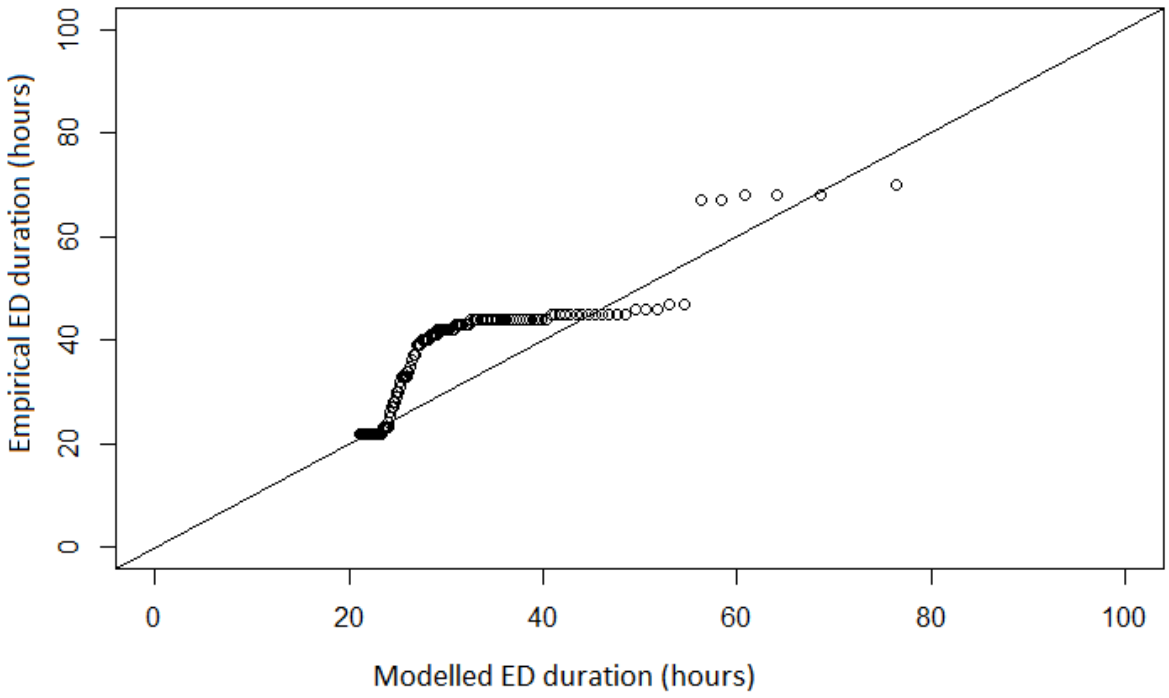

Figure 44: Plot of the extreme ED event dataset when fitted against a simulated exponential distribution based on MERRA data

After transforming the dataset into the shadow variable and back, as described in the methodology, the risk statistics are estimated. As mentioned in the methodology, the upper threshold chosen is calculated to be a factor of 1.5 multiplied with the longest ED duration found empirically. The mean tail value, VaR-95%, CVaR-95%, 50-year ED duration and 100-year ED duration based on the tail of the adjusted extreme dataset based on MERRA data is presented in Table 22. As can be seen from the table, the various risk statistics are lower compared to the results from the ERA-5 generated extreme data.

Table 22: Mean tail, VaR-95%, CVaR-95%, 50-year ED duration, 100-year ED duration values of the adjusted extreme event dataset based on MERRA data

	Mean tail value (hours)	**VaR-95% (hours)**	**CVaR-95% (hours)**	**50-year ED duration (hours)**	**100-year ED duration (hours)**
Extreme event risk – 10% CF threshold	21.8	27.2	41.6	99.0	107
Extreme event risk – 5% CF threshold	17.3	20.0	20.4	34.1	35.0
Extreme event risk – 2% CF threshold	15.2	19.0	19.6	20.2	20.3

The EVA of the ED based on the aggregated CF between technologies for the Netherlands does not consider the lack of stationarity of the solar PV performance. Due to the seasonal characteristics of this performance, the EVA has additionally been conducted when considering only onshore and offshore wind for the Netherlands. Following the same methodology previously used for the aggregated CF for all technologies, based on the ERA-5 data the established threshold for the POT method is 23 hours when excluding solar PV. A visual representation of the included data in this extreme dataset is presented in Figure 45, where red dots are included as extreme events.

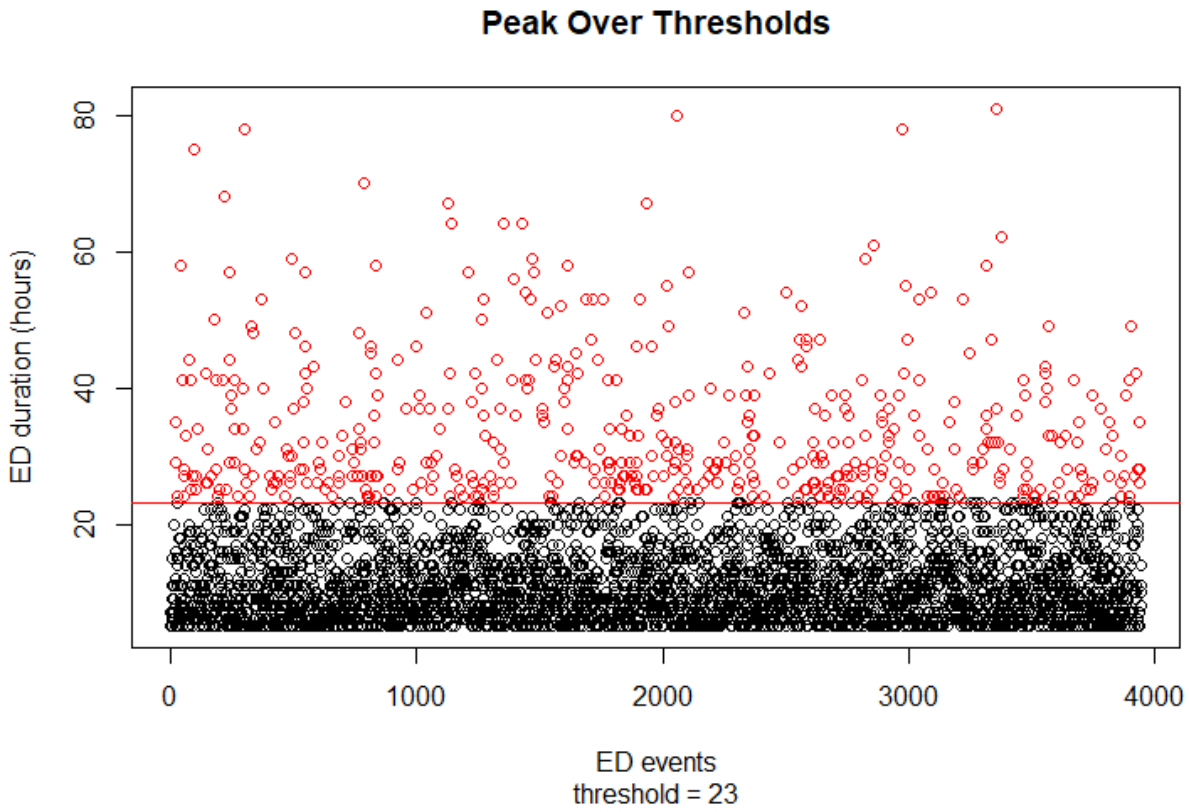

Figure 45: Extreme event selection according to the POT method, where red dots are included as extreme events based on ERA-5 data when excluding solar PV

The extreme value dataset has been fitted by a GP distribution. The fit is presented in Figure 46. As can be seen from the figure, the modelled data follows the empirical data well, and more closely than when solar PV was included. The scale parameter of the distribution is 0.80, whereas the shape parameter is 0.05. Since the shape parameter is below 1, the adjustment of the risk calculations through the use of the shadow variable is not applied.

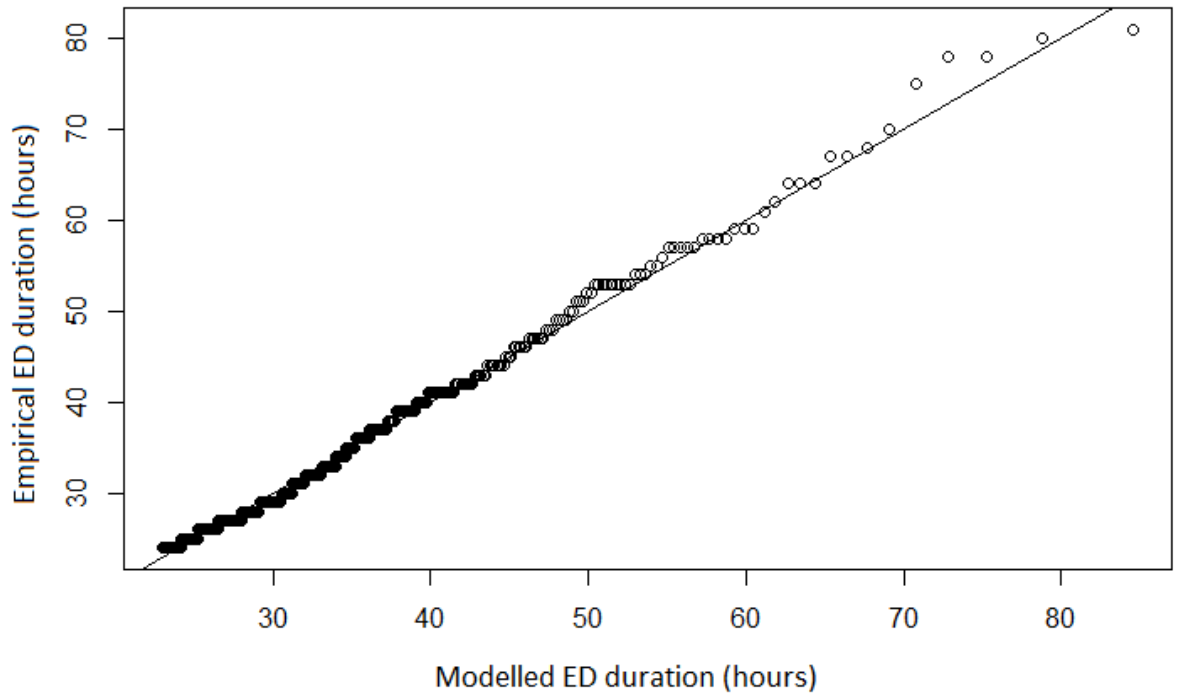

Figure 46: Plot of the extreme ED event dataset excluding solar PV when fitted against a simulated GP distribution based on ERA-5 data

The mean tail, VaR-95%, CVaR-95%, 50-year ED duration and 100-year ED duration values of EVA excluding solar PV based on ERA-5 data are presented in Table 23.

Table 23: Mean tail, VaR-95%, CVaR-95%, 50-year ED duration, 100-year ED duration values of the adjusted extreme event dataset based on ERA-5 data when excluding solar PV

	Mean tail value (hours)	**VaR-95% (hours)**	**CVaR-95% (hours)**	**50-year ED duration (hours)**	**100-year ED duration (hours)**
Extreme event risk – 10% CF threshold	33.3	55.0	63.4	110	115
Extreme event risk – 5% CF threshold	20.0	33.0	38.6	74.6	78.8
Extreme event risk – 2% CF threshold	6.71	7.00	7.67	8.99	9.00

As can be observed from the table, the exclusion of solar PV leads to higher risk values for the analysis based on ERA-5 data. An exception to this is the 2% CF threshold values. These seem to be lower for all measured risk values when excluding solar PV.

A similar approach is taken when considering the MERRA data excluding solar PV. The threshold for the POT method has been established at 22 hours. A visualization of the selected extreme data is presented in Figure 47, where red dots are considered as extreme events.

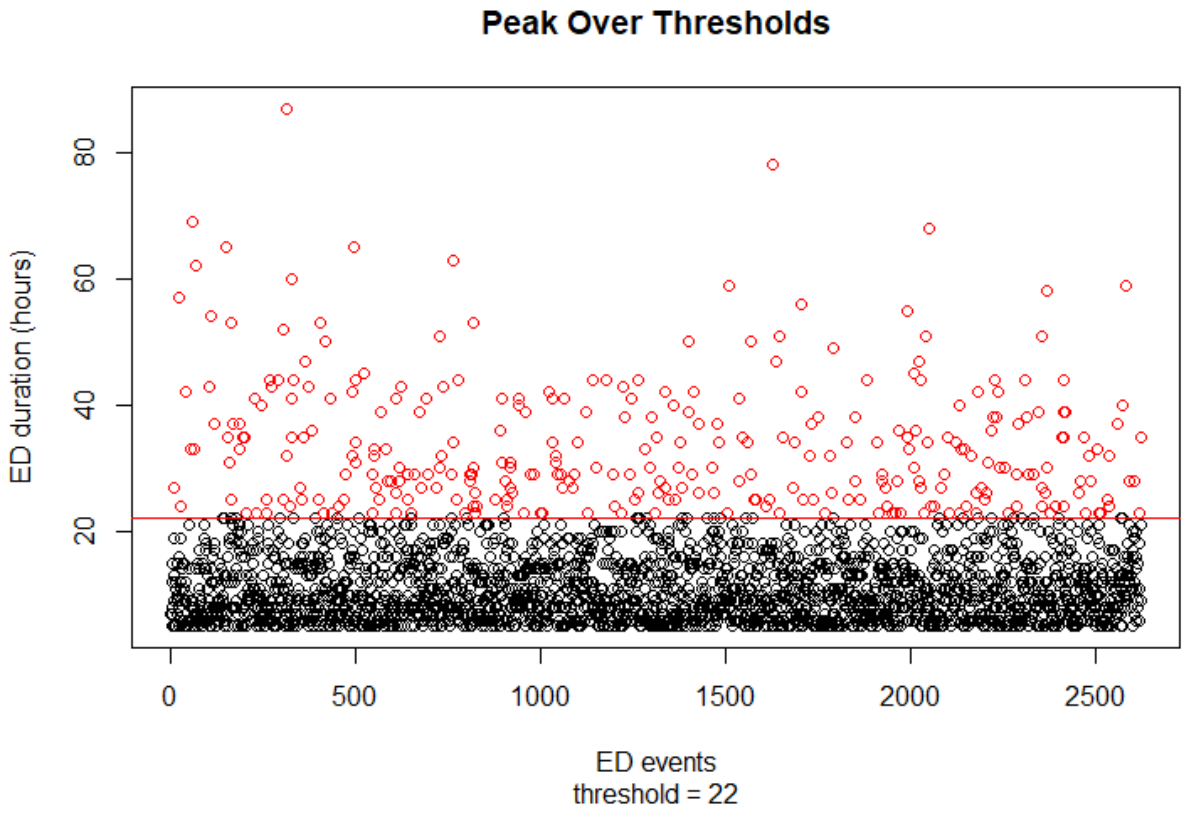

Figure 47: Extreme event selection according to the POT method, where red dots are included as extreme events based on MERRA data when excluding solar PV

The extreme dataset has been fitted by a GP distribution. The fit is presented in Figure 48. The scale parameter of the distribution is 13.2, whereas the shape parameter is -0.12. The simulated data follows the empirical data well, and similar to the ERA-5 results the model performs better when excluding solar PV.

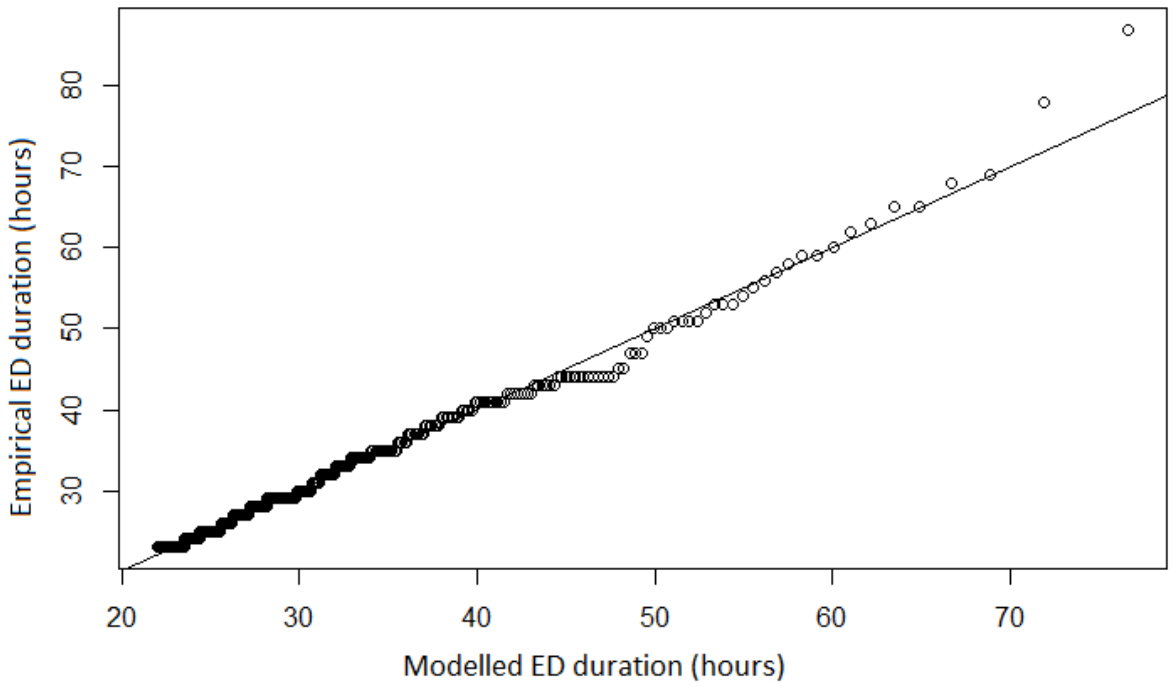

Figure 48: Plot of the extreme ED event dataset excluding solar PV when fitted against a simulated GP distribution based on MERRA data

The mean tail, VaR-95%, CVaR-95%, 50-year ED duration and 100-year ED duration values of EVA excluding solar PV based on ERA-5 data are presented in Table 24.

Table 24: Mean tail, VaR-95%, CVaR-95%, 50-year ED duration and 100-year ED duration values of the adjusted extreme event dataset based on MERRA data when excluding solar PV

	Mean tail value (hours)	**VaR-95% (hours)**	**CVaR-95% (hours)**	**50-year ED duration (hours)**	**100-year ED duration (hours)**
Extreme event risk – 10% CF threshold	32.5	53.0	61.8	97.4	100
Extreme event risk – 5% CF threshold	19.2	28.0	31.5	45.0	46.0
Extreme event risk – 2% CF threshold	9.75	10.0	10.3	10.9	11.0

Similar to the results that exclude solar PV for the ERA-5 data, the results for the MERRA data seem to be associated with higher risk values when excluding solar PV. As was found for the ERA-5 results, an exception is found for the 2% CF threshold. For this threshold, the risk values are lower when excluding

solar PV. The 50 and 100-year ED durations are higher when excluding solar PV for both ERA-5 and MERRA data, except for the 2% CF threshold. This indicates that the contribution of solar PV to extreme ED event occurrence defined by the 2% CF threshold is proportionally larger than wind.

4: Discussion

The aim of this study is to characterize ED events in the Netherlands. There are some aspects of the study that require elaboration for proper interpretation of the results. Firstly, the importance of validation is apparent in any study, however options for extensive sensitivity analysis based on input data are not as extensive as it ideally could be. The two datasets used as climate input data, ERA-5 and MERRA, are widely used in studies modelling wind and solar PV power. If more options for input data were available, the results of this study could be more refined and perhaps lead to other insights. Due to the unavailability of this data and the computational requirement it takes to include more input data, even if it were available, the validation of results is limited. However, the datasets that are included in this study are widely used in the field of wind and solar PV energy simulation, and in some cases are verified to be reliable in assessing renewable energy generation. Namely, the input data used for this research, specifically the ERA-5 climate data is considered to be the most accurate available data for energy conversion and is used in models such as highRES-Europe (Price & Zeyringer, 2022), and CorRES (Koivisto, 2019) in the near future.

Secondly, the results for this research are constrained by the time span of the original climate data that is used, with 1960-2020 for the ERA-5 data and 1980-2020 for the MERRA data. An argument could be made that the availability of more data could influence the found results. Since there are no larger historical climate data sets available for the considered region, a possibility could be to use simulated time series as input data. This has been done in multiple studies, for example in by utilizing a k-nearest neighbor algorithm to model solar PV and wind power production in Texas (Amonkar et al., 2022). Additionally, methods for autocorrelation-based copula models have been used to simulate realistic solar PV power generation time series (Munkhammar & Widén, 2017) and residual load time series (Koivisto et al., 2019). While these techniques could prove useful for future research on ED events in The Netherlands, they do not discredit the results found in this study. Furthermore, the time periods that are considered are large enough to capture a significant amount of ED events for all considered CF thresholds. Nonetheless, future research could place an emphasis on these simulation techniques to validate findings in this research and to model ED events in the future considering effects by climate change on power generation.

Thirdly, the copper plate assumption made in this study might influence the results and their interpretation. The ED characterization does not account for transport constraints of power. The effect of this is that at certain moments in time, power generation is curtailed due to grid congestion. These moments could be of a sufficiently long duration that the effective capacity factor falls below the set ED threshold of 10%. However, it is assumed that this effect is not significant, as most curtailment takes place in periods where there is a high amount of VRE generation. This would therefore mainly be of importance in moments of time where part of the grid is unavailable due to technical issues. The effect of the copper plate assumption is disregarded as energy demand and residual load has not been incorporated in this study.

Additionally, the assumptions made for the installed capacity and in particular the share of installed capacity per technology type are made off of historical figures and might not be representative for the future. With the installation of new wind farms or solar parks, the share of installed capacity per region, whether for provinces, bidding zones or on a national scale, changes for the different technologies. This impacts the amount and duration of ED events, as the results found in this study are based off of static values. However, irrespective of the share of installed capacity per technology for the aggregated CF or share of installed capacity per region, there always exists a zone in which ED events will occur. This is

represented in Figure 49. The dots in the figure represent hourly timesteps of solar and wind performance expressed in CF values. On the left section of the figure, the zone is depicted in which there will always be ED events, regardless of the share of installed capacity for wind and solar PV. The middle and right section of the figure depict situations in which there is a high share of solar PV and wind, respectively. Minimizing the amount of ED events within any configuration requires the minimizing of the amount of hourly timesteps underneath the blue line. It can be observed from the figure that regardless of the configuration, this critical zone depicted on the left side of the figure always exists.

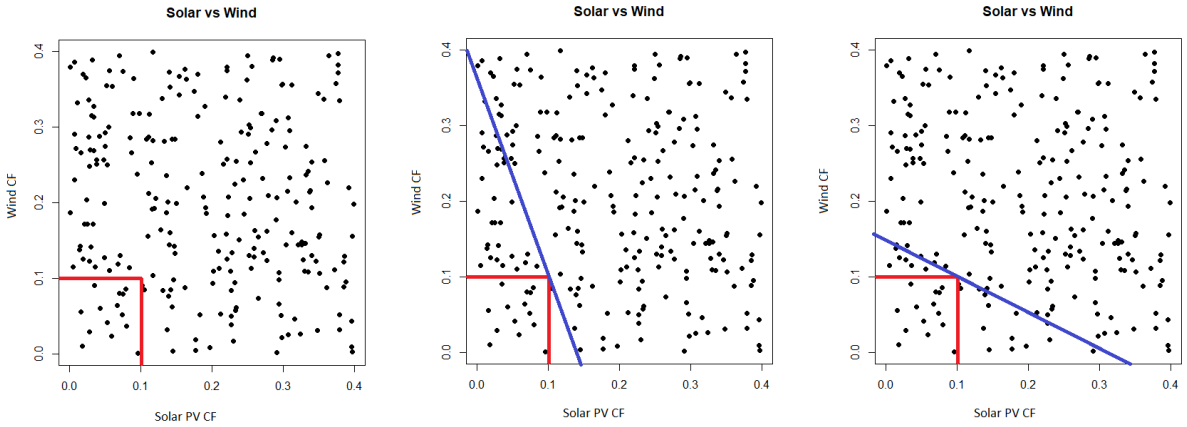

Figure 49: Representation of ED events in a scatterplot depicting solar PV and wind performance expressed in CF with the critical zone (left), a portfolio heavily dependent on solar (middle) and a portfolio heavily dependent on wind (right)

Furthermore, the study assumes an isolated Dutch power system, without considering the possibility of the import of electricity through international cables from for example the UK or Germany. While true, there is a strong correlation between ED event occurrence in the Netherlands and Belgium (0.7), Germany (0.5), Denmark (0.5), and the UK (0.5) (Li et al., 2021a). Consequently, the availability of renewable power from neighboring countries is not guaranteed and perhaps not even likely. Nonetheless, some ED events can certainly be mitigated through the use of these international cables, and it would be interesting for follow-up research to characterize ED events across the interconnected grid of Europe. It is likely that the geographic smoothing effect would reduce the number of ED events, if the copper plate assumption is maintained.

Finally, this research does not include energy demand or residual load. Including this aspect of energy consumption provides a clearer overview of the moments of imbalance between renewable energy production and consumption. While this is true, this study still presents relevant findings from the perspective of energy supply risks of renewable energy technologies. Follow-up research on this study could focus more on the energy demand perspective, especially when considering the local or regional perspective as was done in a study on ED occurrence in Poland by Jurasz et al. (2021)

5: Conclusion

The aim of this study was to characterize the ED events that occur in the Netherlands. This characterization is considered to be useful due to the risks that are associated with the occurrence of such ED events. These risks are present in the form of high electricity prices, rolling blackouts or brownouts. For the simple energy droughts, solar PV is associated with the highest amount of ED events followed by onshore wind and offshore wind. Furthermore, the occurrence of ED events for the historical time periods considered is not equal between provinces. The provinces of Gelderland, Limburg, Noord-Brabant, Overijssel and Utrecht experience higher amounts of ED events than other provinces based on technologically compounding ED characterization. In contrast, the province of Zeeland experiences the least ED events. The maximum duration of such ED events is higher for characterization based on ERA-5 data than MERRA data, lasting 239 hours and 165 hours, respectively. These results relate to the first two sub-questions of the research and provide useful information for policy makers and parties involved in the development of new VRE installations. For these stakeholders, the potential installable capacity of VRE technologies per grid cell provides useful information for future projects. Additionally, the planning of new VRE capacity can consider the provincial differences of VRE performance to minimize ED event occurrence as a result of the findings of this research.

The third sub-question of this research considers the spatially compounding characteristics of ED events. Through the construction of copula models, the dependency between ED occurrence in the two sub-regions of the Netherlands is assessed. For the ERA-5 data, the co-occurrence between ED events in these N1 and N2 regions is captured better with the constructed model than with empirical data at the 5% and 2% / multiple CF threshold ED definition. For the 10%, 5% and 2% CF thresholds the return periods of co-occurring ED events are 6.70, 46.2 and 602 days, respectively. Similarly, for the MERRA data the constructed copula model captures co-occurrence better than the empirical data at the same threshold ED definitions as the model based on ERA-5 data. The return periods of co-occurring ED events between the regions at the 10%, 5% and 2% CF thresholds are 10.4 days, 94.8 days, and 7692 days, respectively. Finally, copula models are constructed to analyze the dependence between solar PV and wind technologies in terms of simple ED co-occurrence. No co-occurrences are modelled or empirically found for the 2% CF threshold. For the ERA-5 data, the return periods are 67.7 days and 1176 days for the 10% and 5% CF thresholds, respectively. Higher values are found for the MERRA data, as the return periods are 117 days and 3030 days for the 10% and 5% CF thresholds, respectively. The results of the copula models are useful for the Dutch TSO, TenneT, in context of the alternative bidding zone proposal submitted that divides the Netherlands from a singular bidding zone to the N1 and N2 regions. The findings can be used to reconsider the energy infrastructure and estimate the requirement capacity for international grid connections for both regions more accurately. In the case of ED occurrence in only one region, zonal pricing can stimulate power transfer from the other region. Since the co-occurrence of ED events necessarily implies no possibility of compensating the lack of power generation in one region with the other, international grid connections are necessary for both regions separately.

The final sub-question of this region considers extremely long duration ED events. Various theories have been applied, including introducing an upper threshold to estimate risk values more accurately for certain distributions. The risk values are measured in the duration of ED occurrence. For the ERA-5 data, the VaR-95% risk value is estimated at 46 hours, 21 hours, and 19 hours for the 10%, 5% and 2% CF thresholds, respectively. Furthermore, the CVaR-95% risk value is estimated at 58.1, 21.6 and 19.4 hours for the 10%, 5% and 2% CF thresholds, respectively. The risk values for the MERRA data calculations are mostly different at the 10% CF threshold when compared to the ERA-5 results. The VaR-95% based on MERRA

data is estimated at 27.2 hours, 20.0 hours, and 19.0 hours for the 10%, 5% and 2% CF thresholds, respectively. Additionally, the CVaR-95% is estimated at 41.6 hours, 20.4 hours, and 19.6 hours for the 10%, 5% and 2% CF thresholds, respectively. 50-year and 100-year ED durations are found to be between 84 and 99 hours and 91 and 107 hours, respectively. To exclude the effect of non-stationarity in the results, the extreme long duration ED events are also characterized excluding solar PV. The results for this EVA are characterized by higher risk values for the 10% and 5% CF thresholds compared to the previous results. For ERA-5 data, the VaR-95% results are 55 hours, 33 hours, and 7 hours for the 10%, 5% and 2% CF thresholds, respectively. Additionally, the CVaR-95% results are 63.4 hours, 38.6 hours, and 7.67 hours for the 10%, 5% and 2% CF thresholds, respectively. The MERRA results are slightly lower than ERA-5, however still higher than the results that included solar PV for the EVA for the 10% and 5% CF thresholds. The VaR-95% results for this data are 53 hours, 28 hours, and 10 hours for the 10%, 5% and 2% CF thresholds, respectively. The CVaR-95% results are 61.8 hours, 31.5 hours, and 10.3 hours for the 10%, 5% and 2% CF thresholds, respectively. Finally, 50-year and 100-year ED durations are found to be between 97 and 110 hours and 100 and 115 hours when excluding solar PV, respectively. Similar to considering other extreme events for risk management such as floodings or droughts, these results provide useful information for grid operators in the Netherlands. Assessing the duration of extremely long duration ED events enables these operators to take appropriate measures to overcome these periods of time with alternative means of supplying power such as battery systems and back-up generators to prevent black outs.

To conclude, this study has characterized the occurrence of ED events in various domains. Periods of low power generation based on technologies in isolation, as well as technologically and spatially compounding events are analyzed. Finally, the risk of extremely long duration ED events is analyzed. Future research of this topic should focus on investigating ED events based on residual load instead of only power supply. Furthermore, valuable insights could be gained from analyzing ED events in the context of an interconnected grid in Europe to assess the influence of international power transfer capacity. Finally, the incorporation of future power generation through simulation techniques such as autocorrelation and k-nearest neighbor could be used to reflect on the findings in this study.

Acknowledgements

Over the course of the past five months, I have spent a considerable amount of time working on this master thesis project. I would like to thank my supervisors, Dr. Jing Hu and Dr. Vinzenz Koning for providing me with the opportunity to research this topic, and to continuously inspire me to strive for a result to be proud of. In the numerous feedback sessions we have had, I always felt free to ask any question relating to the material without limit. Your active contribution to the thesis project is much appreciated. Additionally, I would like to thank the university for granting me access to the remote workstation that most of the research was carried out on. Finally, I would like to thank my family and friends for your unconditional support during the thesis period, it surely would not have been possible to have been successfully completed in time without your help. Besides the stressful moments and hard work, I look back fondly on this period of conducting research, thank you all.

References

Acerbi, C., Nordio, C., & Sirtori, C. (2001). Expected shortfall as a tool for financial risk management. *ArXiv Preprint Cond-Mat/0102304*.

Agarwal, A., & Khandeparkar, K. (2021). Distributing power limits: Mitigating blackout through brownout. *Sustainable Energy, Grids and Networks*, *26*, 100451.

Allen, S., & Otero Felipe, N. (2022). Standardised indices to monitor energy droughts. *Available at SSRN 4312835*.

Amjad, M., Asim, M., Azhar, M., Farooq, M., Ali, M. J., Ahmad, S. U., Amjad, G. M., & Hussain, A. (2021). Improving the accuracy of solar radiation estimation from reanalysis datasets using surface measurements. *Sustainable Energy Technologies and Assessments*, *47*, 101485.

Amonkar, Y., Farnham, D. J., & Lall, U. (2022). A k-nearest neighbor space-time simulator with applications to large-scale wind and solar power modeling. *Patterns*, *3*(3), 100454.

Bali, T. G. (2003). The generalized extreme value distribution. *Economics Letters*, *79*(3), 423–427.

Beurskens, H. J. M., & Brand, A. J. (2012, December 15). *Wind Energy*. https://publications.tno.nl/publication/34627943/816eUK/b13001.pdf

Borchers, H. W., & Borchers, M. H. W. (2022). Package 'pracma.' *Accessed On*, *4*.

Bosch, J., Staffell, I., & Hawkes, A. D. (2018). Temporally explicit and spatially resolved global offshore wind energy potentials. *Energy*, *163*, 766–781.

Bowen, T., Chernyakhovskiy, I., & Denholm, P. L. (2019). *Grid-scale battery storage: frequently asked questions*. National Renewable Energy Lab.(NREL), Golden, CO (United States).

CBS. (2023, March 11). *CBS gebiedsindelingen*. https://www.cbs.nl/nl-nl/dossier/nederland-regionaal/geografische-data/cbs-gebiedsindelingen

Cirillo, P., & Taleb, N. N. (2016). Expected shortfall estimation for apparently infinite-mean models of operational risk. *Quantitative Finance*, *16*(10), 1485–1494.

Copernicus. (2023, June 1). *Copernicus: CLC 2018*. https://land.copernicus.eu/pan-european/corine-land-cover/clc2018?tab=download

Delignette-Muller, M. L., Dutang, C., Pouillot, R., Denis, J.-B., & Siberchicot, A. (2015). Package 'fitdistrplus.' *Journal of Statistical Software*, *64*(4), 1–34.

Eurek, K., Sullivan, P., Gleason, M., Hettinger, D., Heimiller, D., & Lopez, A. (2017). An improved global wind resource estimate for integrated assessment models. *Energy Economics*, *64*, 552–567.

Eurostat. (2023, January 30). *Electricity production capacities for renewables and wastes*. https://ec.europa.eu/eurostat/databrowser/view/NRG_INF_EPCRW__custom_5113418/default/table?lang=en

Gangopadhyay, A., Seshadri, A. K., Sparks, N. J., & Toumi, R. (2022). The role of wind-solar hybrid plants in mitigating renewable energy-droughts. *Renewable Energy*, *194*, 926–937.

Gilleland, E., & Katz, R. W. (2016). extRemes 2.0: an extreme value analysis package in R. *Journal of Statistical Software*, *72*, 1–39.

Gilli, M., & Këllezi, E. (2006). An application of extreme value theory for measuring financial risk. *Computational Economics*, *27*, 207–228.

Gökgöz, F., & Güvercin, M. T. (2018). Energy security and renewable energy efficiency in EU. *Renewable and Sustainable Energy Reviews*, *96*, 226–239.

Grothe, O., & Schnieders, J. (2011). Spatial dependence in wind and optimal wind power allocation: A copula-based analysis. *Energy Policy*, *39*(9), 4742–4754.

Grounds, M. A., LeClerc, J. E., & Joslyn, S. (2018). Expressing flood likelihood: Return period versus probability. *Weather, Climate, and Society*, *10*(1), 5–17.

Gruber, K., Regner, P., Wehrle, S., Zeyringer, M., & Schmidt, J. (2022). Towards global validation of wind power simulations: A multi-country assessment of wind power simulation from MERRA-2 and ERA-5 reanalyses bias-corrected with the global wind atlas. *Energy*, *238*, 121520.

Gruber, S. (2012). Derivation and analysis of a high-resolution estimate of global permafrost zonation. *The Cryosphere*, *6*(1), 221–233.

Hain, L. I., Koelbel, J., & Leippold, M. (2023). Bounding the Impact of Hazard Interdependence on Climate Risk. *Swiss Finance Institute Research Paper*, *23–26*.

Halpern, B. S., Frazier, M., Afflerbach, J., Lowndes, J. S., Micheli, F., O'Hara, C., Scarborough, C., & Selkoe, K. A. (2019). Recent pace of change in human impact on the world's ocean. *Scientific Reports*, *9*(1), 11609.

Hirth, L. (2013). The market value of variable renewables: The effect of solar wind power variability on their relative price. *Energy Economics*, *38*, 218–236.

Hirth, L., & Ziegenhagen, I. (2015). Balancing power and variable renewables: Three links. *Renewable and Sustainable Energy Reviews*, *50*, 1035–1051.

Hu, J., Harmsen, R., Crijns-Graus, W., & Worrell, E. (2019). Geographical optimization of variable renewable energy capacity in China using modern portfolio theory. *Applied Energy*, *253*, 113614.

Hu, J., Koning, V., Bosshard, T., Harmsen, R., Crijns-Graus, W., Worrell, E., & van den Broek, M. (2023). Implications of a Paris-proof scenario for future supply of weather-dependent variable renewable energy in Europe. *Advances in Applied Energy*, *10*, 100134.

Ida, A., Ishimura, N., & Nakamura, M. (2014). Note on the measures of dependence in terms of copulas. *Procedia Economics and Finance*, *14*, 273–279.

Institute, F. M. (2019). Maritime boundaries geodatabase: maritime boundaries and exclusive economic zones (200NM), version 11. *Available Online At:*

Jourdier, B. (2020). Evaluation of ERA5, MERRA-2, COSMO-REA6, NEWA and AROME to simulate wind power production over France. *Advances in Science and Research*, *17*, 63–77.

Jung, C., & Schindler, D. (2023). The Properties of the Global Offshore Wind Turbine Fleet. *Available at SSRN 4446635*.

Jurasz, J., Canales, F. A., Kies, A., Guezgouz, M., & Beluco, A. (2020). A review on the complementarity of renewable energy sources: Concept, metrics, application and future research directions. *Solar Energy*, *195*, 703–724.

Jurasz, J., Mikulik, J., Dąbek, P. B., Guezgouz, M., & Kaźmierczak, B. (2021). Complementarity and 'resource droughts' of solar and wind energy in poland: An era5-based analysis. *Energies*, *14*(4), 1118.

Klopčič, A. L., Hojnik, J., & Bojnec, Š. (2022). What is the state of development of retail electricity markets in the EU? *The Electricity Journal*, *35*(3), 107092.

Koivisto, M. (2019). *CorRES tool: Modelling VRE variability and uncertainty*.

Koivisto, M., Das, K., Guo, F., Sørensen, P., Nuño, E., Cutululis, N., & Maule, P. (2019). Using time series simulation tools for assessing the effects of variable renewable energy generation on power and energy systems. *Wiley Interdisciplinary Reviews: Energy and Environment*, *8*(3), e329.

Lamb, W. F., Wiedmann, T., Pongratz, J., Andrew, R., Crippa, M., Olivier, J. G. J., Wiedenhofer, D., Mattioli, G., Khourdajie, A. al, House, J., Pachauri, S., Figueroa, M., Saheb, Y., Slade, R., Hubacek, K., Sun, L., Ribeiro, S. K., Khennas, S., de la Rue du Can, S., … Minx, J. (2021). A review of trends and drivers of greenhouse gas emissions by sector from 1990 to 2018. *Environmental Research Letters*, *16*(7), 073005. https://doi.org/10.1088/1748-9326/abee4e

Li, B., Basu, S., Watson, S. J., & Russchenberg, H. W. J. (2020). Quantifying the predictability of a 'Dunkelflaute'event by utilizing a mesoscale model. *Journal of Physics: Conference Series*, *1618*(6), 062042.

Li, B., Basu, S., Watson, S. J., & Russchenberg, H. W. J. (2021a). A brief climatology of dunkelflaute events over and surrounding the North and Baltic Sea areas. *Energies*, *14*(20), 6508.

Li, B., Basu, S., Watson, S. J., & Russchenberg, H. W. J. (2021b). Mesoscale modeling of a "Dunkelflaute" event. *Wind Energy*, *24*(1), 5–23.

Mahlknecht, G. (2023). *Greg's Cable Map*. https://cablemap.info/_default.aspx

Malevergne, Y., & Sornette, D. (2003). Testing the Gaussian copula hypothesis for financial assets dependences. *Quantitative Finance*, *3*(4), 231.

Mararakanye, N., Dalton, A., & Bekker, B. (2022). Characterizing Wind Power Forecast Error Using Extreme Value Theory and Copulas. *IEEE Access*, *10*, 58547–58557.

Mashhoodi, B. (2018). Spatial dynamics of household energy consumption and local drivers in Randstad, Netherlands. *Applied Geography*, *91*, 123–130.

Matsuo, Y., Endo, S., Nagatomi, Y., Shibata, Y., Komiyama, R., & Fujii, Y. (2020). Investigating the economics of the power sector under high penetration of variable renewable energies. *Applied Energy*, *267*, 113956.

Mockert, F., Grams, C. M., Brown, T., & Neumann, F. (2022). Meteorological conditions during Dunkelflauten in Germany: Characteristics, the role of weather regimes and impacts on demand. *ArXiv Preprint ArXiv:2212.04870*.

Moraes Jr, L., Bussar, C., Stöcker, P., Jacqué, K., Chang, M., & Sauer, D. U. (2018). Comparison of long-term wind and photovoltaic power capacity factor datasets with open-license. *Applied Energy*, *225*, 209–220.

Munkhammar, J., & Widén, J. (2017). An autocorrelation-based copula model for generating realistic clear-sky index time-series. *Solar Energy*, *158*, 9–19.

Nadarajah, S., Zhang, B., & Chan, S. (2014). Estimation methods for expected shortfall. *Quantitative Finance*, *14*(2), 271–291.

National Centers for Environmental Information. (2023, March 11). *DMSP Publications*. https://www.ncei.noaa.gov/products/dmsp-publications

Neath, A. A., & Cavanaugh, J. E. (2012). The Bayesian information criterion: background, derivation, and applications. *Wiley Interdisciplinary Reviews: Computational Statistics*, *4*(2), 199–203.

Nortier, N. S., Löwenthal, K., Luxembourg, S. L., van der Neut, A., Mewe, A. A., & van Sark, W. (2022). Spatially resolved generation profiles for onshore and offshore wind turbines: A case study of four Dutch energy transition scenarios. *Renewable and Sustainable Energy Transition*, *2*, 100037.

Norton, M., Khokhlov, V., & Uryasev, S. (2021). Calculating CVaR and bPOE for common probability distributions with application to portfolio optimization and density estimation. *Annals of Operations Research*, *299*, 1281–1315.

Ohba, M., Kanno, Y., & Bando, S. (2023). Effects of meteorological and climatological factors on extremely high residual load and possible future changes. *Renewable and Sustainable Energy Reviews*, *175*, 113188.

Ohba, M., Kanno, Y., & Nohara, D. (2022). Climatology of dark doldrums in Japan. *Renewable and Sustainable Energy Reviews*, *155*, 111927.

Ohlendorf, N., & Schill, W.-P. (2020). Frequency and duration of low-wind-power events in Germany. *Environmental Research Letters*, *15*(8), 084045.

Osei, M. A., Amekudzi, L. K., Omari-Sasu, A. Y., Yamba, E. I., Quansah, E., Aryee, J. N. A., & Preko, K. (2021). Estimation of the return periods of maxima rainfall and floods at the Pra River Catchment, Ghana, West Africa using the Gumbel extreme value theory. *Heliyon*, *7*(5), e06980.

Otero, N., Martius, O., Allen, S., Bloomfield, H., & Schaefli, B. (2022). A copula-based assessment of renewable energy droughts across Europe. *Renewable Energy*, *201*, 667–677.

Pickands III, J. (1975). Statistical inference using extreme order statistics. *The Annals of Statistics*, 119–131.

Plötz, P., & Michaelis, J. (2014). The probability of long phases without wind power and their impact on an energy system with high share of renewable energies. *9th Conference on Energy Economics and Technology, ENERDAY 2014*.

Pörtner, H.-O., Roberts, D. C., Adams, H., Adler, C., Aldunce, P., Ali, E., Begum, R. A., Betts, R., Kerr, R. B., & Biesbroek, R. (2022). *Climate change 2022: Impacts, adaptation and vulnerability*. IPCC Geneva, Switzerland:

Pototschnig, A. (2020). *The importance of a sound bidding-zone review for the efficient functioning of the internal electricity market*. European University Institute.

Price, J., & Zeyringer, M. (2022). highRES-Europe: The high spatial and temporal Resolution Electricity System model for Europe. *SoftwareX*, *17*, 101003.

Quarton, D. C. (2005). An international design standard for offshore wind turbines: IEC 61400-3. *Bristol, UK: Garrad Hassan and Partners, Ltd*.

Rajulapati, C. R., Papalexiou, S. M., Clark, M. P., & Pomeroy, J. W. (2021). The perils of regridding: examples using a global precipitation dataset. *Journal of Applied Meteorology and Climatology*, *60*(11), 1561–1573.

Raynaud, D., Hingray, B., François, B., & Creutin, J. D. (2018). Energy droughts from variable renewable energy sources in European climates. *Renewable Energy*, *125*, 578–589.

Rijksoverheid. (2022, September 30). *Factsheet Zon-PV per provincie 2021*. https://www.rijksoverheid.nl/onderwerpen/duurzame-energie/documenten/rapporten/2022/09/30/factsheet-zon-pv-per-provincie-2021

Rinaldi, A., Krajcinovic, D., & Mastilovic, S. (2007). Statistical damage mechanics and extreme value theory. *International Journal of Damage Mechanics*, *16*(1), 57–76.

RvO. (2018, August 27). *Windparken op de Noordzee*. https://www.rvo.nl/subsidies-financiering/windenergie-op-zee/actieve-windparken

RvO. (2022, May 22). *Monitor Wind op Land over 2021*. https://www.rvo.nl/sites/default/files/2022-05/Monitor-wind-op-land-2021_0.pdf

Ryu, G. H., Kim, D., Kim, D.-Y., Kim, Y.-G., Kwak, S. J., Choi, M. S., Jeon, W., Kim, B.-S., & Moon, C.-J. (2022). Analysis of Vertical Wind Shear Effects on Offshore Wind Energy Prediction Accuracy Applying Rotor Equivalent Wind Speed and the Relationship with Atmospheric Stability. *Applied Sciences*, *12*(14), 6949.

Sarykalin, S., Serraino, G., & Uryasev, S. (2008). Value-at-risk vs. conditional value-at-risk in risk management and optimization. In *State-of-the-art decision-making tools in the information-intensive age* (pp. 270–294). Informs.

Schepsmeier, U., Stoeber, J., Brechmann, E. C., Graeler, B., Nagler, T., Erhardt, T., Almeida, C., Min, A., Czado, C., & Hofmann, M. (2015). Package 'vinecopula.' *R Package Version*, *2*(5).

Schleussner, C.-F., Rogelj, J., Schaeffer, M., Lissner, T., Licker, R., Fischer, E. M., Knutti, R., Levermann, A., Frieler, K., & Hare, W. (2016). Science and policy characteristics of the Paris Agreement temperature goal. *Nature Climate Change*, *6*(9), 827–835.

Science, U. C. for E. R. O. and. (1996). *USGS EROS Archive–Digital Elevation–Global 30 Arc-Second Elevation (GTOPO30)*. US Geological Survey (USGS) Reston, VA.

SEARATES. (2023, March 11). *Sea ports of the Netherlands*. https://www.searates.com/maritime/netherlands

Shehata, W., & Yousof, H. (2022). A novel two-parameter Nadarajah-Haghighi extension: properties, copulas, modeling real data and different estimation methods. *Statistics, Optimization & Information Computing*, *10*(3), 725–749.

Shivakumar, A., Dobbins, A., Fahl, U., & Singh, A. (2019). Drivers of renewable energy deployment in the EU: An analysis of past trends and projections. *Energy Strategy Reviews*, *26*, 100402.

Simionescu, M., Strielkowski, W., & Tvaronavičienė, M. (2020). Renewable energy in final energy consumption and income in the EU-28 countries. *Energies*, *13*(9), 2280.

SOLARGIS. (2020). *Solar resource maps of Netherlands*. Https://Solargis.Com/Maps-and-Gis-Data/Download/Netherlands.

Statista. (2023a, January 25). *Leading countries in per capita electricity consumption in Europe in 2021*. https://www.statista.com/statistics/1262218/per-capita-electricity-consumption-europe-by-country/

Statista. (2023b, January 25). *Per capita electricity consumption in Europe from 2000 to 2021*. https://www.statista.com/statistics/1262471/per-capita-electricity-consumption-europe/#:~:text=In%202021%2C%20Europe's%20electricity%20consumption,6.28%20megawatt%20hours%20per%20capita.

Steiner, A., Köhler, C., Metzinger, I., Braun, A., Zirkelbach, M., Ernst, D., Tran, P., & Ritter, B. (2017). Critical weather situations for renewable energies–Part A: Cyclone detection for wind power. *Renewable Energy*, *101*, 41–50.

Stepek, A., & Wijnant, I. L. (2011). *Interpolating wind speed normals from the sparse Dutch network to a high resolution grid using local roughness from land use maps*. KNMI.

Sun, Y., Hof, A., Wang, R., Liu, J., Lin, Y., & Yang, D. (2013). GIS-based approach for potential analysis of solar PV generation at the regional scale: A case study of Fujian Province. *Energy Policy*, *58*, 248–259.

Tedesco, P., Lenkoski, A., Bloomfield, H. C., & Sillmann, J. (2022). Gaussian copula modeling of extreme cold and weak-wind events over Europe conditioned on winter weather regimes. *Environmental Research Letters*.

TenneT. (2022a, June 9). *Bidding Zone Review: TSOs investigate alternative bidding zone configurations*. https://www.tennet.eu/news/bidding-zone-review-tsos-investigate-alternative-bidding-zone-configurations

TenneT. (2022b, December 21). *Landelijk Actieprogramma Netcongestie*. https://tennet-drupal.s3.eu-central-1.amazonaws.com/default/2022-12/Landelijk%20Actieprogramma%20Netcongestie_definitief_0.pdf

The Wind Power: Wind Energy Market Intelligence. (2023). *Manufacturers and turbines*. https://www.thewindpower.net/turbines_manufacturers_en.php

Thompson, P., Cai, Y., Reeve, D., & Stander, J. (2009). Automated threshold selection methods for extreme wave analysis. *Coastal Engineering*, *56*(10), 1013–1021.

Ueckerdt, F., Brecha, R., & Luderer, G. (2015). Analyzing major challenges of wind and solar variability in power systems. *Renewable Energy*, *81*, 1–10.

van den Bergh, K., Wijsen, C., Delarue, E., & D'haeseleer, W. (2016). The impact of bidding zone configurations on electricity market outcomes. *2016 IEEE International Energy Conference (ENERGYCON)*, 1–6.

van der Wiel, K., Stoop, L. P., van Zuijlen, B. R. H., Blackport, R., van den Broek, M. A., & Selten, F. M. (2019). Meteorological conditions leading to extreme low variable renewable energy production and extreme high energy shortfall. *Renewable and Sustainable Energy Reviews*, *111*, 261–275.

Vrieze, S. I. (2012). Model selection and psychological theory: a discussion of the differences between the Akaike information criterion (AIC) and the Bayesian information criterion (BIC). *Psychological Methods*, *17*(2), 228.

WDPA. (2023, March 11). *Protected Areas*. https://www.protectedplanet.net/en/thematic-areas/wdpa?tab=WDPA

Windpowerlib. (2023, February 14). *Model description: Wind power plants*. https://windpowerlib.readthedocs.io/en/stable/model_description.html

Wind-turbine-models. (2023a, February 13). *Vestas V105-3.3*. https://en.wind-turbine-models.com/turbines/891-vestas-v105-3.3

Wind-turbine-models. (2023b, February 13). *Vestas V117-3.3*. https://en.wind-turbine-models.com/turbines/694-vestas-v117-3.3

Wind-turbine-models. (2023c, February 13). *Vestas V126-3.3*. https://en.wind-turbine-models.com/turbines/695-vestas-v126-3.3

Yang, Y., Javanroodi, K., & Nik, V. M. (2022). Climate change and renewable energy generation in europe—long-term impact assessment on solar and wind energy using high-resolution future climate data and considering climate uncertainties. *Energies*, *15*(1), 302.

Yang, Y., Li, H., Aichhorn, A., Zheng, J., & Greenleaf, M. (2013). Sizing strategy of distributed battery storage system with high penetration of photovoltaic for voltage regulation and peak load shaving. *IEEE Transactions on Smart Grid*, *5*(2), 982–991.

Zappa, W., & Van Den Broek, M. (2018). Analysing the potential of integrating wind and solar power in Europe using spatial optimisation under various scenarios. *Renewable and Sustainable Energy Reviews*, *94*, 1192–1216.

Zscheischler, J., Martius, O., Westra, S., Bevacqua, E., Raymond, C., Horton, R. M., van den Hurk, B., AghaKouchak, A., Jézéquel, A., & Mahecha, M. D. (2020). A typology of compound weather and climate events. *Nature Reviews Earth & Environment*, *1*(7), 333–347.

Appendix

A: Spatial analysis

The spatial analysis follows the methodology of Hu et al. (2019) and Jung & Schindler (2023). The respective areas of the Netherlands, both onshore and the EEZ, are assessed based on the possibility of VRE technology installation. The modelling software used for the spatial analysis is ArcGIS Pro. Firstly, the selected available area is filtered through geographical constraints, which differ by technology. The geographical constraints can be found in Table 25.

Table 25: Geographical constraints by VRE technology

Constraint for each VRE technology	Data sources	Resolution of data (NA in case of shapefile)	Onshore wind	Offshore wind	Utility-PV	Rooftop PV
Territory (km^2)	(CBS, 2023)	NA	Administrative terrestrial area	Economical exclusive zone	Administrative terrestrial area	Administrative terrestrial area
Distance to shore (km)	NA	NA	NA	10-185 A minimum distance to shore at ~10 km is set to restrict visibility and environmental impacts of offshore wind farms. The maximum distance to shore is limited to 185 km for cost consideration (Eurek et al., 2007)	NA	NA
Depth (m)	Institute (2019)	0.004° (0.25 arcmin)	NA	≤ 60 Only offshore wind turbines with bottom fixed foundations (no floating) are considered. They usually suit water depth below 60 m (Hu et al., 2019)	NA	NA
Vessel identity and location information	Halpern et al. (2019)	0.1° (6 arcmin)	NA	≤1500. If the grid cell includes more than 1500 vessel locations, it is considered as vessel-intensive areas to be excluded from the available area for offshore wind farms.	NA	NA
Oil rigs	(National Centers for Environmental Information, 2023)	0.008° (0.5 arcmin)	NA	Fully exclusion	NA	NA
Submarine communications cable	(Mahlknecht, 2023)	NA	NA	1 km^2 buffering from both sides of the cable (Bosch et al., 2018)	NA	NA

Distance to port	(SEARATES, 2023)	NA	NA	≤ 80 km to the nearest port (Jung & Schindler, 2023)	NA	NA
Protected areas (km^2)	(WDPA, 2023)	NA	Terrestrial protected areas	Terrestrial & maritime protected areas	Terrestrial protected areas	Terrestrial protected areas
Permafrost (%)	(S. Gruber, 2012)	0.008° (0.5 arcmin)	≤0.1	NA	≤0.01	≤0.01
Elevation (m)	(Science, 1996)	0.05° (30 arcmin)	<=2500 Following Eurek et al. (2017), elevation above 2500 m is considered as too high for onshore wind development due to substantial reduction of wind power density associated air density losses.	NA	NA	NA
Slope (degree)	Calculated based on Elevation	0.05° (30 arcmin)	<11.31 (or 20%) (Eurek et al., 2017)	NA	<4 (0r 6.99%) (Sun et al., 2013)	NA
Land cover	(Copernicus, 2023)	0.003° (1.67 arcmin) for GlobCover 2009 V2.3; 100m for CLC2018	Depending on suitability factor per land cover type	NA	Depending on suitability factor per land cover type	Depending on suitable rooftop areas in built-up area

After the geographical constraints have been applied, the CLC land cover classification system is used to determine the potential suitable area within the available area. The available area is multiplied by a predetermined factor, based on the cover classification. The land cover classification can be found in Table 26.

Table 26: Land cover classification (Copernicus, 2018)

Main Class	1st Sub-Class	2nd Sub-Class	CLC Code	Onshore wind	Offshore wind	Utility - PV	Rooftop PV	
							Tilted roof	*Flat roof*
Artificial surfaces	Urban fabric	Continuous urban fabric	111	0	0	0	0.119	0.007
		Discontinuous urban fabric	112	0	0	0	0.067	0.004
	Industrial, commercial and transport units	Industrial or commercial units	121	0	0	0	0.041	0.045
		Road and rail networks and associated land	122	0	0	0	0	0
		Port areas	123	0	0	0	0	0
		Airports	124	0	0	0	0	0
	Mine, dump and construction sites	Mineral extraction sites	131	0	0	0	0	0
		Dump sites	132	0	0	0	0	0
		Construction sites	133	0	0	0	0	0
		Green urban areas	141	0	0	0	0	0

	Artificial, non-agricultural vegetated areas	Sport and leisure facilities	142	0	0	0	0	0
	Arable land	Non-irrigated arable land	211	0.2	0	0.01	0	0
		Permanently irrigated land	212	0	0	0	0	0
		Rice fields	213	0	0	0	0	0
	Permanent crops	Vineyards	221	0.1	0	0.01	0	0
		Fruit trees and berry plantations	222	0.1	0	0.01	0	0
		Olive groves	223	0.1	0	0.01	0	0
	Pastures	Pastures	231	0.2	0	0.01	0	0
	Heterogeneous agricultural areas	Annual crops associated with permanent crops	241	0.2	0	0.01	0	0
		Complex cultivation patterns	242	0.2	0	0.01	0	0
		Agricultural land with significant natural vegetation	243	0.2	0	0.01	0	0
		Agro-forestry areas	244	0.1	0	0	0	0
Forest and semi natural areas	Forests	Broad-leaved forest	311	0	0	0	0	0
		Coniferous forest	312	0	0	0	0	0
		Mixed forest	313	0	0	0	0	0
	Scrub and/or herbaceous vegetation associations	Natural grasslands	321	0.2	0	0.01	0	0
		Moors and heathland	322	0.1	0	0.01	0	0
		Sclerophyllous vegetation	323	0.1	0	0.01	0	0
		Transitional woodland-shrub	324	0	0	0	0	0
	Open spaces with little or no vegetation	Beaches, dunes, sands	331	0	0	0	0	0
		Bare rocks	332	0	0	0	0	0
		Sparsely vegetated areas	333	0.5	0	0.05	0	0
		Burnt areas	334	0	0	0	0	0
		Glaciers and perpetual snow	335	0	0	0	0	0
Wetlands	Inland wetlands	Inland marshes	411	0	0	0	0	0
		Peat bogs	412	0	0	0	0	0
	Maritime wetlands	Salt marshes	421	0	0	0	0	0
		Salines	422	0	0	0	0	0
		Intertidal flats	423	0	0	0	0	0
Water bodies	Inland waters	Water courses	511	0	0	0	0	0
		Water bodies	512	0	0	0	0	0
	Marine waters	Coastal lagoons	521	0	0	0	0	0
		Estuaries	522	0	0	0	0	0
		Sea and ocean	523	0	0.4	0	0	0

The suitable area per grid cell is retrieved after applying the classification to the available area per grid cell. This suitable area is converted into a potential of installable capacity for solar PV or wind turbines through array spacing. For wind, the area allocated for a single wind turbine is determined to be six diameters by six diameters, based on the rotor diameter of the considered wind turbine. For solar PV, the area considered is the surface area of the solar panel multiplied with a factor to prevent self-shading. As mentioned in the methodology, this value is in the range of 1.40 and differs per grid cell.

B: Offshore wind turbine power curves

The power curves of the onshore turbine types are presented in Table 27 (The Wind Power: Wind Energy Market Intelligence, 2023).

Table 27: Power curves for the different onshore turbine types that are considered in the energy conversion

	Vestas V105 – 3.3 MW	**Vestas V117 – 3.3 MW**	**Vestas V126 – 3.3 MW**
Wind speed (m/s)	**Power (kW)**	**Power (kW)**	**Power (kW)**
0	0	0	0
0.5	0	0	0
1	0	0	0
1.5	0	0	0
2	0	0	0
2.5	0	10	12
3	0	24	30
3.5	40	82	102
4	92	147	179
4.5	155	235	286
5	229	327	397
5.5	330	461	553
6	441	597	711
6.5	617	788	931
7	799	978	1150
7.5	989	1230	1437
8	1178	1482	1723
8.5	1428	1798	2079
9	1677	2114	2434
9.5	1995	2459	2780
10	2313	2803	3090
10.5	2608	3060	3235
11	2903	3216	3290
11.5	3100	3275	3298
12	3227	3297	3300
12.5	3275	3299	3300
13	3281	3300	3300
13.5	3295	3300	3300
14	3300	3300	3300

14.5	3300	3300	3300
15	3300	3300	3300
15.5	3300	3300	3300
16	3300	3300	3300
16.5	3300	3300	3300
17	3300	3300	3300
17.5	3300	3300	3300
18	3300	3300	3300
18.5	3300	3300	3300
19	3300	3300	3300
19.5	3300	3300	3300
20	3300	3300	3300
20.5	3300	3300	3300
21	3300	3300	3300
21.5	3300	3300	3300
22	3300	3300	3300
22.5	3300	3300	3300
23	3300	3300	3300
23.5	3300	3300	3300
24	3300	3300	3300
24.5	3300	3300	3300
25	3300	3300	3300
25.5	0	0	0
26	0	0	0
26.5	0	0	0
27	0	0	0
27.5	0	0	0
28	0	0	0
28.5	0	0	0
29	0	0	0
29.5	0	0	0
30	0	0	0

The power curves of the offshore turbine types are presented in Table 28 (The Wind Power: Wind Energy Market Intelligence, 2023).

Table 28: Power curves for the different offshore turbine types that are considered in the energy conversion

	Vestas V164 9.5 MW	**Siemens Gamesa 8.0**	**Siemens SWT 4.0**	**Vestas V112**	**Vestas V80**	**Vestas V90**
Wind speed (m/s)	**Power (kW)**	**Power (kW)**	**Power (kW)**	**Power (kW)**	**Power (kW)**	**Power (kW)**
0	0	0	0	0	0	0
0.5	0	0	0	0	0	0
1	0	0	0	0	0	0
1.5	0	0	0	0	0	0
2	0	0	0	0	0	0
2.5	0	0	80	0	0	0
3	0	0	193	0	0	0
3.5	115	48	300	36	35	38
4	249	169	479	76	70	77
4.5	430	350	705	134	117	133
5	613	593	916	192	165	190
5.5	900	930	1120	269	225	271
6	1226	1307	1329	346	285	353
6.5	1600	1737	1555	465	372	467
7	2030	2186	1788	584	459	581
7.5	2570	2730	2040	737	580	733
8	3123	3278	2300	890	701	886
8.5	3784	3980	2590	1098	832	1079
9	4444	4687	2872	1306	964	1272
9.5	5170	5400	3170	1514	1127	1484
10	5900	6112	3453	1722	1289	1696
10.5	6600	6690	3700	1942	1428	1901
11	7299	7249	3869	2162	1567	2106
11.5	7960	7570	3970	2352	1678	2298
12	8601	7795	4000	2542	1788	2489
12.5	9080	7895	4000	2701	1865	2643
13	9272	7947	4000	2860	1941	2797
13.5	9410	7990	4000	2930	1966	2874
14	9500	8000	4000	2970	1990	2951
14.5	9500	8000	4000	2983	2000	2972
15	9500	8000	4000	2995	2000	2993

15.5	9500	8000	4000	3000	2000	2996
16	9500	8000	4000	3000	2000	2999
16.5	9500	8000	4000	3000	2000	3000
17	9500	8000	4000	3000	2000	3000
17.5	9500	8000	4000	3000	2000	3000
18	9500	8000	4000	3000	2000	3000
18.5	9500	8000	4000	3000	2000	3000
19	9500	8000	4000	3000	2000	3000
19.5	9500	8000	4000	3000	2000	3000
20	9500	8000	4000	3000	2000	3000
20.5	9500	8000	4000	3000	2000	3000
21	9500	8000	4000	3000	2000	3000
21.5	9500	8000	4000	3000	2000	3000
22	9500	8000	4000	3000	2000	3000
22.5	9500	8000	4000	3000	2000	3000
23	9500	8000	4000	3000	2000	3000
23.5	9500	8000	4000	3000	2000	3000
24	9500	8000	4000	3000	2000	3000
24.5	9500	8000	4000	3000	2000	3000
25	9500	8000	4000	3000	2000	3000
25.5	0	0	0	0	0	0
26	0	0	0	0	0	0
26.5	0	0	0	0	0	0
27	0	0	0	0	0	0
27.5	0	0	0	0	0	0
28	0	0	0	0	0	0
28.5	0	0	0	0	0	0
29	0	0	0	0	0	0
29.5	0	0	0	0	0	0
30	0	0	0	0	0	0

C: Visual comparison of the Frank copula and t copula fitting for aggregated CF in the N1 and N2 region based on MERRA data

The visual comparison between the Frank copula and t copula for the MERRA based aggregated CF for the N1 and N2 region is presented in Figure 50.

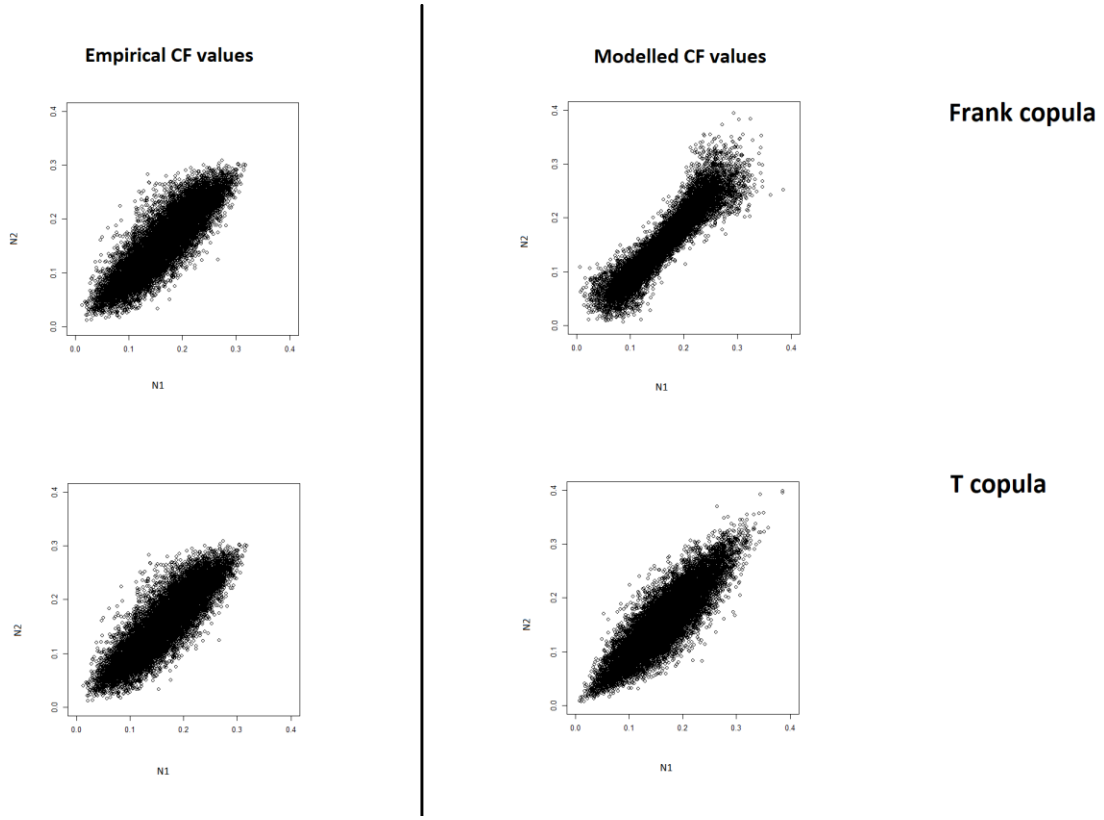

Figure 50: Visual comparison of the Frank copula and t copula of the CF values for the N1 and N2 region based on MERRA data

D: Conventional methodology for calculating CVaR for exponential distributions

The calculation of the CVaR for the exponential distribution is based on the study by Norton et al. (2021) and is presented in (20).

$$CVaR_p = \frac{-\ln(1-p)+1}{\lambda} \quad (20)$$

Where λ is the rate parameter, which is the inverse of the scale parameter β.